Ice core data from Renland

Investigation of firn cores, main cores and evaluation of isotope-enabled GCMs for Renland

Master thesis, 30 ECTS
Center for Ice and Climate

September 20, 2016
Version 2.0

Mika Lanzky

Supervisor: Bo Vinther

University of Copenhagen
Faculty of Science
Niels Bohr Institute

Acknowledgements First, a collective thanks goes to Center for Ice and Climate where I have been around in some form of another throughout the years, doing projects, taking courses, and working in the freezer or isotope lab.

Special thanks goes to Trevor, Lars, Aksel, Vasileios and of course my supervisor, Bo. Although the project might have ended up a tad bigger than planned, the time was both interesting and educational, and I got to work both experimentally and with modelling.

Getting the opportunity to go to the Greenland Ice sheet and stay at the EGRIP camp was a great experience, seeing, and trying, it all "in the flesh".

Thanks also to Anne-Katrine, HC and Martin Werner for providing data for the project. I should also thank Louise and Sandra for companionship throughout the years, even though in the end, they left me behind. The student office at CIC is a good working base, ready with small-talk, help, and cookies.

I will especially like to thank Martin for help with the math and talks about isotopes and feedback on the thesis, and Martin for providing the opportunity for small breaks, proofreading the thesis, and help with meteorology.

Thanks to Iben for help with version 2.0 of the thesis, providing feedback on smaller and bigger mistakes.

Abstract This thesis deals with ice core data from Renland, an peninsula at the East coast of Greenland, in the form of two firn cores and the old and new main core, and evaluates data from two isotope-enabled GCM's, in order to understand the newly drilled core from Renland and the climatic context hereof.

The firn cores was processed and measured for their isotopic composition, a comparison was made to GCM data, and the borehole temperature was modelled for the sites of both the old and new core, using an model with a firn layer and having a density dependency of the thermal parameters.

The firn cores was found to be similar in isotopic value and accumulation, making the old and new main core readily comparable, however, results also suggest that the flow of the two sites are not of the same kind. The GCM data shows good agreement with the measurement data, both in isotopes, precipitation and temperature when viewed separately, while the combination of them still lag improvement.

The agreement of the two sites, the gridded data from a GCM and the temperature modelling run with input from a further away meteorological weather station suggest that the climate experienced at Renland is indicative of a broader, perhaps even regional, signal in the area of Southeastern Greenland.

Resume Dette speciale behandler iskernedata fra Renland, en halvø ved Grønlands øskyst, i form af to firnkerner og den gamle og nye hovedkerne, og evaluerer data fra en global circulations model med isotopkomponent, for at lære om den nyligt borede kerne fra Renland og dens klimatiske kontekst.

Firnkernerne blev processeret og fik målt deres isotopsammensætning, en sammenligning med GCM data blev foretaget, og borehulstemperaturen blev modelleret for stederne for både den gamle og den nye hovedkerne med en model indeholdende et firnlag og en densitetsafhængig af de termiske parametre.

Resultatet var at firnkernerne er enslignende i isotopsammensætning og akkumulation, hvilket muliggør en ligefrem sammenlign af den gamle og nye hovedkerne; det viste sig dog også at flydningen ved de to steder ikke er af samme natur. GCM dataene viser god overensstemmelse med de målte data, både i isotoper, nedbør og temperatur betraget hver for sig, mens sammenføjningen af dem behøver forbedring.

Overenstemmelsen mellem de to steder, det griddede data fra en GCM og temperaturmodelleringen kørt med data fra en meteorologisk vejrstation længere væk tyder på at klimaet oplevet på Renland er indikerende for et bredere, måske endda regionalt, signal i området af sydøstgrønland.

Contents

List of Figures

List of Tables

CHAPTER 1

Introduction

Understanding the processes and mechanisms behind our climate is important as we are in and face a time of increased warming and sea-level rise, with both natural, economic and societal consequences. Paleoclimatic research is a tool to get information about the climate of the past, in order to understand the climate of our future.

One type of such research is that of ice core drilling which provide a diverse archive of different climatic parameters, both proxies and direct. Several cores have been drilled around the world, particularly at Greenland and Antarctica. This thesis makes use of data from cores drilled at the island of Renland off the east coast of Greenland. In 1988, the first core from Renland was drilled at length of 325 meters [Johnsen et al., 1992]. Renland is a good cite for drilling: the ice cap is independent from the main Greenland Ice Sheet, making comparison interesting, and due to the topography of the ice cap, the flow is thought to be complicated, yet stable, and any changes in elevation throughout climatic periods is thought to be very small [Vinther et al., 2009], and its thickness means it has no brittle zone where the ice is often in bad condition.

The old core drilled with an older technique, however, was not in good enough quality for gas or impurity measurements, and a new core was therefore drilled in the summer of 2015, the RECAP project [Vinther], about 2 km away from the old site. A main core of 584 meters was drilled, comprising both all of the Holocene at high resolution and reaching back to the last glacial and even into the Eemian. Radar was used to find the optimum drilling site with low bedrock undulation and high depth, as shown in figure 1.1. In addition to the main core, several shorter firn cores was drilled on the Renland ice cap, two of which where at the old site and close to the new site.
These two firn cores will be compared to gain insight into whether there are differences between the sites, necessary for interpretation of the new main core compared with the old main core. This will be done by cutting them into samples and measuring their isotope values. Data from two isotope-enabled climate models will be compared to the data from the firn cores and to data from the old and new core, by investigating the parameters *temperature, precipitation* and *isotopic composition*.

This enables us to understand the climate of Renland better and tells us about what tools we have available for the interpretation, as this gives information about the performance of climate models for this particular site.

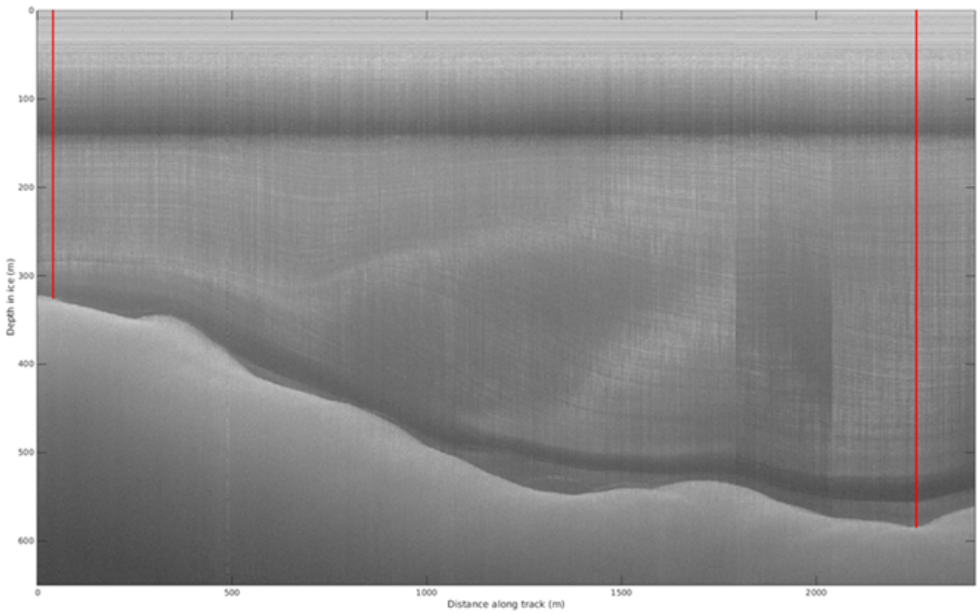

Figure 1.1: *Processed radar image taken in summer of 2015 of the Renland ice cap as part of the RECAP campaign. Overlayed with red lines are locations of the old 1988 core (left) and the new 2015 core (right). Depths are approximately 325 and 584 metres. The black band towards the bottom is the glacial ice. Picture courtesy of Christian Panton.*

The thesis is structured as such:

Chapter 2 and 3 deals with the theoretical background, divided into the main core glaciological (2) and the isotope and climate related topics (3).

Chapter 4 contains the description and result of the firn core experimental work and their comparison.

Chapter 5, 6 and 7 investigates the iso-gcm models. First, we make a validation check of the models with weather stations (5), then we compare the isotopic values of the models and firn cores (6), and in (7) we model borehole temperature from ECHAM input and compare with measurement profiles at old and main Renland RECAP core holes. and finally

Chapter 8 and 9 discusses the various results individually and in context of each other (8), and summarizes to a concluding answer (9).

CHAPTER 2

General glaciology

Wherever snowfall exceeds the melting (and/or runoff), a glacier will form, as a mountain glacier, ice cap or ice sheet, such as those of Greenland or Antarctica. An ice cap is divided into zones, mainly the accumulation zone where precipitation is higher than melting/evaporation and you have positive mass balance, and the ablation zone, where you have negative mass balance. The balance of the masses in those zones then determine the overall mass balance of the ice cap.

Due to gravity, the ice flows downwards, and an ice cap will often take on a flat rounded oval shape, seen as a 2D cross-section (of Greenland) in figure 2.1. After the snow falls onto the surface in the accumulation zone, it will compact into ice and move down and to the sides, stretching the yearly layers horizontally which become thinner. The *ice divide* is defined as where ice to either side of it flows in their respective directions. Idealized, the accumulation happening right on the spot of the ice divide will only move downwards, thus creating an old, layered sequence of the snowfall, with the ice at the bottom being infinitely old, if nothing melted off at the bottom and nothing disturbed the deeper layers.

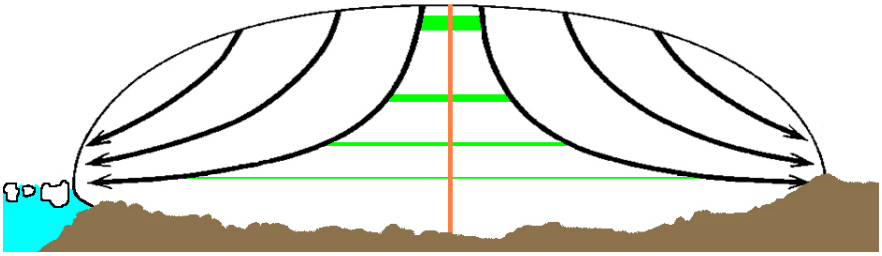

Figure 2.1: *Drawing of cross section of an idealized ice cap for Greenland with flow lines from the surface to the sides and internal layers getting thinner going deeper. The orange line marks the ice divide, from where the ice flows in opposite horizontal directions. Picture credit: CIC, NBI, University of Copenhagen.*

For Greenland, the central ice divide, running almost north-south, is about 3 kilometres thick and the oldest, undisturbed ice goes back to about 125,000 years at NGRIP, to the start of the previous warm period, the Eemian. On Antarctica, the elevation is similar, but the annual snowfall is much smaller, so here the ice can be almost a million years old at Dome C and F.

This sequence of layered ice can be sampled by drilling *ice cores* and investigating the ice in different ways, such as stable water isotopes, impurities, the gas content in the air bubbles trapped in the ice, and the ice crystals themselves. All these measurements, some proxies and others direct or indirect, enables us to evaluate the state of the climate in the past.

2.1 Deformation of ice sheets

If the ice did not flow, and it did not melt away, the ice sheets on Earth would just continue to grow and grow. Since it does not, flow of ice must be a factor. When viewing a "parcel" of the

ice sheet, what goes in must also be what goes out, otherwise there would be either loss or build up of material. In all of geophysics, we need to have conservation of mass. From that, we get the continuity equation:

$$\frac{\partial \rho}{\partial t} + \frac{\partial \rho u}{\partial x} + \frac{\partial \rho v}{\partial y} + \frac{\partial \rho w}{\partial z} = 0 \tag{2.1}$$

where u, v and w refers to the velocity in the x, y and z direction, and ρ the density. If we ignore the second horizontal dimension and assume the ice is incompressible, i.e. constant density, the continuity equation simplifies greatly and gives us a relation between the change in the horizontal and vertical speed:

$$-\frac{\partial u}{\partial x} = \frac{\partial w}{\partial z} \tag{2.2}$$

2.1.1 Velocity model

Let us consider a slab of size x of the ice sheet, in two dimensions, close to the ice divide. On the surface it snows with an annual accumulation of λ_H in the z-direction. This ice, with a (two-dimensional) volume of $x\lambda_H$, must go somewhere, and if there is no bottom melting, the only way it can go is out in the x-direction, leaving through the "side" the full height of the ice cap, H; the negative x-direction is bounded by the ice divide, meaning the movement is mirrored on its other side. If the entire vertical ice column moved as one, the horizontal velocity profile would be a straight line, making what goes out the velocity times the ice height.

Another velocity model, $u(z)$, is the "kink model", proposed by Dansgaard and Johnsen [1969]. It assumes steady state in ice cap height and accumulation rate, and that the horizontal velocity is constant, u_H, down to a certain depth, h, called the kink height, from where it linearly decreases with depth, $u_H((1 - f_B)z/h + f_B)$, until reaching bottom velocity, as seen on figure 2.2. The bottom sliding factor f_B, defined as the ratio of the bedrock to surface horizontal velocity, will determine the lowest horizontal velocity, and in the case of no bottom sliding, the velocity will decrease to zero at the bottom.

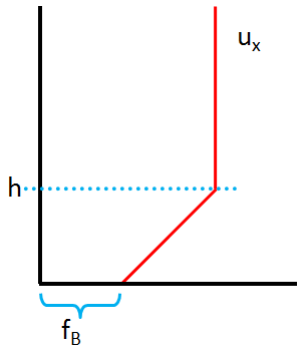

Figure 2.2: *Qualitative representation of the horizontal velocity with depth for the kink-model. The kink height is given as h, and f_B is the bottom sliding.*

Using "what comes in must come out", we can now find an expression for the surface velocity

given by the accumulation and the kink height:

$$\begin{aligned}\lambda_H x &= \int_0^H u(z)dz = \int_0^h u_H[(1-f_B)\frac{z}{h}+f_B]dz + \int_h^H u_H dz \\ &= u_H[(1-f_B)\frac{h^2-0^2}{2h} + f_B(h-0)] + u_H(H-h) \\ &= u_H\left((1-f_b)\frac{h}{2}+f_Bh\right) + u_H(H-h) = u_H\left[(1-f_B)\frac{h}{2}+f_Bh+H-h\right] \\ &\Rightarrow u_H = \frac{\lambda_H x}{H_e}, \qquad \text{where} \quad H_e = H+\frac{h}{2}(f_B-1)\end{aligned} \tag{2.3}$$

where H_e is called the "effective height". As we now have an expression for the horizontal velocity, u, we can use the continuity equation 2.2 to find an expression for how the ice moves vertically, w:

$$dw = -\frac{du}{dx}dz \Rightarrow \int_{w(0)}^{w(z)} dw = -\int_0^z \frac{du}{dx}dz' \Rightarrow w(z)-w(0) = -\int_0^z \frac{du}{dx}dz' \tag{2.4}$$

The expression for u is different above and below the kink height, so we must divide the derivation into two parts. First the lower, from $0 \le z \le h$. If we assume no bottom melting, there is no ice "going into" the bedrock, making $w(0) = 0$:

$$\begin{aligned}w(z) &= -\int_0^z \frac{\partial}{\partial x}\left[u_H\left((1-f_B)\frac{z}{h}+f_B\right)\right]dz' = -\int_0^z \frac{\partial}{\partial x}\left[\frac{\lambda_H x}{H_e}\left((1-f_B)\frac{z}{h}+f_B\right)\right]dz' \\ &= -\frac{\lambda_H}{H_e}\left[(1-f_B)\frac{z'^2}{2h}+f_Bz'\right]_0^z = -\frac{\lambda_H}{H_e}\left[(1-f_B)\frac{z^2}{2h}+f_Bz\right]\end{aligned} \tag{2.5}$$

and for the upper part, $h \le z \le H$, we get the velocity of the kink height, $w(h)$ from the expression just derived:

$$\begin{aligned}w(z) &= w(h) - \int_h^z \frac{\partial}{\partial x}(u_H)dz' = w(h) - \int_h^z \frac{\partial}{\partial x}\frac{\lambda_H x}{H_e}dz' = w(h) - \left[\frac{\lambda_H}{H_e}z'\right]_h^z \\ &= -\frac{\lambda_H}{H_e}\left[(1-f_B)\frac{h^2}{2h}+f_Bh\right]\left[-\frac{\lambda_H}{H_e}(z-h)\right] = -\frac{\lambda_H}{H_e}\left[\frac{h}{2}-\frac{h}{2}f_B+f_Bh+z-h\right] \\ &= -\frac{\lambda_H}{H_e}\left[z-\frac{h}{2}(1-f_B)\right]\end{aligned} \tag{2.6}$$

As can be seen, the equations simplify if there is no bottom sliding.

Assuming steady state of the accumulation, each annual layer of ice moves exactly its own thickness down each year, while thinning. In this way, the velocity profile also yields the thicknesses, $\lambda(z)$ of the layers per year, τ, or $\lambda(z) = -w(z)\tau$. The shape of the profile of the vertical velocity is the same as for the annual thickness, as seen in figure 2.3.

2.2 Dating ice cores

If an ice core is undisturbed, the relative age of the layers are known, in that simply deeper lying parts are older than upper parts, and perhaps it is also possible to know the duration of a piece of the core. But it is also of interest to know the *absolute* dating of the layers, both for evaluating the core itself, but especially for comparing it to other ice cores and other climate records. High-precision dating is furthermore needed to determine if a certain event, present in

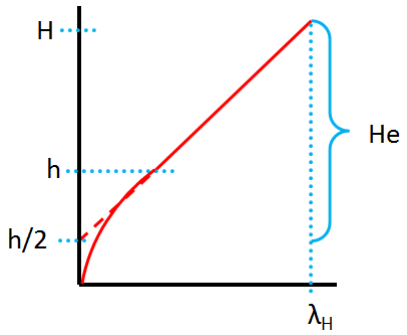

Figure 2.3: *Qualitative representation of the annual layer thickness as given by the kink velocity model. By extending the linear part of the profile, one finds half the kink height.*

more than one record, was simultaneously occurring or had a delay, and especially when comparing events of different parameters and their interaction, for instance in the case of greenhouse gases and temperature.

The current used time scale for the Greenland ice cores is the GICC05 (overview of publications available at [Center of Ice and Climate, 2016]), synchronizing the different cores to the same chronology, using a variety of the techniques available, making it possible to get an comprehensive, dated overview of the paleoclimate.

Dating of the top part of an ice core is often done by seasonal layer counting of the δ^{18}O-profile, where summers will have high values and winters low, corresponding to higher and lower temperatures (see section 3.3.) After a certain depth, the layers become too thin to distinguish the individual layers in the isotope measurements (due to sampling resolution or diffusion), but the isotope profile can still be used for horizons, dated references.

The ice in an ice core is not pure ice, but contains particles, solubles, that creates ions. Electrical conductivity measurements of the ice, ECM, also has an annual signal due to the impurity content differing between summer and winter. When the ice layers get too thin for annual detection, ECM can be used to find volcanic eruptions, the dates of which sometimes can be known from historical records, which releases sulfur into the atmosphere that then precipitates onto the ice surface.

When there are no more physical measurements to be made that can help find horizons for dating, a mathematical model based on the velocity scheme is used to create a time scale for chronology.

2.2.1 Modelling time

If we integrate up the velocities for a depth interval starting at the top, H, we will get the age:

$$w(z) = \frac{\mathrm{d}z}{\mathrm{d}t} \quad \Rightarrow \quad \int_{t(h)}^{t(z)} dt = \int_{H}^{z} \frac{dz'}{w(z')} \quad \Rightarrow \quad t(z) - t(H) = \int_{H}^{z} \frac{dz'}{w(z')} \tag{2.7}$$

Obviously, the time at the surface, $t(H) = 0$. The expression for the vertical velocity, $w(z)$ is taken from previous section 2.1.1, and likewise, we therefore need to split the calculation into two parts, an upper and a lower. Since we are now integrating from the top down as opposed to before, this

time the upper part, $h \leq z \leq H$, is first:

$$\begin{aligned} t(z) &= \left(\frac{\lambda_H}{H_e}\right)^{-1} - \int_H^z \frac{dz'}{z' - \frac{h}{z}(1-f_B)} = \frac{H_e}{\lambda_H}\int_z^H \frac{dz'}{z' - \frac{h}{2}(1-f_B)} \\ &= \frac{H_e}{\lambda_H}\left[\ln\left(z' - \frac{h}{2}(1-f_B)\right) - \ln\left(z' - \frac{h}{2}(1-f_B)\right)\right]_z^H \\ &= \frac{H_e}{\lambda_H}\left[\ln\left(\frac{H - \frac{h}{2}(1-f_B)}{z - \frac{h}{2}(1-f_B)}\right)\right] = \frac{H_e}{\lambda_H}\left[\ln\left(\frac{H_e}{z - \frac{h}{2}(1-f_B)}\right)\right] \end{aligned} \tag{2.8}$$

For the lower part, $0 \leq z \leq h$, we get the time at the kink height, $t(h)$, from the expression just derived, similar to the derivation for the velocity:

$$\begin{aligned} t(z) &= t(h) + \int_h^z \frac{dz'}{w(z')} = t(h) - \left(\frac{\lambda_H}{H_e}\right)^{-1}\int_h^z \frac{dz'}{(1-f_B)\frac{z'^2}{2h} + f_B z'} \\ &= t(h) + \frac{H_e}{\lambda_H}\int_z^h \frac{dz'}{(1-f_B)\frac{z'^2}{2h} + f_B z} = t(h) + \frac{H_e}{\lambda_H}\left(-\frac{1}{f_B}\left[\ln\left(1 + \frac{f_B}{(1-f_B)\frac{z'}{2h}}\right)\right]_z^h\right) \\ &= t(h) + \frac{H_e}{\lambda_H f_B} - \left[\ln\left(1 + \frac{2f_B}{1-f_B}\right) - \ln\left(1 + \frac{f_B 2h}{z(1-f_B)}\right)\right] \\ &= t(h) + \frac{H_e}{\lambda_H f_B}\ln\left(\frac{1 + \frac{f_B 2h}{z(1-f_B)}}{1 + \frac{2f_B}{1-f_B}}\right) = \frac{H_e}{\lambda_H}\ln\left(\frac{H_e}{\frac{h}{2}(1+f_B)}\right) + \frac{H_e}{\lambda_H f_B}\ln\left(\frac{1 + \frac{f_B 2h}{z(1-f_B)}}{1 + \frac{2f_B}{1-f_B}}\right) \\ &= \frac{H_e}{\lambda_H}\left[\ln\left(\frac{H_e}{\frac{h}{2}(1+f_B)}\right) + \frac{1}{f_B}\ln\left(\frac{1 + \frac{f_B 2h}{z(1-f_B)}}{1 + \frac{2f_B}{1-f_B}}\right)\right] \end{aligned} \tag{2.9}$$

Note that this equation, for the lower part, is not valid if there is no bottom sliding. In that case, the age can be found from doing the same derivation but for the velocity profile without bottom sliding (i.e. $f_B = 0$):

$$t(z) = \frac{H_e}{\lambda_H}\left[\ln\left(\frac{2H_e}{h}\right) + 2\left(\frac{h}{z} - 1\right)\right] \tag{2.10}$$

2.3 Temperature in ice sheets

An ice sheet is a massive slab of ice, so naturally it must be below zero where there is ice present or else it would be melting away. While bottom melting can happen due to the pressure of the overlaying load and the heat from below, and sometimes melt layers happen on the surface and percolate down through the top layers in warm summers, the ice sheet near the ice divide is in general all below the *pressure melting point*, which is colder than zero degrees Celsius due to the weight above.

By measuring the temperature profile of a borehole (the hole left after drilling an ice core), it is possible to infer temperatures of the past, as done in Dahl-Jensen [1998]. Simplified, the snow falling on the surface "records" the ambient temperature which then gets transported downwards into the ice sheet.

From below comes the geothermal heat, which is both a heat from the radiation from the core and mantle itself and the product of radioactive decay of uranium and thorium in the granite in the bedrock below the ice sheet. From above comes "the cold" in the form of precipitating snow.

This creates a profile where, apart from the top metres dominated by the diurnal and seasonal cycle, the temperature is increasing downwards into the glacier.

2.3.1 Modelling borehole temperature

Viewed in the simplest way, the changes of temperature in time at a given place in the ice sheet will be from the conduction of the heat in the ice, and from the advection of ice with a different temperature at the given place. This takes the mathematical form of

$$\frac{\partial T}{\partial t} = \kappa \frac{\partial^2 T}{\partial z^2} - w(z)\frac{\partial T}{\partial z} - u(x)\frac{\partial T}{\partial x} \tag{2.11}$$

where the conduction is in the form of diffusivity with the diffusivity term, κ; $w(z)$ and $u(x)$ is the vertical and horizontal velocities as described in section 2.1.1; and the coordinate system chosen is so that z is positive upwards, i.e. the height above bedrock, and x is in the direction the of horizontal flow.

Advection in the horizontal direction, $u(x)(\partial T/\partial x)$, is often ignored: even though the horizontal velocity is not always small, the temperature differences will be. Additionally, when close to an ice divide, the velocity is also small, making the combined term even smaller.

If the temperatures do not change over a given time period, the term to the left of the equality will be zero, and the ice sheet is said to be in *steady state*.

The diffusivity of ice is given in terms of the thermal conductivity, K, density, ρ, and thermal specific capacity, c, as $\kappa = K/\rho c$. The density of ice is constant at ~917kg/m^3 (see section 2.4). The thermal conductivity and specific capacity depends on the temperature of the ice and the relations are found empirically:

$$K_{ice} = 9.828e^{-0.0057T} \qquad \text{and} \qquad c = 152.5 + 7.122T \tag{2.12}$$

where temperature, T, is given in Kelvin, and the units of the conductivity and capacity is (W/mK) and (J/kgK), respectively. From Cuffey and Paterson [2010]

However, an ice sheet also has a top layer of firn, which changes the temperature profile. In firn, the density is not constant, but depends on the given depth. Additionally, the thermal conductivity naturally depends on density, as the contact area of the individual ice grains changes with density. The thermal capacity's dependency on density is negligible, as the amount of air between ice grains does not change the heating scheme. This means that the thermal diffusivity vary with density as the thermal conductivity depends on density. This relation is not well constrained, but Weller and Schwerdtfeger [1970] found the following dependence on density:

$$K(T,\rho) = K_{ice}\left(\frac{\rho(z)}{\rho_{ice}}\right)^{1-0.5\rho(z)/\rho_{ice}} \qquad \text{and thus} \qquad \kappa(T,\rho) = \frac{K_{ice}}{\rho_{ice}c}\left(\frac{\rho(z)}{\rho_{ice}}\right)^{1-0.5\rho(z)/\rho_{ice}} \tag{2.13}$$

where the density profile $\rho(z)$ could be found as described in section 2.4.

Taking all this into account requires a new equation for the temperature for the non steady state ice sheet with a firn layer:

$$\begin{aligned}\frac{\partial T}{\partial t} = \kappa\frac{\partial^2 T}{\partial z^2} + \left[\left(\frac{\kappa}{\rho} + \frac{\partial \kappa}{\partial \rho}\right)\frac{\partial \rho}{\partial z} - w(z)\right]\frac{\partial T}{\partial z} - u(x)\frac{\partial T}{\partial x} \\ + \left[\frac{\partial \kappa}{\partial T} + \frac{\kappa}{c}\frac{\mathrm{d}c}{\mathrm{d}T}\right]\left(\frac{\partial T}{\partial z}\right)^2 + L\frac{\Lambda}{\rho^3}\frac{d\rho}{dz}\frac{g}{c}\end{aligned} \tag{2.14}$$

as given by Johnsen [1977]. The last term is a compaction term, taking into account the heating produced when the firn compacts into ice, where Λ is the annual rate of accumulation in weight

per area, L the overlying load at a given depth and g the acceleration of gravity. The term in front of the squared vertical advection, $(dT/dz)^2$, takes care of the thermal dependency of the parameters on temperature, while the extra term in front of the vertical advection non-squared, (dT/dz), contains the dependency on density.

2.4 Densification of snow to ice

Precipitation over an ice cap is in the form of sometimes rain but most often snow. Newly fallen snow, with densities as low as ~310 kg/m^3 and sometimes even less, will compact and densify until it eventually becomes ice with a density of 917 kg/m^3 [Cuffey and Paterson, 2010].

Snow being packed is called *firn*. It packs by consolidating the ice grains, bustling closer together, and "shaving" off the well-known six-pointed ends. At a certain depth, known as *pore close-off*, the permeability becomes zero, but the porosity remains non-zero. This is when any gas present will be trapped in the air pockets, and that depth also represents the *delta time* between the age of the ice and the age of the gas. The firn is now said to be ice, which will eventually reach the maximum density, by continued compaction.

2.4.1 Schytt model

There are different models for the densification of ice, some based more on the physical processes and other based more on direct observations. An empirical model by [Schytt, 1958] is a simple exponential increase from the surface density, ρ_0, to ice density, ρ_{ice}, (or the decrease from ice density to surface density), where the parameter k is the inverse folding depth, essentially saying how many meters it takes for a 1e increase:

$$\rho(d) = \rho_{ice} - (\rho_{ice} - \rho_0)\exp(-kd) \tag{2.15}$$

where d is the depth from the surface. By integrating the density model, it is possible to estimate how much of the ice column is air: this is simply the relative difference between the density from top to bottom to that of the ice, summed up:

$$\begin{aligned} l_{air} &= \int_0^H \frac{\rho_{ice} - \rho(d)}{\rho_{ice}}\, dz = \int_0^H \frac{(\rho_{ice} - \rho_0)\exp(-kd)}{\rho_{ice}}\, dz = \\ &= \frac{(\rho_{ice} - \rho_0)}{\rho_{ice}}\left(-\frac{1}{k}\right)\exp(-kd)\Big|_0^H = \frac{(\rho_{ice} - \rho_0)}{\rho_{ice}}\left(-\frac{1}{k}\right)[0-1] \\ &= \frac{1}{k}\frac{\rho_{ice} - \rho_0}{\rho_{ice}} \end{aligned} \tag{2.16}$$

where H is the height of the ice sheet. Since the height of the ice sheet is (usually) many times larger than the folding depth, the evaluation of the upper limit can be taken as to be zero, and we thereby get an expression for the length of the vertically integrated "air column".

The Schytt-model has the advantage that it is a straightforward model, easily implementable, while fitting the data reasonably well. An example of a more detailed and intricate model based on the physics governing densification is the Herron-Langway model [1980].

CHAPTER 3

Stable water isotopes

Isotopes are variations of an element where the number of neutrons in the nucleus differ. The number of protons are the same and determines the element, but the atomic number, and thereby mass of the atom, differs as the element can have less or more neutrons. Some isotopes are radioactive and will decay with a certain half-life, while others are stable.

Water is a molecule comprised of two hydrogen atoms and one oxygen atom, H_2O, forming covalent bonds, H–O–H. Both hydrogen and oxygen have isotopes: the most common form of hydrogen has no neutrons, ${}^{1}_{1}\mathrm{H}$, where superscript indicates the mass number (sum of neutrons and protons) and subscript the number of protons, which of course is also given by the element, H. Two other isotopes of hydrogen are the stable deuterium with one neutron, ${}^{2}_{1}\mathrm{H}$, and the unstable tritium with two neutrons, ${}^{3}_{1}\mathrm{H}$. Of the stable isotopes of oxygen, the most common is ${}^{16}_{8}\mathrm{O}$, followed by ${}^{18}_{8}\mathrm{O}$ and ${}^{17}_{8}\mathrm{O}$.

Since all isotopes of an element has the same number of protons, the definition of an element, the subscript is often omitted. For hydrogen, regular hydrogen, deuterium and tritium are also often denoted just H, D and T, respectively.

This, in theory, gives many different possible combinations for the molecule of water where either one or both regular hydrogen molecules could be replaced by a heavier isotope, and paired with either of the oxygen isotopes.

The four most common isotopologues are $\mathrm{H_2^{16}O}$, $\mathrm{HD^{16}O}$, $\mathrm{H_2^{18}O}$ and $\mathrm{H_2^{17}O}$, where the first is by far the most abundant. When speaking of a molecule that consists of one or more isotopes, the formally correct term is *isotopologue*, while *isotope* is reserved for a single atom: In practise, however, this distinction is not paid much attention and they are used interchangeably, especially when dealing with water.

3.1 Delta notation and definitions

When dealing with isotopes, they are often measured as concentrations rather than absolute amounts. Furthermore, they are reported as ratios of the rare isotopologue compared to the common isotopologue, for instance

$$R_{18} = \frac{[\mathrm{H_2^{18}O}]}{[\mathrm{H_2^{16}O}]}, \qquad R_{17} = \frac{[\mathrm{H_2^{17}O}]}{[\mathrm{H_2^{16}O}]} \qquad \text{and} \qquad R_{\mathrm{D}} = \frac{[\mathrm{HD^{16}O}]}{[\mathrm{H_2^{16}O}]} \tag{3.1}$$

where the square brackets denotes concentration, measured in mass/volume. If the known quantity is the concentrations of the isotope itself as opposed to the isotopolouges, the ratios are given as

$$R_{18} = \frac{[{}^{18}\mathrm{O}]}{[{}^{16}\mathrm{O}]}, \qquad R_{17} = \frac{[{}^{17}\mathrm{O}]}{[{}^{16}\mathrm{O}]} \qquad \text{and} \qquad R_{\mathrm{D}} \approx 2\frac{[\mathrm{D}]}{[\mathrm{H}]} \tag{3.2}$$

What we wish to know is the number of common water *molecules*, not atoms, that have been replaced with a rarer one. When you measure the amount of hydrogen atoms relative to deuterium atoms, you are also counting the non-replaced hydrogen atom, which is what the factor of two for the deuterium ratio corrects for. For oxygen, there is no such factor, as there is only one oxygen-atom to be replaced in each molecule.

In order to readily compare measurements of different samples, the value of a given isotope is often reported in *delta*-values. This is defined as the ratio of the difference to a reference value and that reference value, R_ref, or rather, the ratio of the sample to a reference value subtracted by one, since the value is often very close to 1:

$$\delta_i = \left(\frac{R_i - R_{ref}}{R_{ref}} \right) \cdot 1000‰ = \left(\frac{R_i}{R_{ref}} - 1 \right) \cdot 1000‰ \tag{3.3}$$

The factor of 1000 ‰ is introduced because isotopic values are very small numbers: multiplying them with a factor is purely for the benefit of humans, and is commonplace in geochemical isotopic research[i].

The full equations for δ^{18}O and δD then reads:

$$\delta^{18}\mathrm{O} = \left(\frac{\left(\frac{[^{18}\mathrm{O}]}{[^{16}\mathrm{O}]}\right)_{sam}}{\left(\frac{[^{18}\mathrm{O}]}{[^{16}\mathrm{O}]}\right)_{ref}} - 1 \right) \cdot 1000‰ \qquad \delta\mathrm{D} = \left(\frac{2\left(\frac{[\mathrm{D}]}{[\mathrm{H}]}\right)_{sam}}{2\left(\frac{[\mathrm{D}]}{[\mathrm{H}]}\right)_{ref}} - 1 \right) \cdot 1000‰ \tag{3.4}$$

Obviously, a value equal to zero has the same ratio of concentrations as the reference value. A positive value is *enriched* in the rare isotope, in this case the heavier ^{18}O or D, which means that it has a greater amount of that isotope compared to the reference value. Likewise, a negative value means the sample is *depleted* of the rare isotope, i.e. it has less of them. For water isotopes, enriched and depleted are synonymous to heavy and light, but this is only the case since the rare isotopes are heavier than the common.

Commonly used standards are VSMOW, Vienna standard mean ocean water, and SLAP, standard light Antarctic precipitation, both "produced"/maintained by the IAEA, the International Atomic Energy Agency. VSMOW is made up of collections of seawater around the world and can as such be seen as a mean of the isotopic values of waters on Earth. The formulation of δ-values based on commonly used standards makes comparison of isotopic values of different water samples possible.

Deuterium excess was defined by Dansgaard [1964] as $d = \delta\mathrm{D} - 8\ \delta^{18}\mathrm{O}$. The factor of eight comes from the size of the relative mass differences for ^{18}O and ^{16}O and D and H ((18-16)/16 vs. (2-1)/1). Excess is also often denoted d-XS or simply XS.

3.2 Fractionation

The differing number of neutrons gives isotopes different masses which results in different physical behaviour, an effect which is called *fractionation*. The fractionation factor, α, is defined in the general case as the ratios of the ratio of one sample compared to the other:

$$\alpha = \frac{R_1}{R_2} \tag{3.5}$$

[i] Although the denotations and factors used differ among different scientific communities, some examples of factors are ε-values, which is multiplied by a factor of 10^4, or μ-values, which are multiplied by 10^6, the factor of multiplication appropriately chosen for a given species.

For water isotopes, this mass-depended fractionation results in the heavy species ($HD^{16}O$, $H_2^{18}O$ and $H_2^{17}O$) being prone to stay in the liquid phase, while the lighter species ($H_2^{16}O$) will evaporate more easily, due to, simplified, the different vapour pressures and binding energies. Given in terms of the fractionation factor, $R_c = \alpha R_v$, where subscripts c and v stands for the condensate and the vapour, and α is greater than 1. In the presented δ-notation, the value of the condensate can be found from the vapour in terms of the fractionation factor:

$$\delta_c = \alpha(\delta_v + 1) - 1 \tag{3.6}$$

This means that that vapour evaporating from a pool will be depleted, as the heavy isotope remains behind, making the pool enriched; and vise versa, water condensation will be enriched as the heavy isotope leaves behind a depleted vapour.

The fractionation of water isotopes can be divided into three types, characterised by the relevant physical mechanisms [Mook, 2001]: *equilibrium* fractionation (some times also referred to as thermodynamic), *kinetic* fractionation, and *diffusive* fractionation (also referred to as transport fractionation), with the last two often lumped together under the umbrella of non-equilibrium fractionation, sometimes called kinetic fractionation.

Equilibrium fractionation is the best understood and most quantified of the types, and describes the case of when water vapour is in equilibrium with a body of water or for instance ice, which means the air is saturated with water vapour, i.e. the relative humidity is 100%. The fractionation factors have been determined empirically by Majoube [1971] and they depend on the temperature, phase of the condensate and of course the isotopic species. For a equilibrium between water vapour and liquid:

$$\begin{aligned} {}^{18}\alpha &= \exp(1137/T^2 - 0.4156/T - 0.00207) \\ {}^{2}\alpha &= \exp(24844/T^2 - 76.248/T + 0.052612) \end{aligned} \tag{3.7}$$

However, in nature, evaporation is usually not an equilibrium process, and a different fractionation factor is therefore needed. Often defined is the *effective* fractionation factor $\alpha_e = \alpha_k \alpha$[ii] as the product of the equilibrium fractionation factor, α, and the kinetic fractionation factor, α_k, for instance given by Merlivat and Jouzel [1979]:

$$\alpha_k = \frac{1 - kRH_{sst}}{1 - k} \tag{3.8}$$

where RH_{SST} is the relative humidity with respect to the sea surface temperature. The constant k differs for the isotopic species, and is a measure of how windy it is, i.e. the "roughness" of the sea surface.

If condensation from vapour happens in the form of rain, it could be approximated as an equilibrium condition with 100% relative humidity. But in the case of snow, this becomes a non-equilibrium process due to sublimation on the ice crystals. A kinetic fractionation factor for this is given by Jouzel and Merlivat [1984]:

$$\alpha_k = \frac{S}{1 + \alpha(S-1)D/D'} \tag{3.9}$$

which contains the regular equilibrium fractionation factor, α. $S = c - FT$ is the super-saturation ratio for ice at temperature T, and c and F are tunable parameters. D/D' are the diffusion constants for the light and heavy isotope in air, depended on the reduced mass of the different isotopic species.

[ii] Some literature denote the equilibrium fractionation factor with a subscript e, though, and the effective one without or differently.

3.3 Isotopes and climate

Evaporation and condensation under both equilibrium and non-equilibrium conditions are the relevant physical processes that control the fractionation and thereby the value of a water sample. As just outlined in the previous section, this mass-depended fractionation is temperature-dependent. This has given rise to the use of the isotope values of water as a proxy for temperature. By drilling ice cores, the isotope values back in time can be obtained, thereby providing a record of paleoclimatic conditions such as temperature. Such a relationship between isotopes and temperature was found empirically by e.g. Dansgaard [1964] which showed quantitatively that cold surface temperatures matched low isotopic values for samples taken from Greenland.

This overall general relationship also holds for glacial and interglacial times, which will have lighter and heavier values, respectively. However, while the mentioned samples represented a spatial slope, a temporal slope is also needed when dealing with paleoclimatic data, as the exact relationship is not constant in time, and furthermore, on these time scales, changes can also occur for the ice sheet height and accumulation rate, which complicates the translation of the isotopes to temperature.

However, the isotopes remain a temperature proxy, and the cold-warm relationship can even be seen as expressed by the seasons of the year. The isotopic signal is governed by the amount of cooling an air mass experiences from evaporation until condensation on its way to Greenland. Taking the approximation that all evaporation happens at roughly the same temperature at the thermal equator, that means that summer precipitation will have higher isotopic values and winters will have lower, and the same applies to inter-glacial and glacial periods, where the temperature is higher and lower outside the tropics.

In reality, source regions do differ. Craig [1961] found that natural waters have a deuterium excess value of 10 ‰, describing the *global meteoric water line*. Equilibrium fractionation results in a the deuterium excess value close to zero. Simplified, the parameter and its deviation from this line has therefore been used as a measure for the evaporation in the origin region of the moisture.

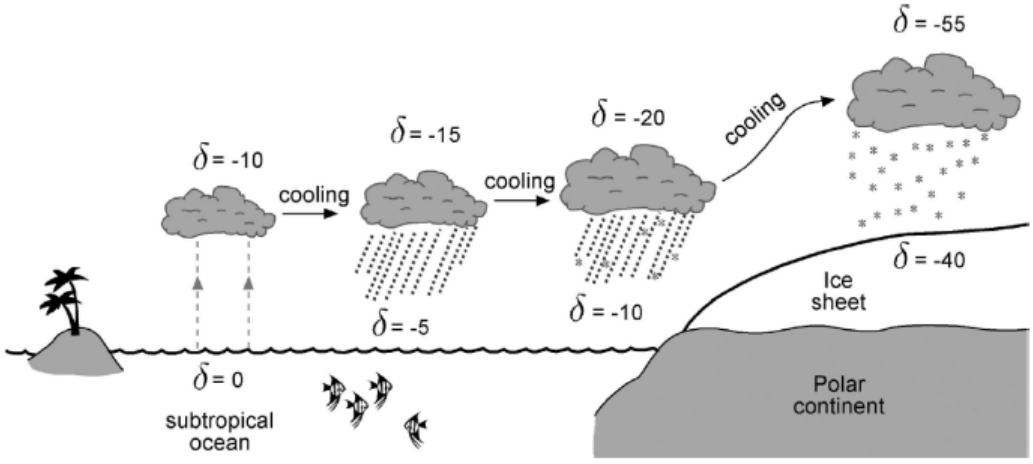

Figure 3.1: *Sketch of the idealized transport of moisture from the subtropics to the Arctics. Not included in this is the complicating factors of differing pathways, nor the possible additional uptake of moisture, nor the influence of sea ice. From Cuffey and Paterson [2010].*

In the context of moisture transport in the natural world, there are a range of different effects affecting the isotopic value of the cloud and its precipitate. Obvious is the general effect of temperature: the colder the air, the less moisture it can contain, and the cloud will therefore become depleted. When travelling northward, temperatures generally become cooler and the same happens. When staying at the same latitude, but increasing in altitude, the vapour will also become more depleted as the air temperature decreases. In addition, situations like travelling across continents or precipitation a heavy amount also decreases the value of the cloud.

The idealized journey of a water parcel from the subtropics to Greenland can be seen in figure 3.1. The isotopic value of the ocean is zero, meaning equal to VSMOW. The formed water vapour is more negative, and as it moves northward, it cools down, making it rain out the heavy isotopes, becoming even lighter. As the vapour mass moves up in elevation along the ice sheet, the air mass cools further and it snows, with quite depleted values of both precipitate and the remaining cloud. During winter, or a glacial period, the water parcel will experience a greater amount of cooling, making the isotopic value of the snow even lighter. This simplified picture does not take into account that the transport pathway does not stay the same for all times, and furthermore, there is the possibility of uptake of additional moisture along the path, which is also complicated by the the presence or lack of sea ice.

What remains is that isotopic values are a complex parameter, but can still be used as a proxy for temperature.

3.4 Rayleigh condensation

A simple model for the transport of moisture to the Arctic is the *Rayleigh condensation scheme* (e.g. Mook [2001] and many others), also knowns as Rayleigh distillation or fractionation. It describes the isotopic values of the process of a vapour mass that is cooling and raining out, under equilibrium conditions, but with the removal of the precipitate.

In terms of the saturation water vapour mixing ratio, w_s[iii], the ratio of the masses of wet and dry air, mass conservation reads:

$$w_s R_v = (w_s + dw_s)(R_v + dR_v) - dw_s R_c \tag{3.10}$$

where the isotopic ratio are defined as in previous section, and any d-term represents a small change. The amount of rare isotopes (the product of mixing ratio and isotopic ratio) in the vapour before any change (left side) must equal the amount of rare isotopes (right side) left in the vapour (the two parenthesis) and in the leaving condensate (the negative term), of which the isotopic value is given by equilibrium fractionation:

$$R_c = \alpha(R_v + dR_v) \tag{3.11}$$

Substituting the isotopic value of the condensate into 3.10:

$$\begin{aligned} w_s R_v &= (w_s + dw_s)(R_v + dR_v) - dw_s \alpha(R_v + dR_v) \\ w_s R_v &= w_s R_v + w_s dR_v + dw_s R_v + dw_s dR_v - \alpha dw_s R_v - \alpha dw_s dR_v \end{aligned} \tag{3.12}$$

The cross terms of small changes are negligible. Reducing:

$$\begin{aligned} 0 &= w_s dR_v + dw_s R_v - \alpha dw_s R_v \\ 0 &= w_s dR_v + dw_s R_v(1 - \alpha) \end{aligned} \tag{3.13}$$

Sorting isotopic ratio and mixing ratio and assuming that α is constant for small changes of temperature allows us to integrate.

$$\begin{aligned} \frac{dw_s}{w_s}(\alpha - 1) &= \frac{dR_v}{R_v} \\ \int_{w_{s0}}^{w_s} \frac{dw'_s}{w'_s}(\alpha - 1) &= \int_{R_{v0}}^{R_v} \frac{dR'_v}{R'_v} \end{aligned} \tag{3.14}$$

where subscript 0 refers to the initial conditions, and prime is used to mark the difference between integrations terms and the limits. What we wish to know is the isotopic ratio of the remaining

[iii] Lecture notes by Bo Vinther, unpublished.

vapour, and from that we can also get the condensate:

$$\ln\left(\frac{w_s}{w_{s0}}\right)(\alpha-1) = \ln\left(\left(\frac{w_s}{w_{s0}}\right)^{\alpha-1}\right) = \ln\left(\frac{R_v}{R_{v0}}\right)$$

$$R_v = \left(\frac{w_s}{w_{s0}}\right)^{\alpha-1} R_{v0} \tag{3.15}$$

$$R_c = \alpha\left(\frac{w_s}{w_{s0}}\right)^{\alpha-1} R_{v0}$$

Often we wish to know this in isotopic values, and these are found by dividing with the reference value:

$$\delta_v = \left(\frac{w_s}{w_{s0}}\right)^{\alpha-1}(\delta_{v0}+1) - 1$$

$$\delta_c = \alpha\left(\frac{w_s}{w_{s0}}\right)^{\alpha-1}(\delta_{v0}+1) - 1 \tag{3.16}$$

The saturation water vapour mixing ratios, w_s and w_{s0}, can be found by knowing the air temperature and pressure. We need to know the start isotopic composition, and often this is taken to be $\delta = 0$, i.e. VSMOW. The integration was made with the assumption that the fractionation factor does not change with temperature, and to satisfy this approximation, small steps in temperature is used and the fractionation factor is often calculated in the half space of these steps.

3.5 Isotope-enabled GCM's

Such simple models as the Rayleigh scheme presented in the previous section which only uses equilibrium fractionation, or variations hereof with additional details (e.g. Johnsen et al. [1989] with also non-equilibrium fractionation) are not sufficiently complex enough to model the natural processes of moisture transport. With the advent of increasing computer processing power, isotope-enabled general circulation models (GCM's) are being used. These are GCM's with an additional isotope module, simulating the fractionation processes through the hydrological cycle.

This is useful both for using the isotope values a final product of the model combined with other climatic parameters, but also as a tracer for the hydrological cycle, and indeed as a test for the model's performance. Idealized, having a full suite of a range of physical climate parameters from a GCM run in modern times, the relationship between them can be derived and quantified, increasing the understanding of similar proxy parameters from paleoclimatic records by illuminating the physical processes, which makes it possible to make findings of the climate of the past, and thereby also possibly the future.

The isotopes are also a good tracer of the hydrological cycle, as a parameter describing water parcels physically moving, going through changes, mainly condensation and evaporation, brought on by the changing atmospheric conditions as it moves through the cycle. And indeed, if a model is able to adequately simulate some parameters but fail with the isotopes, this would be a clue to problems with the underlying physical processes build in the model, either with the isotopic processes or with the more general meteorological background or even both.

In that vain, the isotope module of a GCM is of course only as good as the model itself, and if there are any errors in the representation of the circulation scheme, then even with a correct isotopic treatment, the final output would not be correct. Additionally, GCM's are run on a grid, so parameterisation is needed for the processes taking place at smaller scales. The temporal resolution also matters: if a model produces the right annual behaviour but simulate the seasonal variability wrong in e.g. timing and/or magnitude, this would indicate problems with model per-

formance.

There are of course a wide range climate parameter products from GCM's that would be interesting to investigate. *Temperature, precipitation and isotopic composition* constitute a small, yet still fruitful selection. As described, the latter is to a first order controlled by the first and of course influenced by the second: to have isotopic measurements to compare with model output, precipitation events are necessary if the data record is in the form of an ice core.

Chapter 4

Firn core experiment

This chapter will present the stable water isotope data from two firn cores, A6 and A9, drilled in the RECAP campaign including background, the experimental work, how isotopes are measured, the processing of data and various results.

The A6 and A9 cores were among ten firn cores drilled alongside the main ice core in the RECAP campaign carried out in the summer of 2015. The firn cores where drilled in various locations around Renland, and the purpose of drilling multiple short cores is to investigate the spatial variability of accumulation and δ^{18}O.

A9 was drilled at the location of the old 1988 core, while A6 was drilled ~100 meters north of the new site, at approximately 71.30708N, 26.76548W and 71.30363N, 26.7132W, respectively. According to the radar prospecting made during the RECAP campaign, A6 lies ~12 meter higher than A9.

The A6 and A9 core was drilled on June 6th and 14th, respectively. A9 was drilled from the bottom of a snow pit 1.1 meters in depth, which was sampled with 42 bottles, while A6 was drilled from the snow surface. Both cores where made with a 3 inch hand auger, as opposed to the main core which is 4 inches in diameter and uses the Hans Tausen drill(ing technique) developed by CIC (Centre for Ice and Climate).

4.1 Cutting and melting

Both A6 and A9 consists of 20 bags of 55 cm core each, apart from two cores in A9 logged as 52 and 58 cm. This means that both cores are 11 meters long, but A9 goes deeper, since it was drilled at the bottom of a pit, making it terminate at 12.1 meters depth. The pit was sampled with 42 bottles for the 1.1 meter on top of A9. Thus, A6 is comprised of bag #1–20 and A9 of bag #3–22 plus pit samples.

The two firn cores where cut in the fall of 2015 at CIC's second freezer work space at the Hans Christian Ørsted Institute. Before cutting, the cores were weighed in-bag, measured for length, and then cut into the standard 11[i] equal length samples per 55 cm bag, giving a sample size of 5 cm, which were put in individual isotope bags.

During transportation and handling, some cores became smaller than when originally drilled, due to compaction and/or breaking. Melt layers were observed at several places throughout the cores. Due to the coring starting from the very surface, the cores basically resembled snow compacted into rough cylindrical snow balls, and only further down, started to look more like ice. Handling, measuring and cutting cores all made a lot of surface snow crystals fall off the cores, due to which they were weighed in bag.

[i] Some of the A6 cores were cut in 9 or 10 samples due to experimental reasons.

Since the discrete isotope samples are firn, not ice, they also have a much higher surface area. Therefore, to avoid (excessive) melting in the sample bags, the samples where transferred to the air-tight tobacco tins used for melting while *in* the freezer and *then* brought out for melting at around 20 degrees. The samples where transferred to Kautex bottles for frozen storage to avoid any fractionation/diffusion. In total, there was 215 discrete isotope samples for A6 and 262 for A9 of which 42 are pit samples.

Prepping and measuring had a total of 16 runs, including re-runs and re-preps. For all measurements, a sample size of ~1.2 mL was used. This volume was moved from the Kautex bottles to the sample vials using a Finn-pipette, changing pipette tips between each different sample in order not to mix water samples.

4.2 Measuring isotopes

Initially, the samples were measured in batches of 53 samples in each run, later transferring to a scheme of 39 samples per run with the remaining 14 vials filled with millique-water in order to prevent potential bad injections or damage to the syringes themselves from being too dirty.

Measurements of samples started with the A6 core and ran on the Picarro, version L2120-i. Hereafter, towards the end of A6 samples, measurements were moved to another Picarro, version L2130-i. Since this machine performed better for these samples, it was decided to re-prep and re-run the first two thirds of A6 again on L2130-i. Thus, there are data for all samples from the same Picarro, L2130-i, and duplicates of some of A6 from L2120-i.

4.2.1 Laser spectroscopy

Previously, water stable isotope were measured using mass spectrometers, which utilizes the fact that electrically charged ions of different masses follow different paths when subjected to a magnetic field. In practise, a mass spectrometer measures on gas, so the special isotope was "switched" from the water to the gas, for instance CO_2 for the oxygen atoms. Now, it is more common to use laser spectrometers, and for this experiment, the type used was a near-infrared *cavity ring down spectrometer*, CRDS.

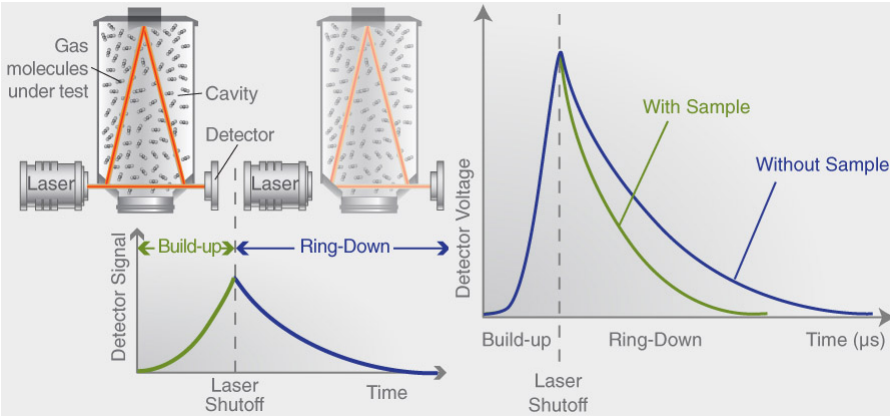

Figure 4.1: *Schematic of a NIR-CDRS Picarro. The vapour is in then cavity where a laser is turned on. The reflective mirrors give it an effective pathway long enough to be sufficiently absorbed enough for measuring. The laser is then turned off, and the difference in the so-called ring-down time with and without sample give a measure for the concentration. Picture from Picarro.*

They details of how they work are a whole subject in itself and are described in great detail in de Groot [2004]. A simplified explanation follows here: The laser spectrometer utilizes the spectral

absorption lines of gasses, in this case water vapour, which, with enough precision, can also be distinguished for individual isotopologues.

The water sample is vaporized which happens instantly and accurately in order to ensure full transfer of the content. The vapour is this moved into the cavity which contains ultra-reflective mirrors. A laser is turned on, and due to the mirrors, the effective pathway of the laser is many kilometres, enabling the absorption to be high enough to measure the small amount of trace gases. After a time the laser is turned off, and the intensity in the cavity decreases, due to the absorption and the leakage of the not-perfect mirrors. The difference in ring-down time with and without sample is then used to determine the concentration in the vapour of the sample.

4.2.2 Calibration and validation

When measuring on a Picarro, each machine has its own "instrument values", so in order to get the actual values of the samples, a calibration is needed, for both δ^{18}O and δD. This was done by using two standards whose values covers the range of the samples, and a third standard used to check the goodness of the calibration. For RECAP A9 and A6, the set of three standards used were -22, -40 and NEEM. These three are CIC in-house standards calibrated against both VSMOW and SLAP. The values shown in table 4.1 and used throughout this thesis are with reference to VSMOW.

Table 4.1: *CIC standards calibrated to VSMOW*

standard	δ^{18}O [‰]	δD [‰]
−22	-21.88 ± 0.06	-168.45 ± 0.09
NEEM	-33.50 ± 0.03	-257.45 ± 0.20
-40	-39.98 ± 0.08	-311.11 ± 0.35

By "plotting" the true and measured values of the two standards against each other, the calibration line is found by linear regression. With this, the calibrated values of the third standard is then found by the following equation:

$$\delta_{cali} = \alpha \cdot \delta_{meas} + \beta \tag{4.1}$$

where α is of course the slope and β the intercept. The true value of the third standard is then compared to the calibrated value, giving an offset for both isotopes. If this offset is too big, the run needs to be repeated. This threshold is an experimentally found guideline, based on the sample under examination and the uncertainty of the machine.

The third standard is also used to detect possible instrument drift in the values by being measured multiple times throughout the run. Generally, a small drift is to be expected, and here the same threshold as for the calibration-offset applies.

When injecting samples into the cavity, the needle might not empty completely, which could result in a memory effect. This contamination from previous measurement can also be the case for the cavity and the vaporizer. To counteract this, standards and samples are measured multiple times. This is especially pertinent for the standards, as their values vary greater than those of the samples. Therefore, the standards are measured 20 times, but only the latter half is used for calculating average values; for the first sample, eight injections are made but only the latter half used, and for the rest of the samples four injections are made with the first not used; and interspersed are the measurements of the third standard used for drift correction. The injection scheme is summarised in table 4.2.

Even if the measurements of the standards are determined to be good, based on checking offset and drift, the measurements of each sample need also to be good. The value of a sample is taken

Table 4.2: *Measurement procedure used for the firn samples.*

type	name	N of injections
standard	-22	20
standard	NEEM	20
standard	-40	20
standard	NEEM	8
sample	# 1	8
sample	# 2-53	4
standard	NEEM	16

as the mean of the three injections used. This value is validated by computing the standard deviation of the three used injections: if it is below the same thresholds as for the offset, the value is trustworthy. If not, its value can be found by interpolating from its neighbours, if the sampling resolution is believed to be high enough that the trend of the values of the samples does not change significantly. If there are too many bad samples with high uncertainty, and especially if these are sequential making the interpolation-method less reliable, a re-run is needed.

Additionally, injections are occasionally not executed well; especially dust and other micro-scale impurities can affect the water concentration of the injection, simply by blocking the transfer of the water. Measurements made at a much lower or higher water concentration (~1k ppmv) compared to the rest of the batch are not comparable, and will also influence the value of the sample itself. If injections of too different water concentration occur, they will be excluded from the calculations, and in turn this yields a new mean but also a new standard deviation that is based on fewer data points.

A graphic representation that summarises the validation process can be seen in figure 4.2.

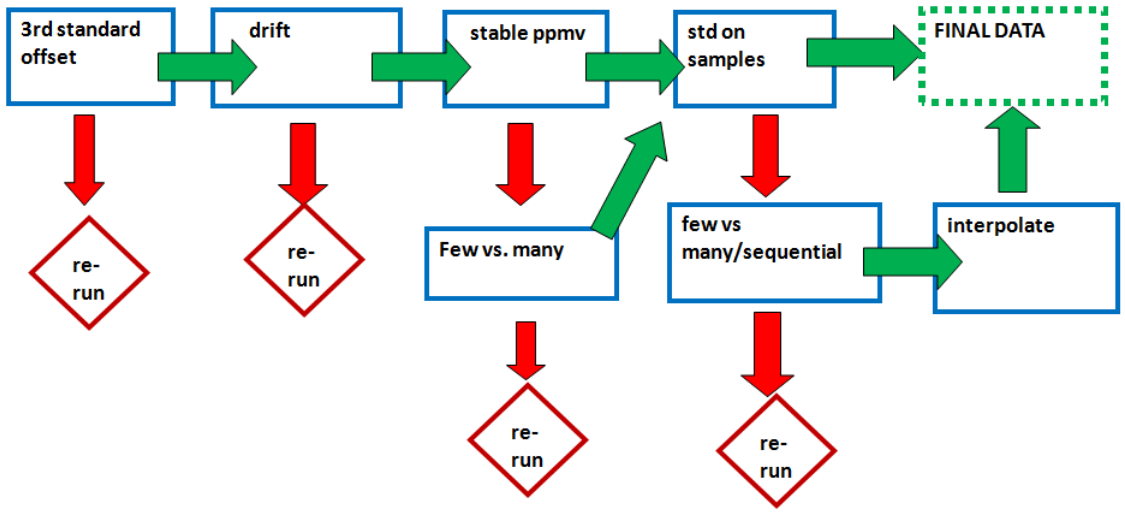

Figure 4.2: *Flowchart showing the measurement data validation process. First step is checking the offset between the true and calibrated value of the third standard; second step is checking whether any drift is too high and a correction or re-run is needed; third step has to do with the water concentration level, and whether it is only a few samples that are bad, in which case these are discarded, or if it is a general trend, then re-run; final step of the validation is checking the standard deviation of the samples and whether there are too many or if they are sequential, and if so, the possibly remedy step of interpolation; before having the final data.*

4.3 Results

Some injections of RECAP A6 were so bad in terms of too low water concentration, probably due to dirty water, that they had to be discarded: For some, one of the three data points where discarded,

but for two samples, two of the three data points were bad. Excluding these of course results in a value with no standard deviation, and as such, no way of validating the single measurement. The usual strategy is then to interpolate from the neighbouring values, however, this was not done for this experiment but the two samples do not affect the overall interpretation and results. For neither A6 and A9, no complete sample triplets had too high a standard deviation that required interpolation to the neighbours, when using the best run of those that have duplicates.

The end processed data, on a firn depth scale, after validation is presented in figures 4.3 and 4.4 for A9 and A6, respectively.

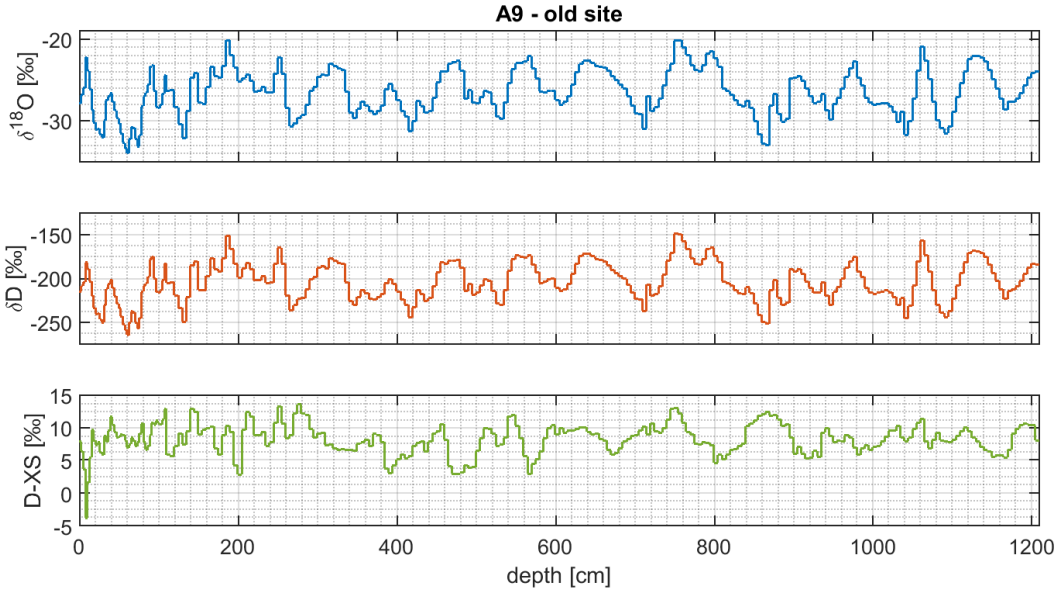

Figure 4.3: *RECAP A9 isotopic values on firn depth scale. Marked are interpolated values, if any. The span of the depth axis is the same for A9 and A6, so they can more readily be compared.* δ^{18}O *is in blue,* δD *in red, and* δXS *in green.*

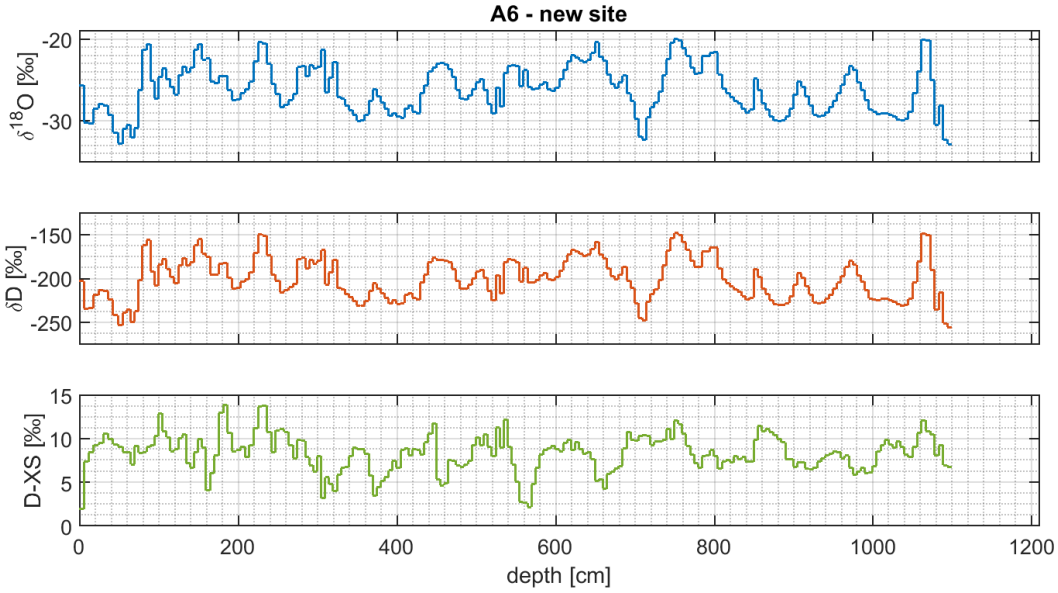

Figure 4.4: *RECAP A6 isotopic values on firn depth scale. Marked are interpolated values, if any. The span of the depth axis is the same for A9 and A6, so they can more readily be compared.* δ^{18}O *is in blue,* δD *in red, and* δXS *in green.*

Even though a depth in one core does not necessarily translate to the same depth in the other core (since you cannot be sure both cores have same precipitation amount), it is still readily apparent how similar the two cores are, both in overall values and in the variation and timing hereof.

As mentioned earlier, the A9 core reaches deeper than A6; indeed, it also goes back further in time by an extra year, based on the behaviour of the isotope values, where, at this resolution, the summer and winter of a year is easily seen.

What is also shown is that, in terms of time, the A9 core starts later than A6: the very near-surface values of A9 seems to not match up with those of A6, but rather instead, the top values of A6 fit values of A9 that are offset deeper by about ~15 cm.

There are some certain samples that looks like outliers. For some of them, they are present in both cores, making them trustworthy. For other values, while care *was* taken to be precise and meticulous during the experimental process, it is possible that mistakes could have been made, affecting single samples and/or the sequence of the samples.

Overall, the lows and highs of the cores are easily discerned in δ^{18}O and δD, and some cyclic behaviour is also observed, although this becomes clearer when taking the δXS into account. The very top samples from the first two-three metres or so seem more "noisy" than the rest, for all the isotopic parameters. This is due to diffusion and densification having not yet affected these samples, which would smooth out the isotopic values.

4.3.1 Density

For a full comparison of the cores, and eventual transfer to a time scale, the cores will need to be on the same depth scale, for which we need the density of the samples. From the weights of the 20 bags per core, the density for core A9 and A6 was calculated.The length of the core for calculating the bag volume is of course the drilled, logged length, since this reflects the density the firn ice had in the field. Since the cores were measured in bag, the weight of the plastic bag, 25 g, needs to be subtracted to get the weight of the cores.

$$\rho_{firn} = \frac{m_{bag+core} - 25\text{g}}{V_{core}} = \frac{m_{core}}{l_{core}\pi r_{core}^2} \tag{4.2}$$

The density profile can be seen in figure 4.5. It is not possible to use the pit samples to measure density; when taking these samples, the snow is already being compacted, and, the volume, thus mass, taken in one "glass" is also very low compared to the weight of the glass itself.

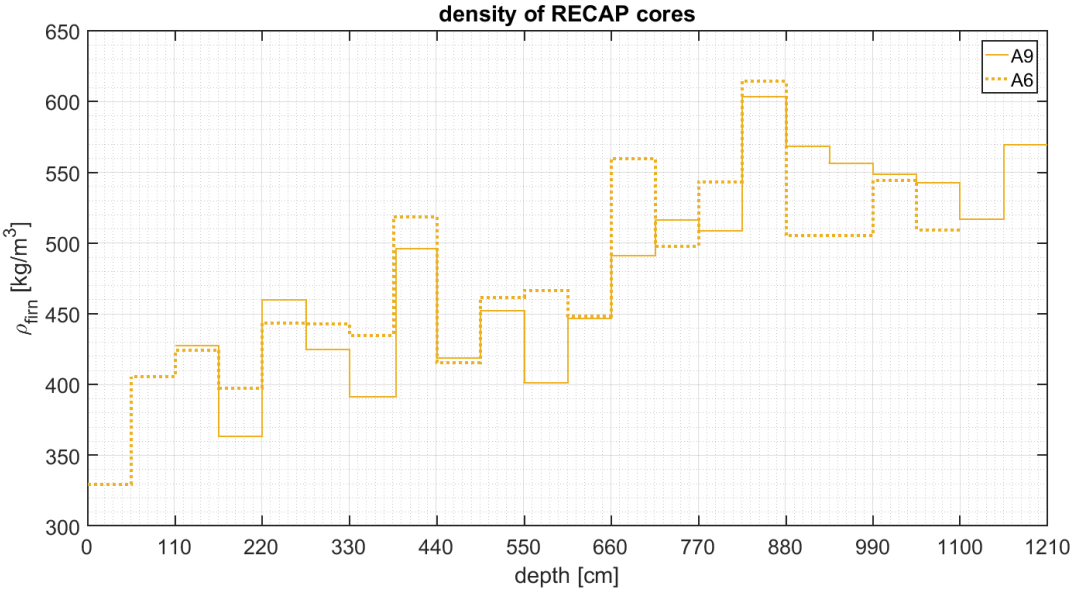

Figure 4.5: *Density profile of A9 and A6. A9, solid line, starts at bag #3 at 110 cm at the bottom of the pit and A6, dashed line, at bag #1 at 0 cm, the surface.*

The density starts out at low ~400 kg/m^3 near the surface, and of course becomes denser with depth. However, at these depths it does not reach ~917 kg/m^3, the requirement for ice. In general, the years are similar. Inconsistencies can be due to possible melt layers: these will impact the density towards higher values, and might not necessarily occur in both cores at the same time, due to percolation. The density variations for the same depth should not be an artefact of the experimental processing, as the cores were measured in-bag, so any breaks and/or grinds or similar that would remove material from the core itself would still be in the bag.

The density of the cores can be used to put the isotope values on a water equivalent depth scale, instead of the original measured, physical (firn) depth scale. Likewise, this could be an ice depth scale. Both of these are readily used, and having the same "material" depth scale will make it possible to compare these results to other data.

This is simply done by factoring the physical depth with the ratio of the measured density (that of the firn) to a reference density (1000 kg/m^3 for water, 917 kg/m^3 for ice):

$$l_{ref} = l_{firn} \frac{\rho_{firn}}{\rho_{ref}} \tag{4.3}$$

Regarding the pit samples of A9, the density used is that of A6 for which depth interval a given pit sample lies.

4.3.2 Time scale

Using either material depth scale for the core A9 and A6, since they are so similar even with original firn depths, we can now put these on a time scale. This is done by looking at the cycles of lows and highs of δ^{18}O and saying these correspond to winter and summer seasons, respectively. Since these yearly cycles are not absolutely clear, we also look at the behaviour of δXS, which, in general, should have high values in the fall. Dating A9 and A6 by cross-referencing between them yields a higher certainty of the timing of the individual years. The chosen time scale can be seen in figures 4.6 and 4.7 for A9 and A6.

When dating the cores, it is convention to choose the minimum value as the beginning of that year, e.g. first of January. Since the sample of course spreads over a time interval given by the length of the sample, the bottom of the sample represents the earliest time. The samples in between two horizons are given a date by simple linear interpolation, meaning that each will correspond to a n'th of a year, where n is the number of samples per year. This means that the dating is only fixed in one place, the winter and start of the year; for increased precision, two fix points of for instance both winter and summer could be used, as could another assumption than evenly spread precipitation over the course of a year.

Naturally, since the cores were drilled in the summer of 2015, they start at high values. This also gives us the first dating "horizon", year 2015, at the first minimum. Dating for the years 2014 and 2013 is more difficult and it almost looks like they have double seasons. Placing the remaining horizons, but with out labelling years, are easiest done by moving forward in time, meaning backwards from the bottom of the core. A6 is a bit uncertain in this regards, since it ends on what is a low value which means we cannot be sure whether this *is* the start of the year or from later: comparing with A9f gives some certainty to this being a horizon.

Year 2008 in core A6 is interesting: it reaches lower values during the year than at the start of itself or the following year; however, when comparing with A9, the start of both 2008 and 2009 seem somewhat more clear, although the year itself is still "odd".

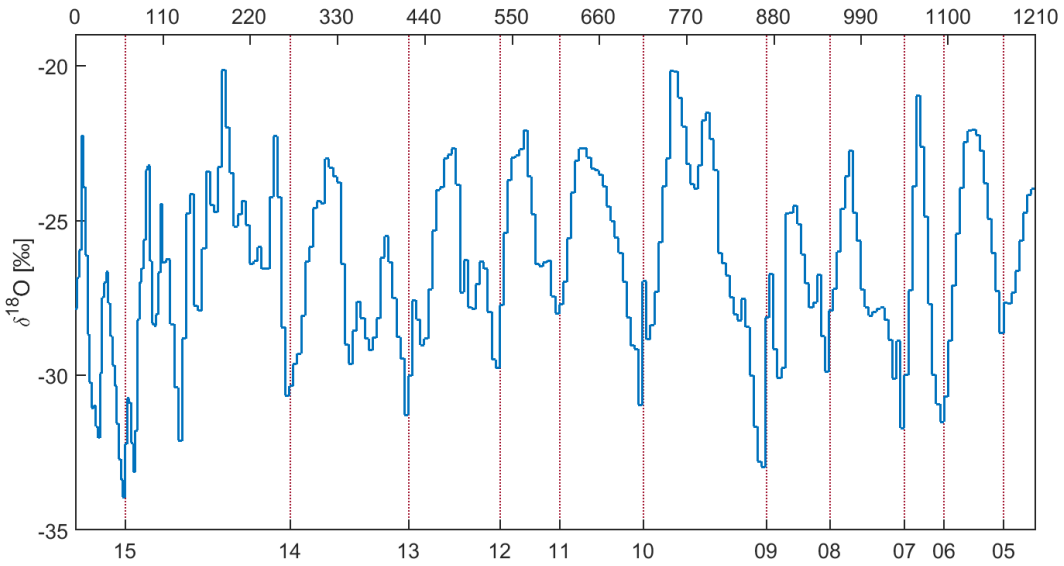

Figure 4.6: *Chosen placement of yearly horizons for A9. Top axis is physical depth in centimetres and bottom axis is the start of the years 2015-2005.*

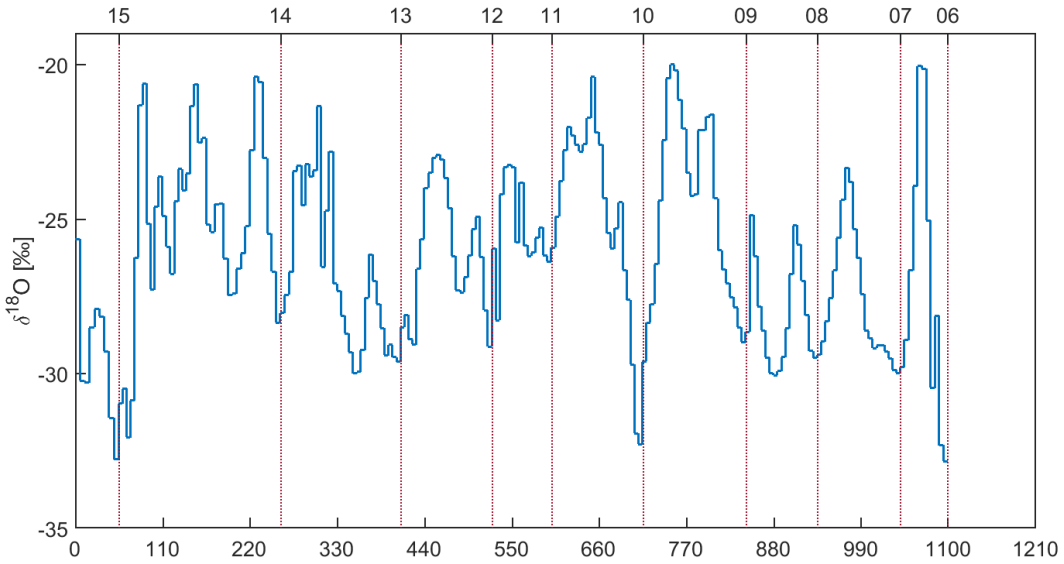

Figure 4.7: *Chosen placement of yearly horizons for A6. Top axis is the start of the years 2015-2006 and bottom axis is physical depth in centimetres.*

Yearly precipitation

Having the isotope values on a water (or ice) depth scale *and* a time scale enables us to compute the precipitation throughout the years for A9 and A6. The mean yearly precipitation is 545 mm for A9 and 559 mm for A6 in ice equivalent, and figure 4.8 shows the precipitation in ice equivalent for the different years. The summed precipitation can be seen in figure 4.9.

Comparison of A6 and A9

Now that they are on a time scale, it is possible to compare A9 and A6 and see if there are any differences. This is shown in figure 4.10. For completeness, the extra year of 2005 is included for A9. In general we can see that the timing of the years are similar, although the most recent year 2014 is somewhat messy, both due to less diffusion of the isotopes, but also due to it being

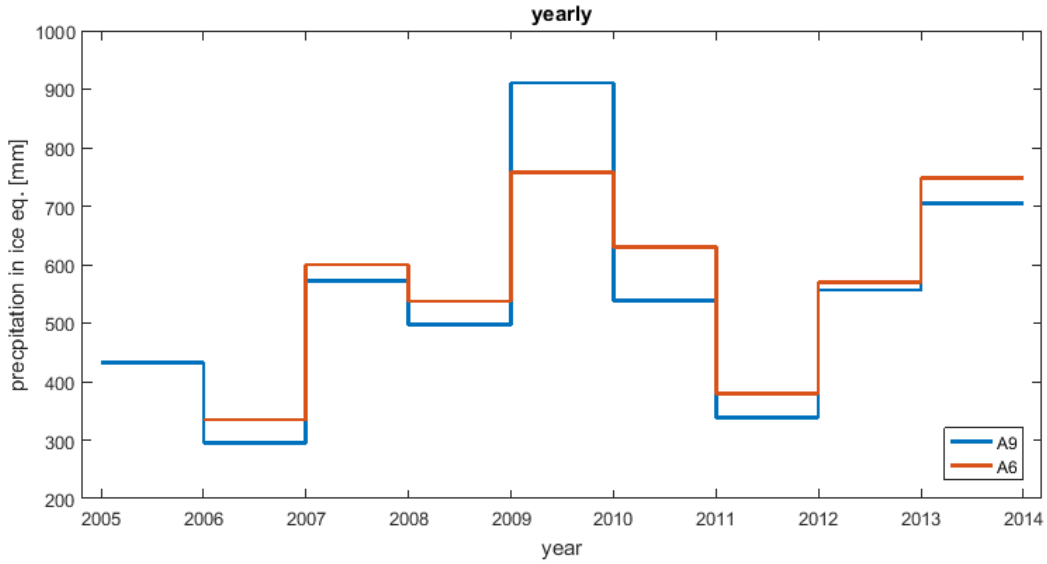

Figure 4.8: *The yearly precipitation for A9 (blue) and A6 (red) in ice equivalent.*

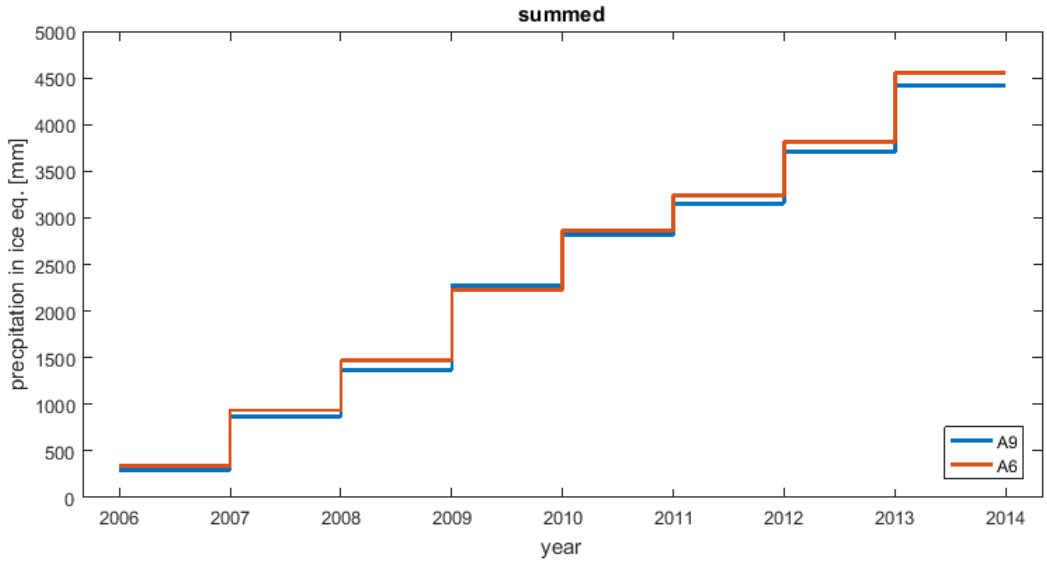

Figure 4.9: *Summed precipitation for A9 (blue) and A6 (red) for the years 2006-2013 in ice equivalent.*

the part with the lowest density and thus the biggest length being visually "compressed". Year 2008 has discrepancies between the two cores in the timing of the isotope highs and lows within the year, although they match up at both ends. It is possible that precipitation truly did happen at different times of the year, but if we believe that high tops means summer, it would be odd if summer happened at that different times months apart. Both the timing and the values agree between the two cores very well in general, although for instance the two transitions of 06-07 and 08-09 have a lower value for A9 than A6.

In order to compare the means of isotopic values of one year to another or of any time duration, a precipitated weighted mean is needed. This is simply the isotope value for a given precipitation "event" (in this case, our samples) weighted against the full precipitation:

$$\mu_{prec.weigh.} = \frac{\sum_{i=n}^{N} I_i \cdot P_i}{\sum_{i=n}^{N} P_i} \tag{4.4}$$

where I is the isotopic value of the sample, P is the precipitation, or rather length of the sam-

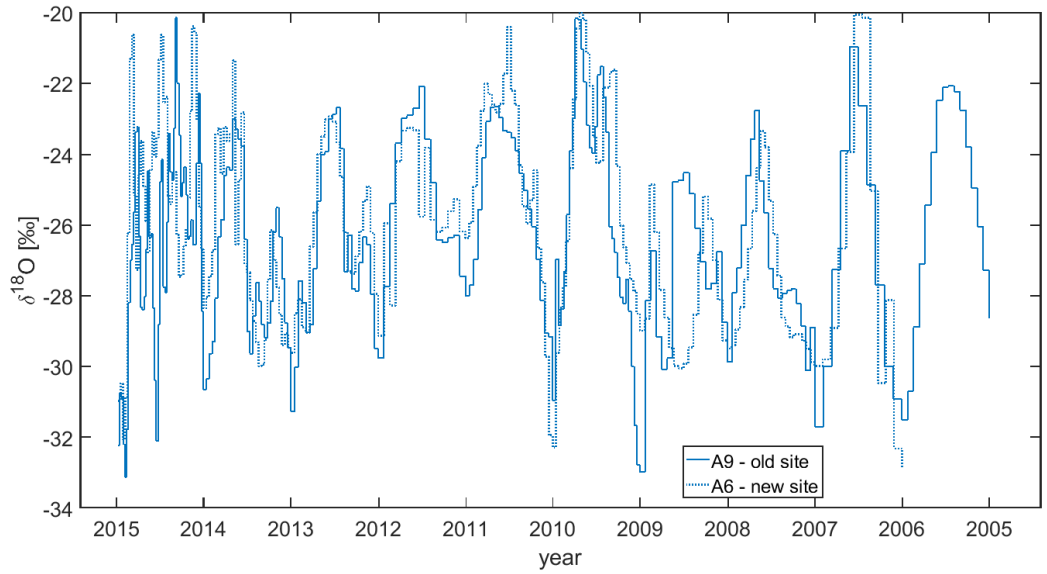

Figure 4.10: *Comparison of A9 and A6 on time scale. A9 is solid line, A6 is dashed line.*

ple, and the interval $n - N$ determines what duration or range the mean is for. Conceptually, it is analogous to having a big (ideal closed system) bucket standing outside, collecting precipitation, in any form, for the specified period of time that you wish to find the mean value of: if all the precipitation is contained herein, a well-mixed sample will have the isotopic value of interest.

For A9, in the comparable interval of the years 2006-2014, the mean isotopic value of δ^{18}O is -26.49 ‰, and for A6 it is -26.08 ‰. However, when comparing the years to each other, the difference between A9 and A6 is not statistically significant: the mean difference between A9 and A6 for δ^{18}O is -0.28 ‰ (meaning A9 is lower in value), but the standard deviation is 0.73 ‰, and the error on the mean is 0.24 ‰. This can also be seen graphically in figure 4.11, where the precipitated weighted means of δ^{18}O within each year are shown.

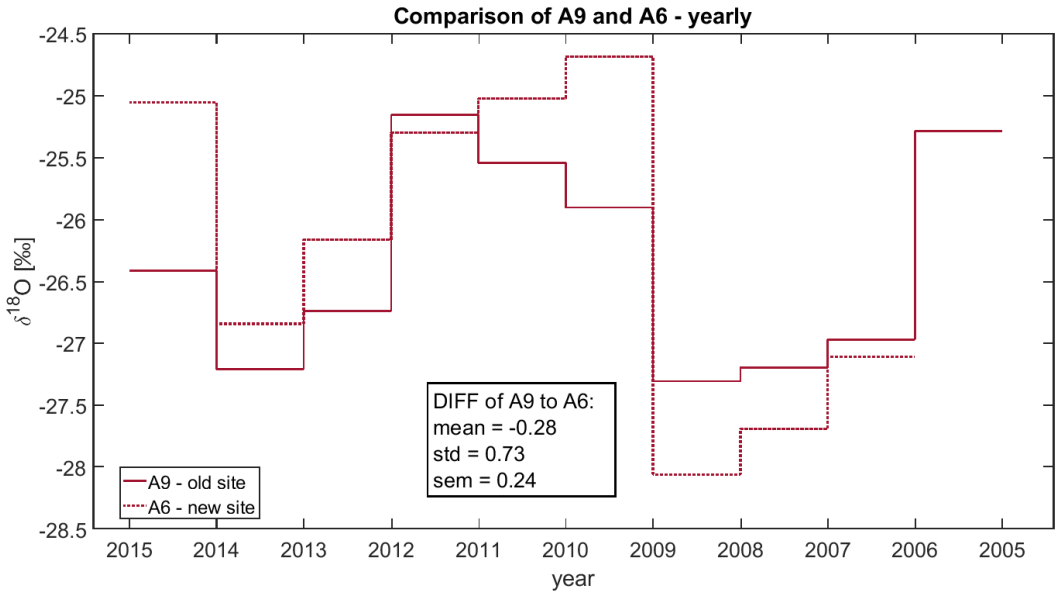

Figure 4.11: *Precipitated weighted yearly δ^{18}O-values. A9 is solid line, A6 is dashed line. For completeness, the year of 2005 for A9 is also plotted, but was of course not used for the statistical analysis.*

Comparison of A9 and Renland 1988

Since A9 and the old Renland 1988 core was drilled at the same location, it is interesting to compare these two. Figure 4.12 shows the 5 year means of δ^{18}O going back to year zero (2000 years b2k, before 2000). There is a gap in data, obviously, between the years 1985 and 2005; also, since the firn core only comprises ten years, there is obviously only two data points. It can however still be seen that the isotopic values of the last 10 years are on the warmer side of Renland values, and also, while there are some single warm data points back in time, two sequential values as high as for the last ten years are not seen unless going back ~550 years.

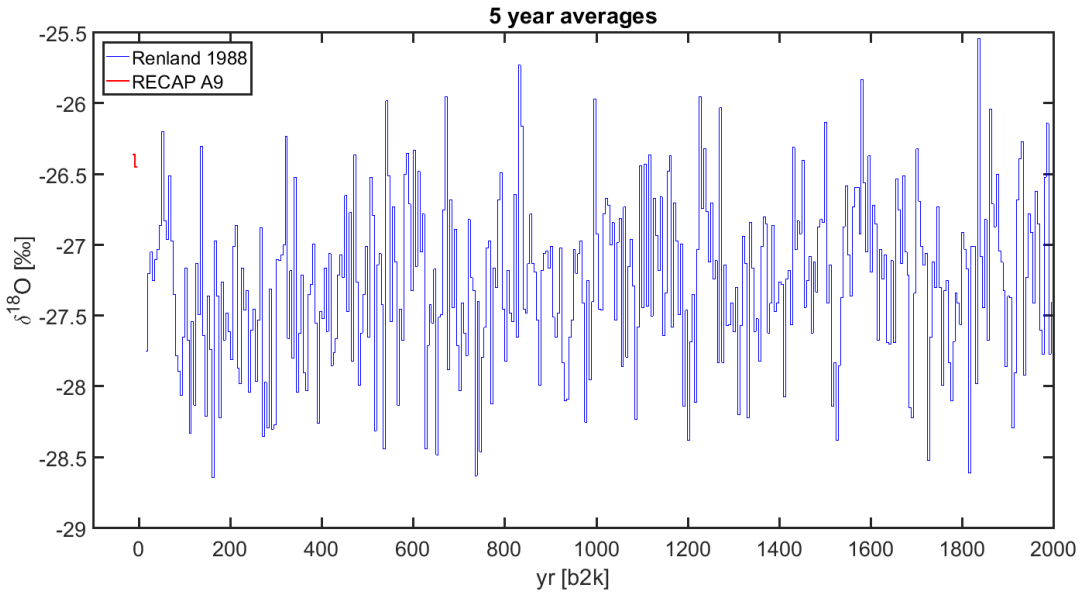

Figure 4.12: *5 year averaged δ^{18}O-values for Renland 1988 main core (blue) and RECAP A9 firn core (red).*

CHAPTER 5

DMI observations and GCM data

Meteorological data from DMI stations in Greenland and from two isotope-coupled GCM's are used in this thesis. This chapter presents the data sources and makes a simple, quick validation of the models. Then we compare the isotopic values and the precipitation from the models to ice cores data (chapter 6) and the temperature data to borehole measurements (chapter 7) from Renland.

The GCM-data are used mainly to perform a check of whether we can use the models' data to enlighten our investigation/understanding of the climate of Renland.

5.1 DMI

DMI (the Danish Meteorological Institute) handles the weather reporting and research for also the Fareo Island and Greenland. They publish their technical reports [DMI, 2016] containing the measurements from several weather stations for a wide range of meteorological parameters. Report 16-10 (16 being the year of publication, 10 the number given to the report) gives an overview of all the data available, free and per request, for the three countries and for different time intervals. Report 16-08 contains the explanation of the parameters and overview of the daily and hourly measurements and in the recent years for several weather stations for Greenland with accompanying data files. Report 16-04 gives the historical account with measurement series for certain selected stations of Greenland for certain parameters in a variety of daily, monthly and yearly resolution.

This thesis have used the monthly data files from report 16-04 for the station 4339 Ittoqqortoormiit (Danish name Scoresbysund, hereafter denoted Itt.) and 4360 Tasiilaq. Both stations are on the east coast, and the placement of Itt. can be seen in figure 5.2. Report 16-04 also details the meta data for the stations, for instance the moving of the weather stations and missing data or fill-in of data from other station measurements.

For Itt., we use the precipitation and the temperature measurements for intervals within 1960-2013 for comparison with GCM data. The temperature record has a few missing months in this interval, and especially for the precipitation, there are also problems[i].

For Tasiilaq, we have used the temperature data from 1895 to 2015. August in 1924 and July in 1937 are missing, as is September 1910 to August 1911, but otherwise the record is complete. This makes it the temperature record from the east coast of Greenland reaching the longest way back without significant holes, and it will be used for borehole temperature modelling.

[i] It is mentioned in report 15-10 that the automatic rain gauge of the V98 weather station for this location has permanent problems. Also, some months will have missing days, and some years have monthly gaps, in the record, and in contrast to temperature, precipitation is not a trend in the time span of a month, and as such, missing just one or precipitation events can have big impact on the cumulated sum. Additionally, the measuring of temporally highly resolved precipitation, especially as snow, is tricky and more ambiguous than temperature.

5.2 GCM data

The two GCM's used in this thesis are from the models ECHAM and ISOCAM. The parameters in question are two-meter temperature (in order to compare with the DMI data), precipitation, and the isotopic values of that precipitation. The ECHAM data was provided by Martin Werner and the ISOCAM data by Anne-Katrine Faber.

For both ECHAM and ISOCAM, the data was given in monthly resolution and from there the annual values was calculated. The grid points were chosen as the nearest match with the real-world locations of Renland and Itt., with coordinates listed in table 5.2. For ECHAM, we have data from 1960-2013 and for ISOCAM a shorter period of 2004-2014. The resolutions of the two models are similar at approximately 1°; ECHAM is 1.125x1.121 and ISOCAM is 1.25x0.9424. ISOCAM is free-running, producing data from an initial input. ECHAM is a nudged model, which means that output is being forced to match reanalysis data.

5.3 Validation

By comparing meteorological measurement data to the model's output data, we can make an initial validation of whether we ought to use the model output data from ECHAM and ISOCAM. The intervals for which we will be comparing temperature and precipitation data are 2004-2013, including, for where ECHAM and ISOCAM overlap, and 1960-1986, including, where only ECHAM will be looked at. We choose to use monthly and yearly resolution data to avoid too much noise, and also, this way, the yearly development can be checked, and with monthly, the seasonal behaviour can be seen.

We make this comparison for the DMI station 4339 Itt. and with the applicable grid cell with matching coordinates from the two models. We cannot do this comparison for the grid point of Renland, as we do not have a long period of meteorological measurements from there.

Table 5.1: *Summary of the comparison of DMI and ECHAM and ISOCHAM model data for the location of Itt. for the recent interval of 2004-2013 including. As mentioned, the precipitation for DMI is not a reliable check.*

		temperature [C]		**precipitation [mm]**	
		mean	amp	mean	sum
	ISOCHAM	-8.7	11.8	976	9763
Itt.	**ECHAM**	-7.3	8.5	1223	12230
	DMI	-4.9	10.8	*310*	*3100*

A summary of the comparison for the recent interval can be seen in table 5.1. It was found that ECHAM performs better in terms of the overall temperature, but the seasonal amplitude of ISOCAM fits better. The "seasonal amplitude" is defined as the mean of the mean offset of the highest and lowest value to the mean of a year. For precipitation, there is no proper comparison with measurements, but the two models agree somewhat, with ECHAM being wetter in some months.

5.3.1 Geographical representation

The coordinates used for the locations of Itt. and Renland are given in table 5.2 for the models and the measurements. Since the models are on a grid, we do of course not expect to have a perfect location match, neither between the real world and the models or the models themselves, and since these grids do not resolve the detailed topography of the coast, the elevation of the points will not match.

Table 5.2: *Coordinates and elevation coordinates of Itt (Scoresbysund) and Renland for the measurements and models. The heights of the old and new site are from the best-matching grid cell of GIMP.*

		latitude	longitude	elevation [m]
Itt.	**ISOCAM**	70.2094 N	21.2500 W	28
	ECHAM	70.0927 N	22.5000 W	167
	DMI	70.4833 N	21.9500 W	70
Renland	**new site**	71.30363 N	26.7132 W	2331
	old site	71.30708 N	26.76548 W	2340
	ISOCAM	71.1518 N	26.2500 W	870
	ECHAM	71.2141 N	27.0000 W	1105

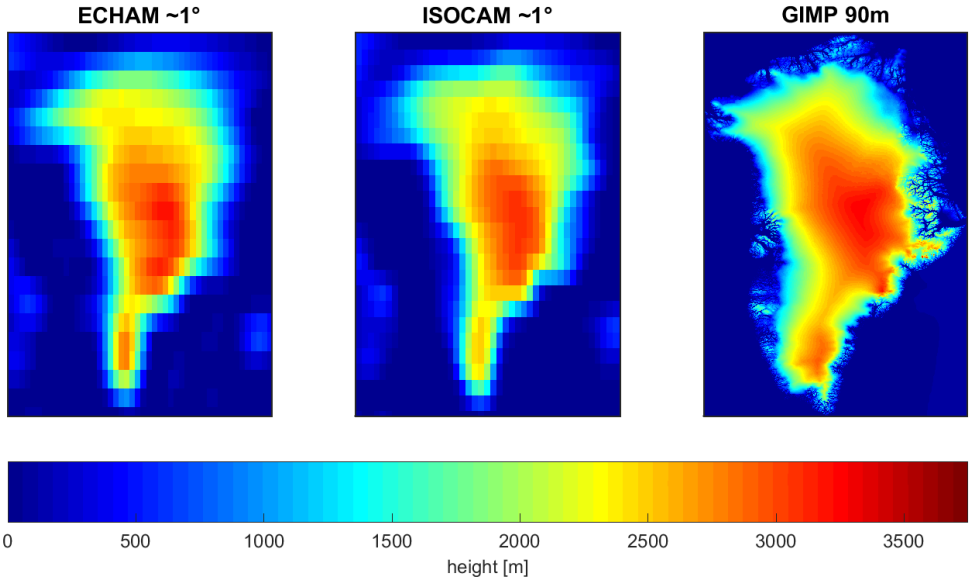

Figure 5.1: *The models ISOCAM and ECHAM both have about 1 degree resolution, and the shown topographic data from GIMP is of the 90 meter resolution. The aspect ratio of the GIMP cutout is not the same as of the models, and do not show the exact same area. where the resolution is 90 in the GIMP product*

The cell for Renland has lower elevation in both ECHAM and ISOCAM, but for Scoresbysund, ISOCAM is lower while ECHAM is higher. In GIMP, A6 and A9 has the same elevation difference, little more than 10 metres, but the sign are switched from that of the radar data: the difference in height between the two sites are not thought to be significant. Topographic maps of Greenland from GIMP and from the models can be seen in figure 5.1, [The Ohio State University, 2016]. Most important to note is that neither Itt. nor Renland is a point in the ocean, as it has positive elevation. Figure 5.2 shows the detail of the area, and it is clear that the *sund* is not resolved, nor can even be seen.

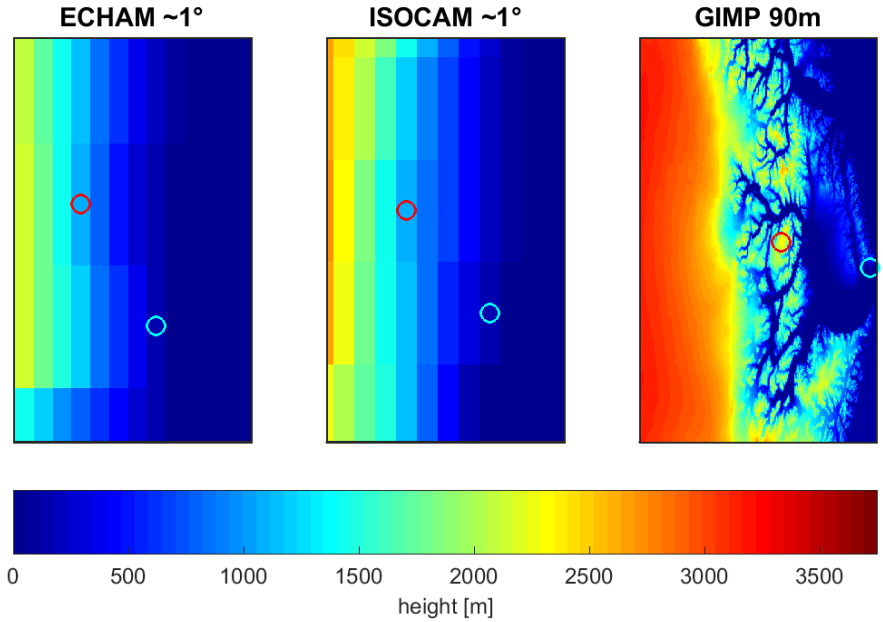

Figure 5.2: *Zoom in of the area around Renland. The "sund" is not seen. The aspect ratio of the GIMP cutout is not the same as of the models, and do not show the exact same area. Red circles denotes Renland and blue circle denotes Itt.*

5.3.2 Temperature

The data comparison for the recent interval is shown in figured 5.3 for yearly. Both models are too cold, with ISOCAM being colder than ECHAM compared to the measurements: As seen by the monthly data, figure 5.4, it is the combined effect of both winter and summer seasons being too cold in the case of ISOCAM. For ECHAM, it is only the summer that are not hot enough. It is not surprising that ECHAM matches the yearly development more closely than ISOCAM, since it is nudged to observational data. The mean seasonal amplitude of the models are more offset for ECHAM than ISOCAM compared to the measurements, but in opposite directions, with ECHAM being too small at and ISOCAM a bit too high.

In the old interval, we only have model data from ECHAM, which can be seen in figures 5.5 for yearly and 5.6 for monthly. Again, ECHAM is too cold, more so before ~1980 than after. This could be due to the advent of using satellites for measuring sea ice presence. The behaviour is more apparent in the monthly profile, where it can be seen that it is especially the winter temperature that has a warming trend, while the summer offset to the measurements stays the same. The temperature of the year 1981 for the DMI measurements are due to missing the four months of July to October, as can be seen in the monthly data too, offsetting the yearly mean to colder.

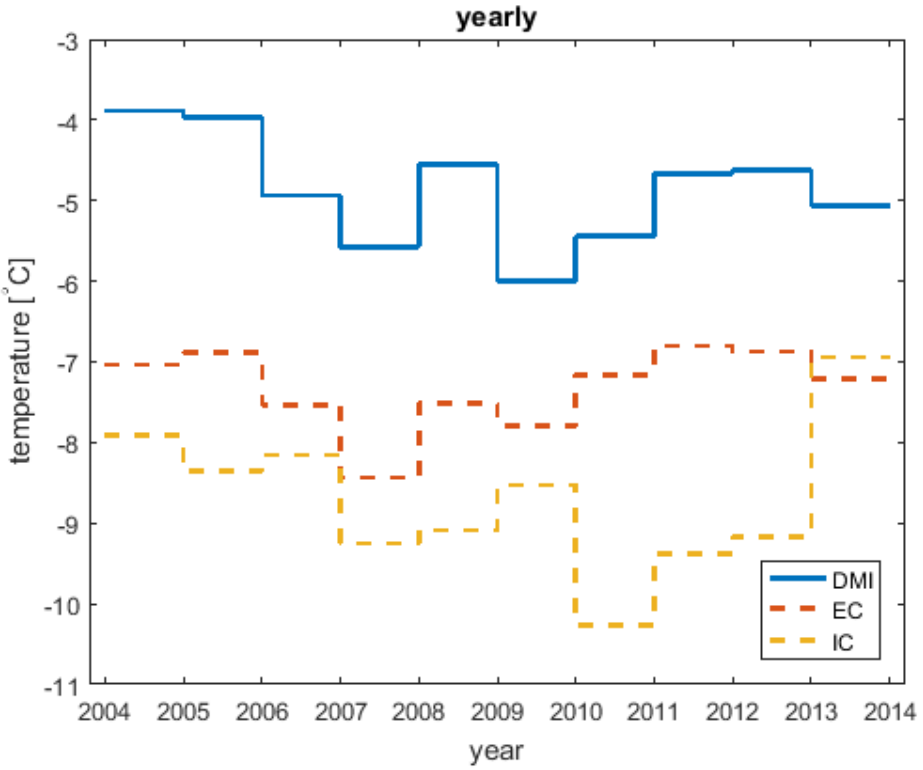

Figure 5.3: *Yearly temperature data from the period 2004-2013 including, for DMI measurements from station Itt. 4339 (blue full line) and from models ISOCAM and ECHAM (yellow and red dashed lines).*

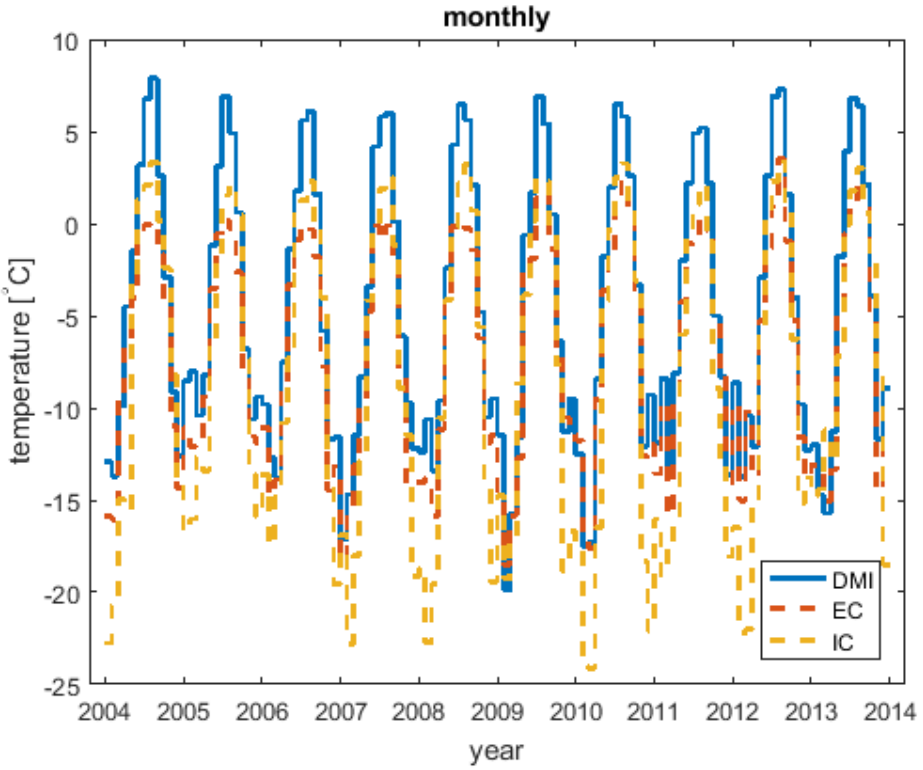

Figure 5.4: *Monthly temperature data from the period 2004-2013 including, for DMI measurements from station Itt. 4339 (blue full line) and from models ISOCAM and ECHAM (yellow and red dashed lines).*

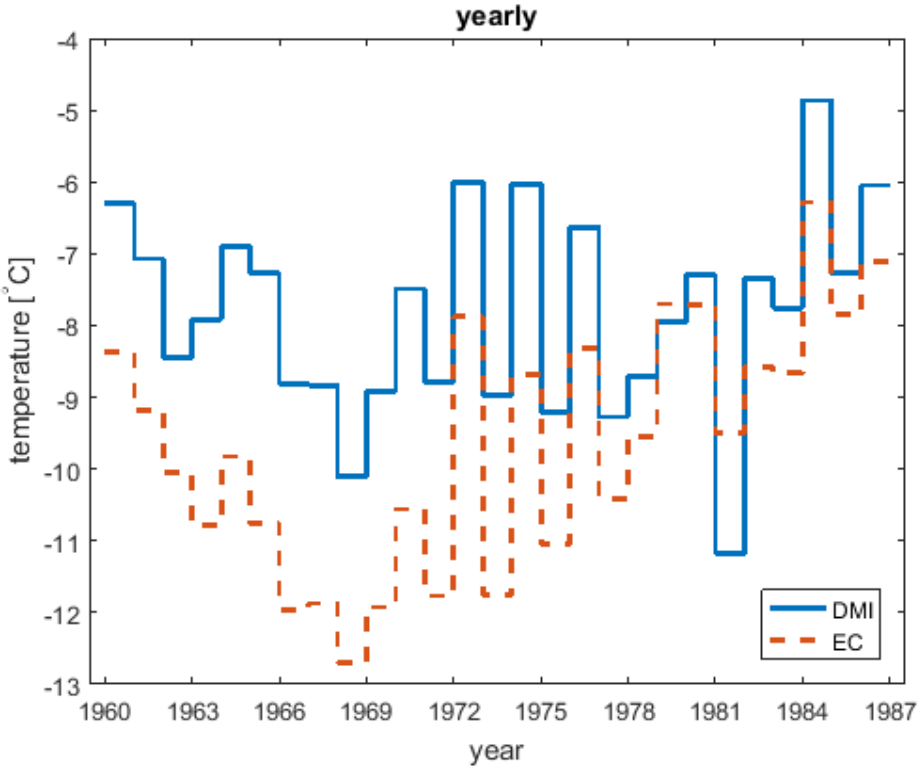

Figure 5.5: *Yearly temperature data from the period 1960-1986 including, for DMI measurements from station Itt. 4339 (blue full line) and from model ECHAM (red dashed lines). Year 1981 is missing July-October, offsetting the mean negatively.*

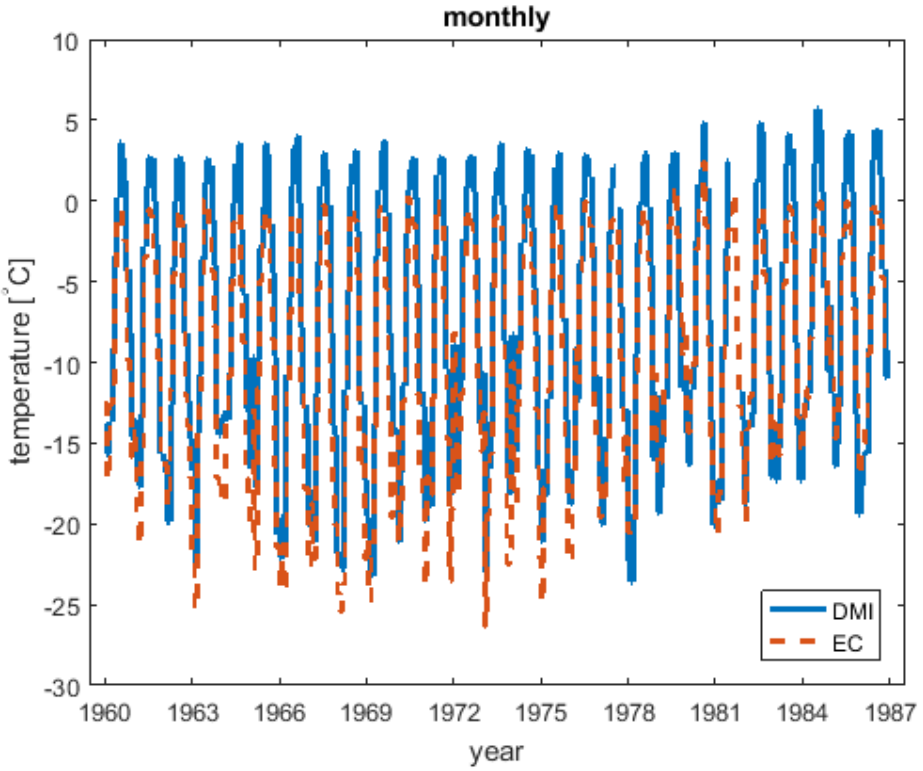

Figure 5.6: *Monthly temperature data from the period 1960-1986 including, for DMI measurements from station Itt. 4339 (blue full line) and from model ECHAM (red dashed line).*

5.3.3 Precipitation

Despite the problematic precipitaton record, we still make this comparison, as it will also tell us about how well ISOCAM and ECHAM agree, which can be seen in figures 5.7 for yearly and 5.8 for monthly for the recent interval. There are continuous gaps in months of 2008-09 and 2011-13, so overall the measured precipitation is too low, as expected. The models agree somewhat, with ECHAM having a higher amount than ISOCAM, with sums of 12230 mm and 9763 mm, respectively. From the monthly data, it seems that this is not due to a always consistently higher level of precipitation for ECHAM, but rather sets of one or two months throughout the years having a bigger amount of precipitation.

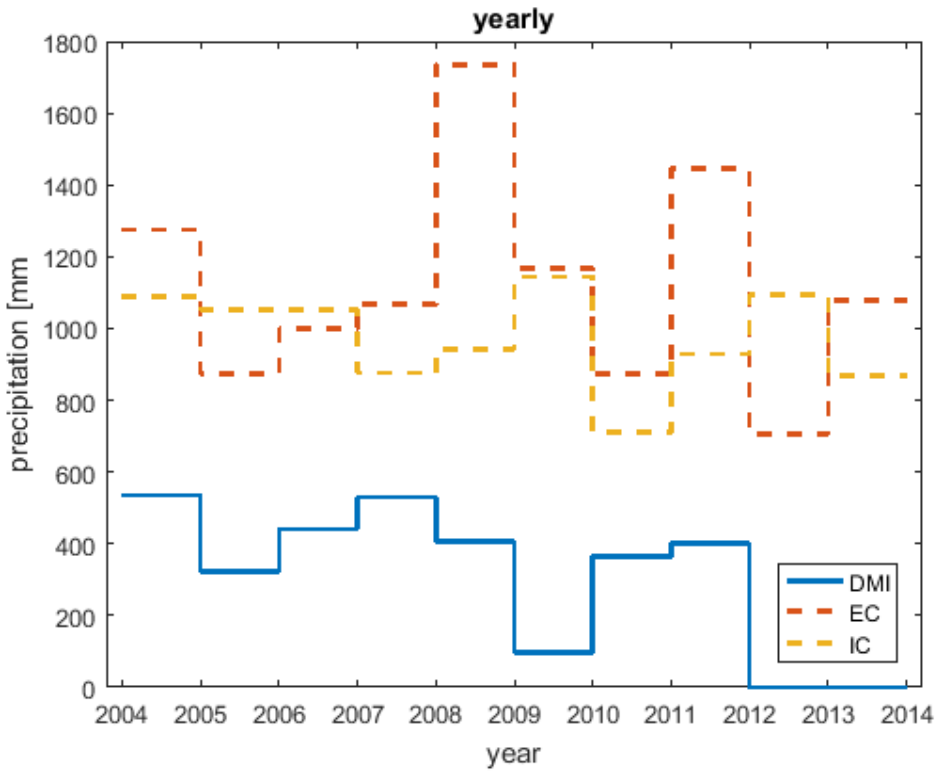

Figure 5.7: *Yearly precipitation data from the period 2004-2013 including, for DMI measurements from station Itt. 4339 (blue full line) and from models ISOCAM and ECHAM (yellow and red dashed lines).*

For the old period, figures 5.9 for yearly and 5.10 for monthly where we only have ECHAM and DMI data to compare, the amount for ECHAM is higher, which could be due to the rain gauge with problems. The average yearly precipitation for the recent and old period are similar, at 1223 mm and 1020 mm, respectively.

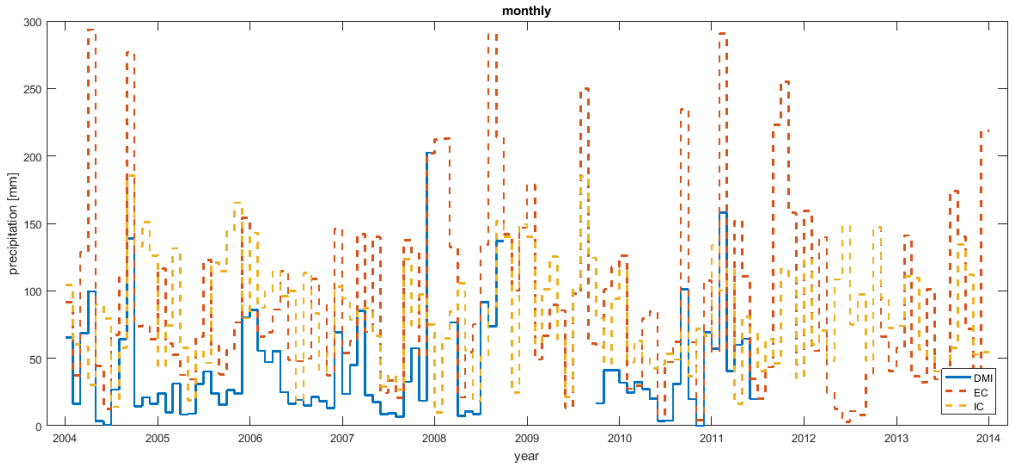

Figure 5.8: *Monthly precipitation data from the period 2004-2013 including, for DMI measurements from station Itt. 4339 (blue full line) and from models ISOCAM and ECHAM (yellow and red dashed lines).*

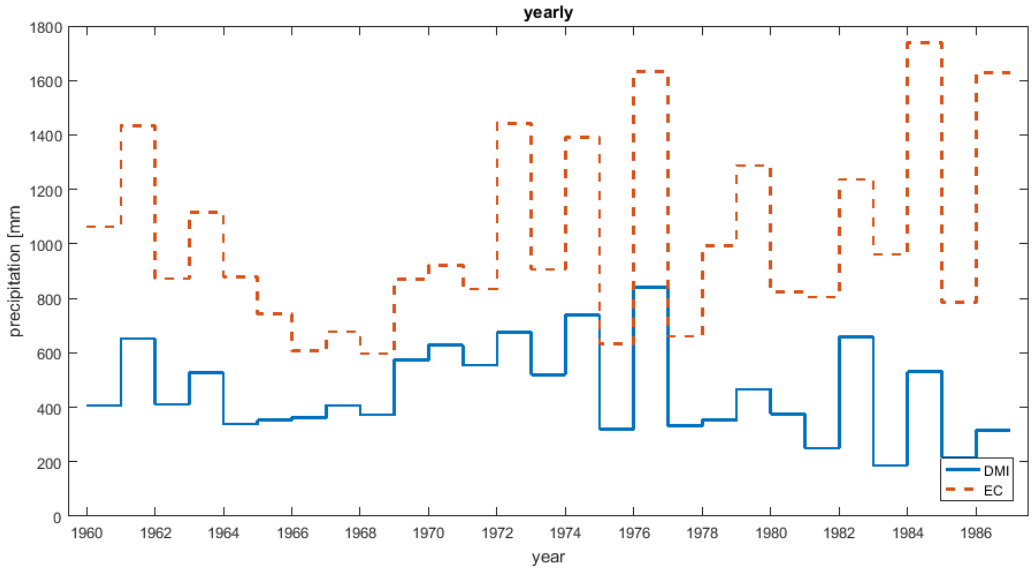

Figure 5.9: *Yearly precipitation data from the period 1960-1986 including, for DMI measurements from station Itt. 4339 (blue full line) and from model ECHAM (red dashed lines).*

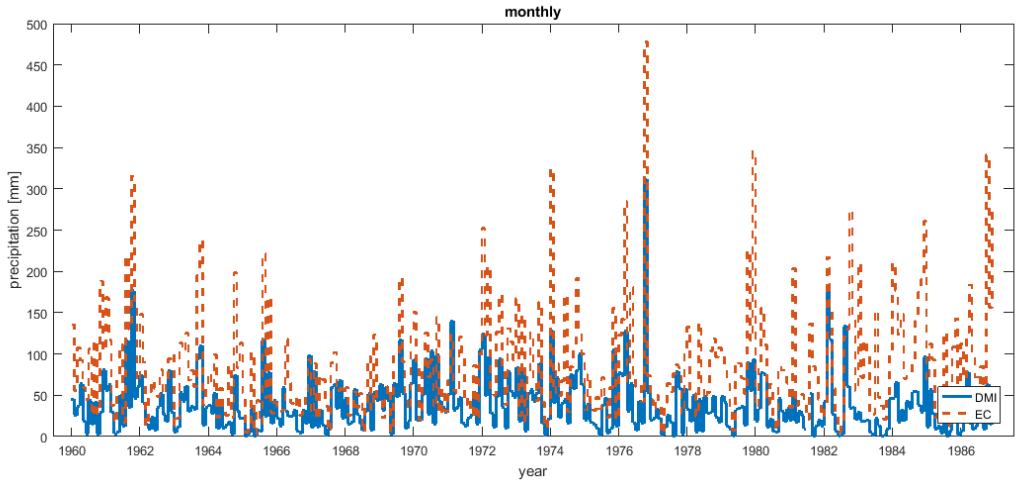

Figure 5.10: *Monthly precipitation data from the period 1960-1986 including, for DMI measurements from station Itt. 4339 (blue full line) and from model ECHAM (red dashed lines).*

CHAPTER 6

Ice core data and GCM

By comparing isotopic model data to that from ice cores, we get a measure of how well the model is reproducing the mechanisms of the climate. In this thesis, the goal is not to do a check of the models ECHAM and ISOCAM themselves, but rather how well the data matches for Renland, and if it is possible to use the model data from Renland to investigate, interpret and understand our ice core data from and paleoclimate of Renland. A proper assessment of an isotope-coupled GCM would require investigation of more than just a single grid cell.

6.1 ECHAM and ISOCAM and firn cores

As we saw in chapter 4, the dated part of the firncores A9 and A6 covers the time period of 2005-2014 and 2006-2014, respectively. We can compare this with model data from the Renland grid cell (see section 5.3.1) for the interval 2006-2013, where ISOCAM, ECHAM and both firn cores overlap; as we saw, the year of 2014 is "busy", since the isotopes have not been diffused, and A6 and A9 do not agree well there, so this is no great loss.

We will compare the isotopic values of mainly δ^{18}O but also show XS, as well as see if the amount of precipitation fits with what we see in the firn cores. Having both precipitation and isotopic values would also make it possible to create an "artificial" ice core based on the model data: that way, we are less dependent on our dating of the firn cores, since we are then comparing depth to isotope values rather than time to isotopic values.

Table 6.1: *Summary of the comparison of ice core data from firn cores and GCM models ECHAM and ISOCAM for the recent interval of 2006-2013.*

		δ^{18}O [‰]		**XS** [‰]		**precipitation** [mm]	
		mean	amp	mean	amp	mean	sum
Renland	**new site**	-26.36	4.12	8.17	3.19	523	4180
	old site	-26.50	4.23	8.26	3.46	506	4048
	ISOCAM	-17.52	3.68	5.08	4.67	499	3995
	ECHAM	-22.62	5.36	8.15	3.60	495	3957

For completeness, the different plots includes 2005, but the values in the summary table 6.1 is based on 2006-2013. The precipitation matches very closely, but the isotopic values of δ^{18}O are offset to higher, lighter, values. This could be due to the difference in height between the real ice cap and the grid point elevation for both models, which also fits with ISOCAM being lower at Renland than ECHAM. For the seasonal amplitudes, ISOCAM again fits slightly better, but the evaluation are uncertain. For XS, ECHAM is best both in mean and amplitudes.

6.1.1 Isotopes

The isotopic values of δ^{18}O and XS are shown in figures 6.1 and 6.2 for yearly and 6.3 and 6.4 for monthly for the models and from "monthly" to "biweekly" approximations for the firn cores, as the number of samples per year differ throughout the profile, as seen in section 4.3.2.

Both ECHAM and ISOCAM have too high, lighter, values of δ^{18}O but it is clear that ECHAM follows the trend of the years a lot better than ISOCAM, with falling values from 2005, rising again in 2009, and then falling till 2013. ISOCAM has the trend of the two declines, but lacks the rise, or has the rise too late, 2011. For XS, ECHAM is clearly better than ISOCAM for the overall values.

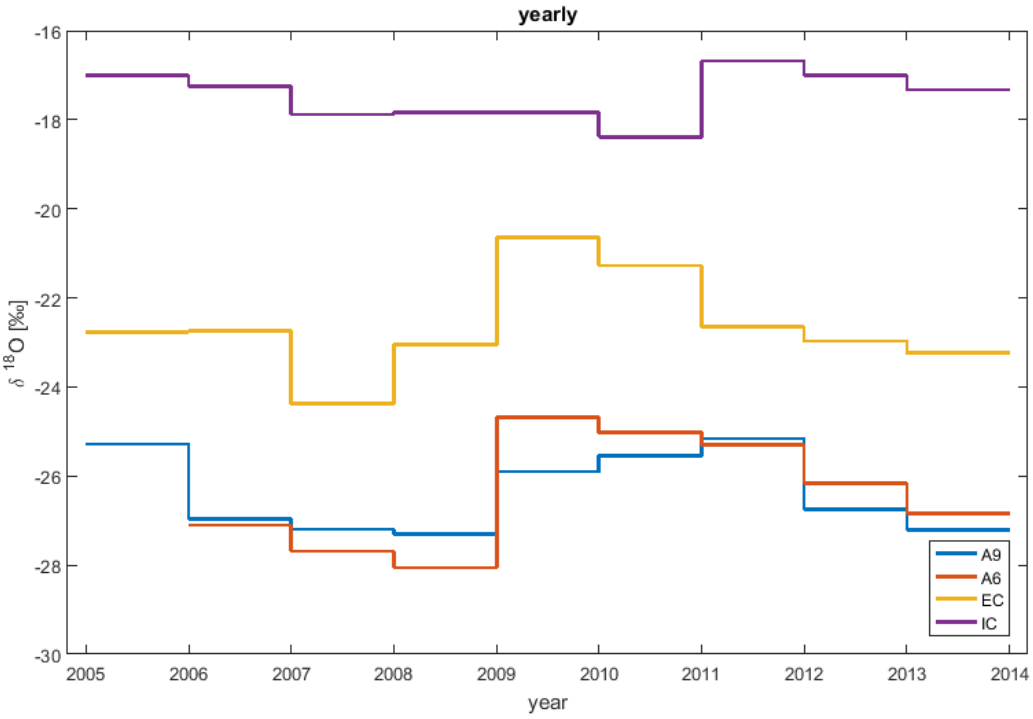

Figure 6.1: *Yearly δ^{18}O-values for 2006-2013, including, from both firn cores (A6 red and A9 blue) and models (ISOCAM purple and ECHAM yellow).*

When looking at the seasonal trend of δ^{18}O for the monthly resolved data, the comparison becomes more muddy. It appears that ECHAM has a periodic behavior, coordinating somewhat with the two firn cores. ISOCAM, however, does seem to have warm and cold periods, but it does not appear to display a seasonal cycle. The mean seasonal amplitude fits better with A9 and A6 for ISOCAM than ECHAM, but since it is simply taking the mean of the maximum and minimum values within a year, it is disputable whether that is a meaningful value. In XS, a seasonal cycle can be seen for ISOCAM, but less apparent so for ECHAM from 2010 onwards. ECHAM, however, seem to fit better with the firn cores in regards to the timing of the cyclus, moreso for the years 2007-2009.

For clarity, the δ^{18}O and XS-values are shown in figures 6.5 and 6.6 for the models alone.

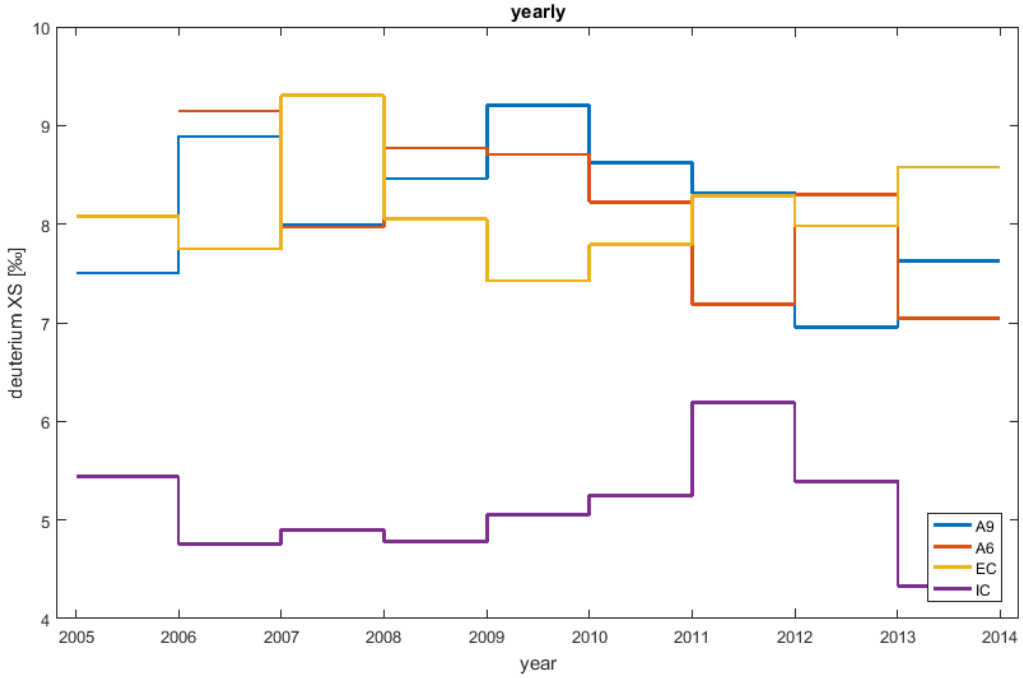

Figure 6.2: *Yearly XS-values for 2006-2013, including, from both firn cores (A6 red and A9 blue) and models (ISOCAM purple and ECHAM yellow).*

Figure 6.3: *Monthly δ^{18}O-values for 2006-2013, including, from both firn cores (A6 red and A9 blue) and models (ISOCAM purple and ECHAM yellow). For the firn cores, the temporal resolution is about monthly to bi-weekly.*

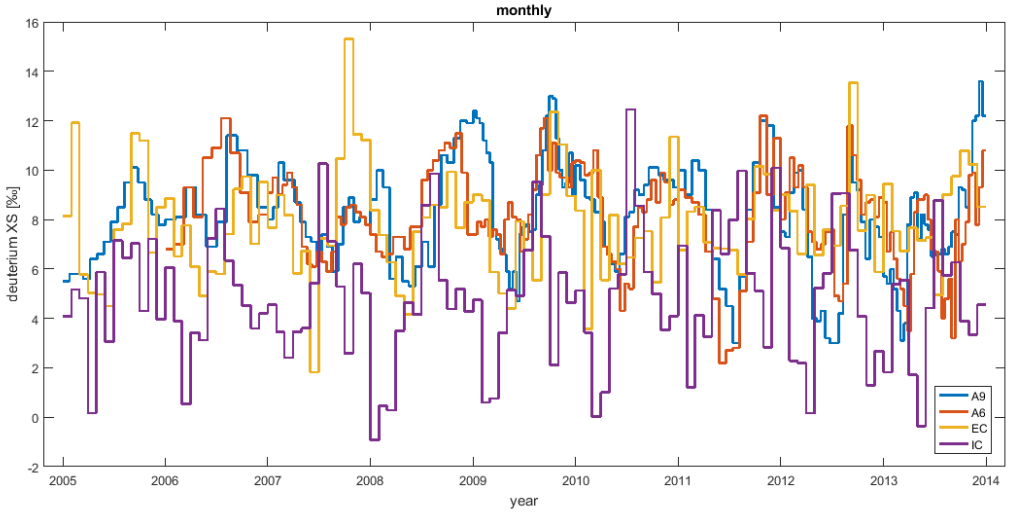

Figure 6.4: *Monthly XS-values for 2006-2013, including, from both firn cores (A6 red and A9 blue) and models (ISOCAM purple and ECHAM yellow). For the firn cores, the temporal resolution is about monthly to bi-weekly.*

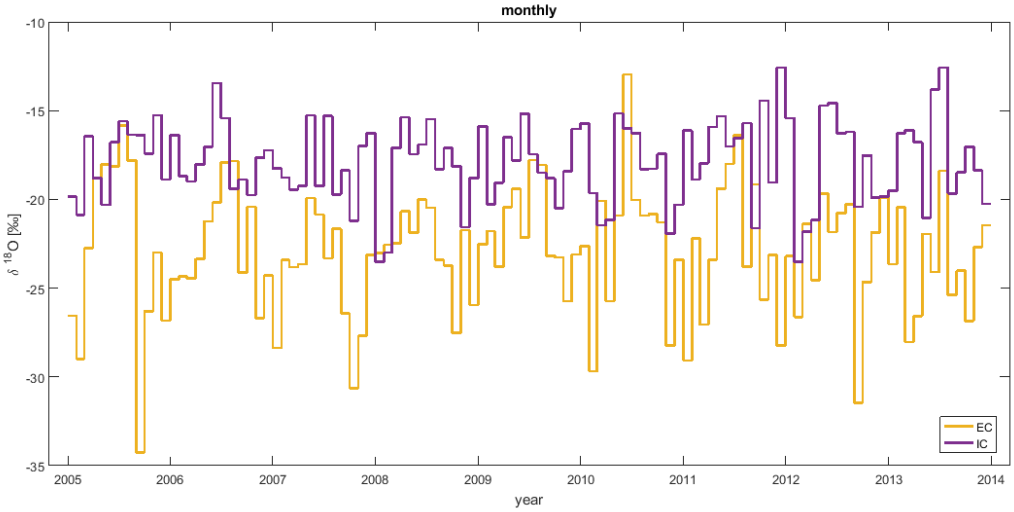

Figure 6.5: *Monthly δ^{18}O values for 2006-2013, including, from models (ISOCAM purple and ECHAM yellow).*

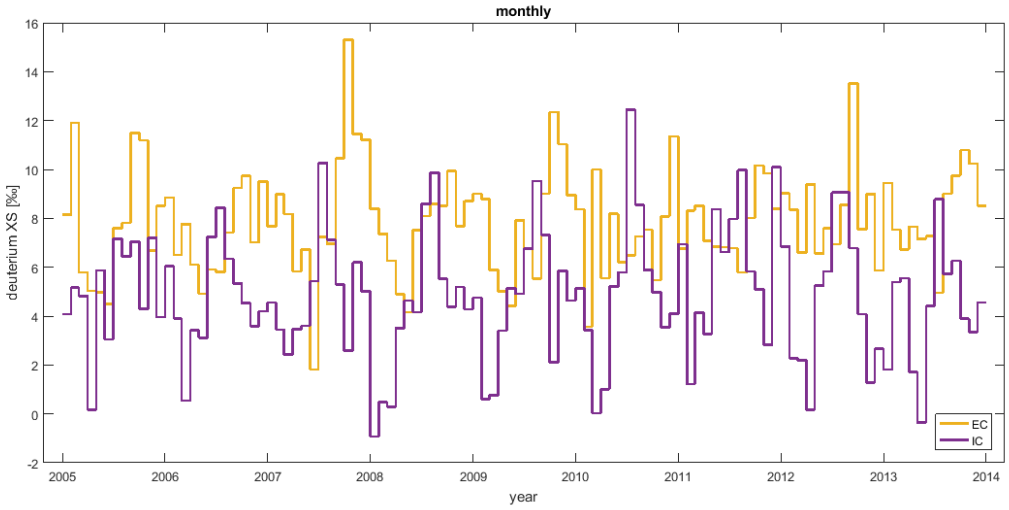

Figure 6.6: *Monthly XS-values for 2006-2013, including, from models (ISOCAM purple and ECHAM yellow).*

6.1.2 Precipitation

For the precipitation, it does not make sense to look at the monthly data, as the spread of the precipitation in the firn cores are completely dependent on where we dated winters, and as such, all months are simply a twelveth of a year length. Instead we look at the yearly precipitation, shown in figure 6.7: Although the distribution of the precipitation within the period is not a match due to certain years being off in both or either ISOCAM and ECHAM, it can be seen in figure 6.8 that the cumulated amount for the overall period match very well.

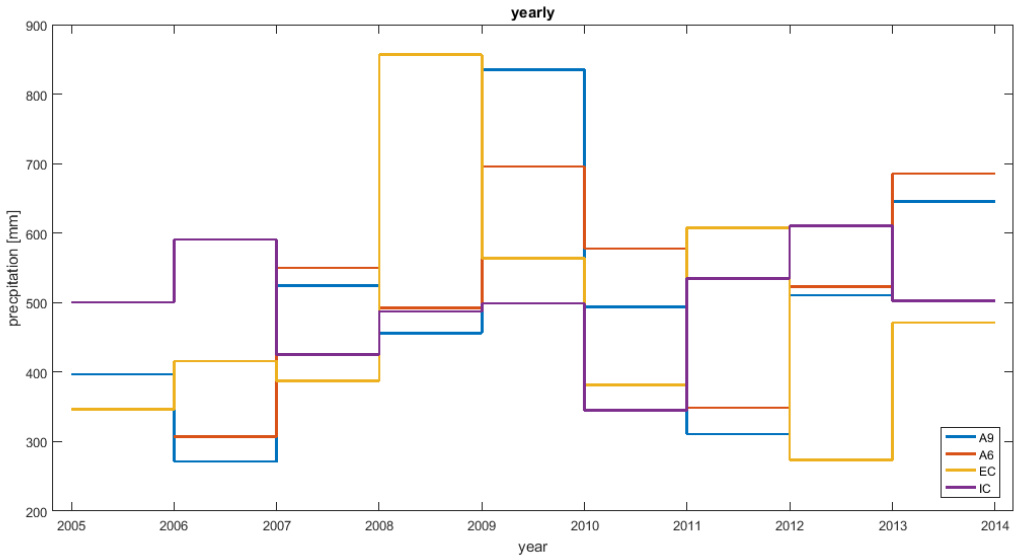

Figure 6.7: *Yearly precipitation data from the period 2006-2013 including, from both firn cores (A6 red and A9 blue) and models (ISOCAM purple and ECHAM yellow).*

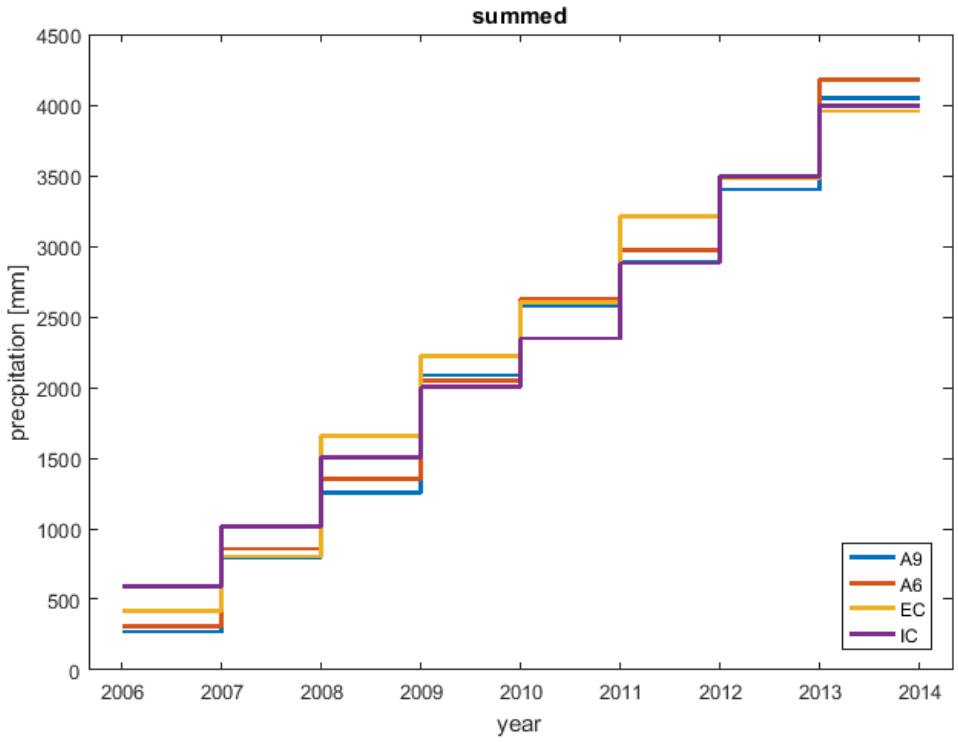

Figure 6.8: *Summed precipitation data from the period 2006-2013 including, from both firn cores (A6 red and A9 blue) and models (ISOCAM purple and ECHAM yellow).*

6.2 ECHAM and Renland 1988

The new main core of RECAP has not yet been put on a time scale, but we can compare the old 1988 core to ECHAM data, in the interval of 1960-1986, where the dating was done by annual layer counting of the δ^{18}O-profile. In general, we see the same behaviour for this interval as for the recent, with matching precipitation (means of 400 mm and 402 mm for ECHAM and the old core), and with small offset in the isotopic value (δ^{18}O means of -23.05 and -27.36 for ECHAM and old core).

6.2.1 Isotopes

Only δ^{18}O-data was measured for the old core and are shown in figures 6.9 for yearly and 6.10 for monthly. ECHAM has higher, lighter values, but the overall trend throughout the years is reproduced well, although not all years match. The higher mean for ECHAM is due to the summer part being too warm compared to the measurements for the old core, as the winters in the first part of the period agree somewhat well. After the winter of 1982, the two data series seem to diverge more, with winters becoming a bit heavier for the old core compared to a lighter ECHAM.

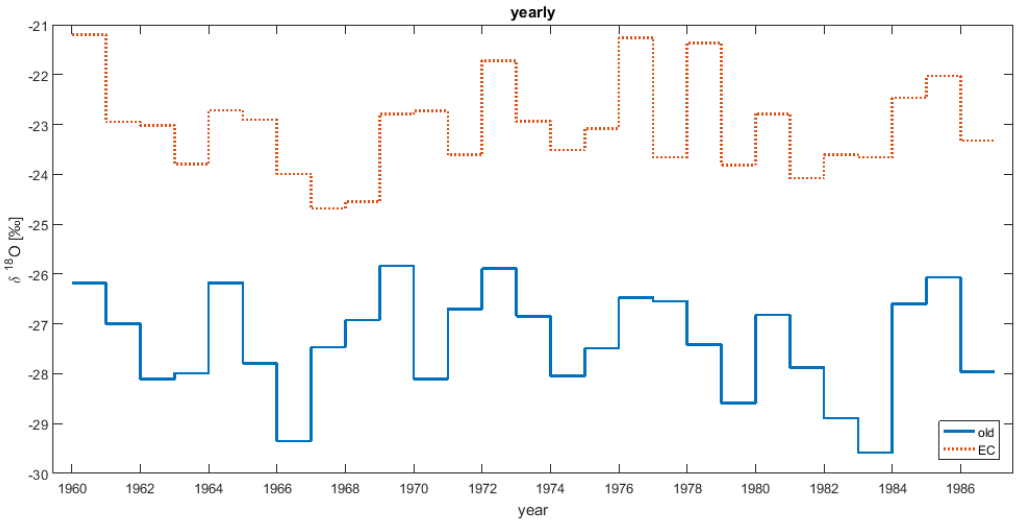

Figure 6.9: *Yearly δ^{18}O-values for 1960-1986, including, from the old Renland core blue full line and model ECHAM red dotted line.*

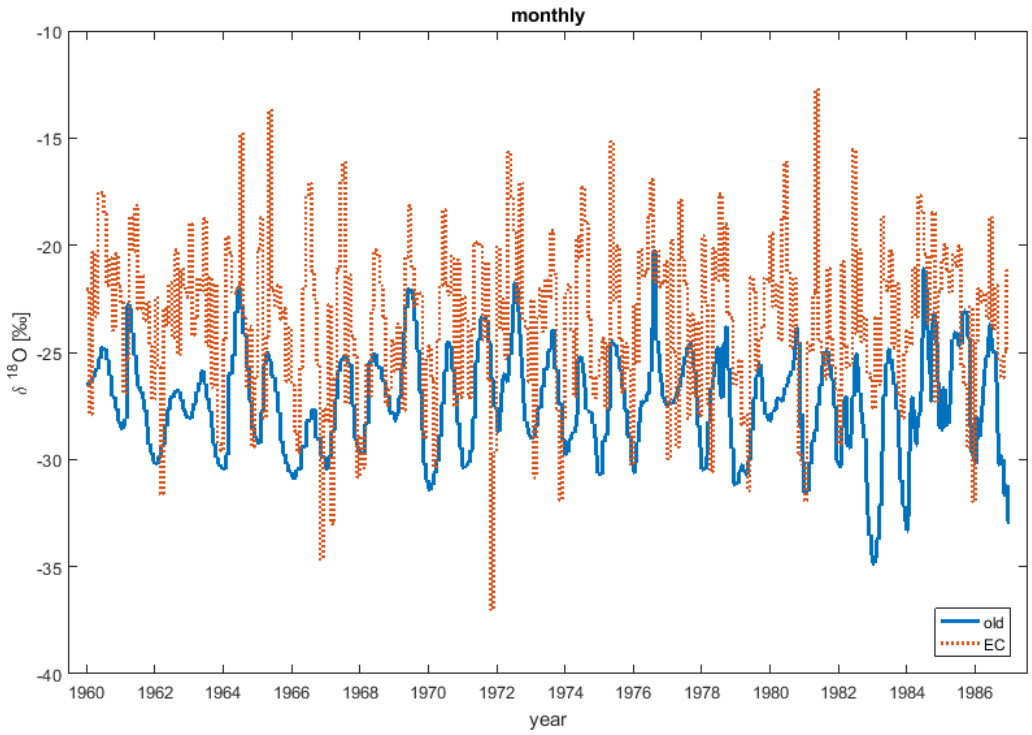

Figure 6.10: *Monthly δ^{18}O-values for 1960-1986, including, from the old Renland core blue full line and model ECHAM red dotted line.*

6.2.2 Precipitation

Again we look at the yearly precipitation: the distribution and overall sum is shown in figures 6.11 and 6.12. As we saw for the recent interval, the precipitation agrees quite well, though with ECHAM both under- and over-estimating the precipitation somewhat in certain years, but with an overall sum nearly identical.

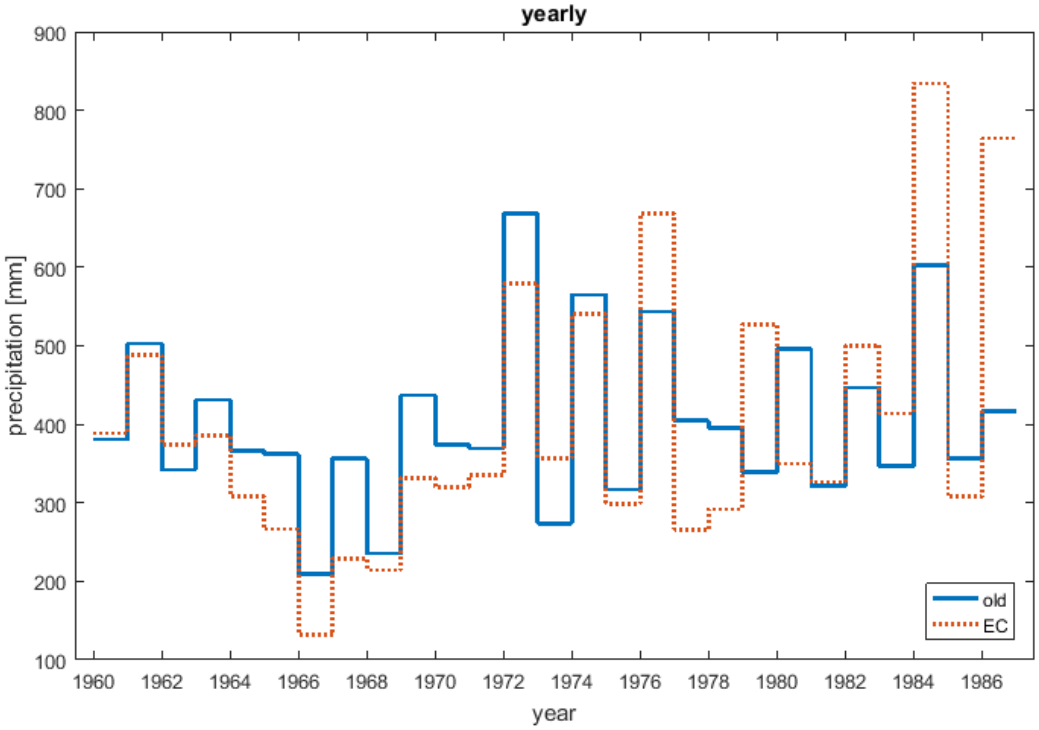

Figure 6.11: *Yearly precipitation data from the period 1960-1986 including, from the old Renland core blue full line and model ECHAM red dotted line.*

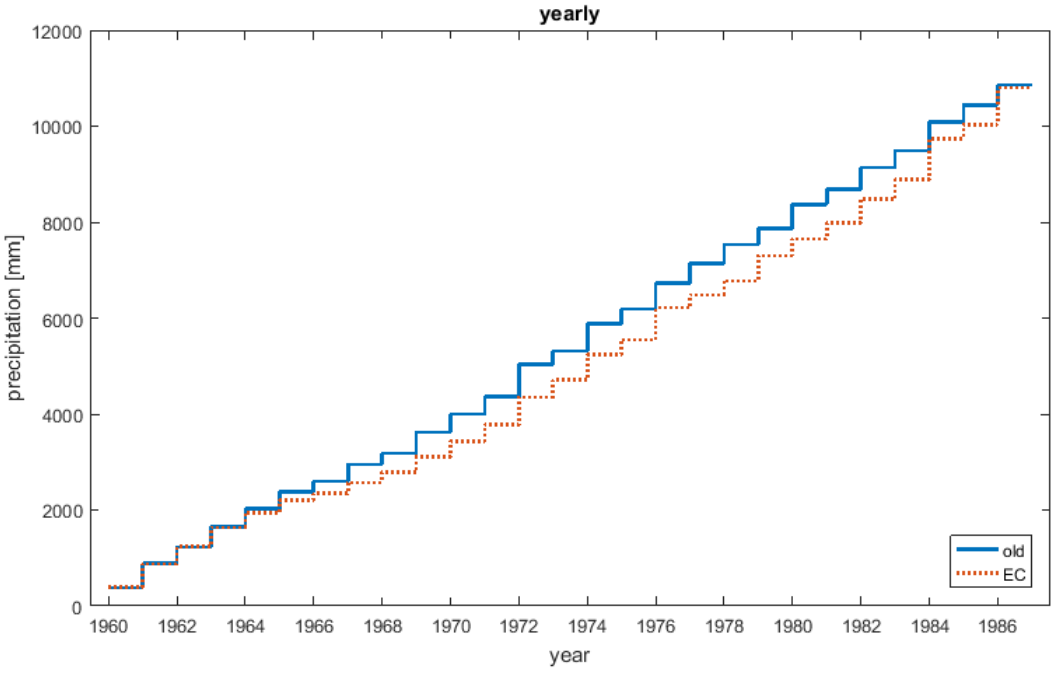

Figure 6.12: *Summed precipitation data from the period 1960-1986 including, from the old Renland core blue full line and model ECHAM red dotted line.*

CHAPTER 7

Temperatures from GCM and boreholes

An other way to evaluate the data from ECHAM is to compare the temperature data of the model to those measured at Renland. As mentioned, there is not/has not been a weather station on Renland for those years, so we do not have direct measurements of the temperature. However, as mentioned in section 2.3, the history of the surface temperatures are recorded in the ice and can be measured in the borehole as a temperature profile after drilling an ice core.

This was done both at the old site in 1988 and at the new site in 2015. The measurements can be seen in figure 7.1. There is an obvious kink in the temperature profile of the new site at 90 meters depth due to the adding of drilling liquid, which increases the temperature. The effect of the liquid is less from 130 meters and downwards.

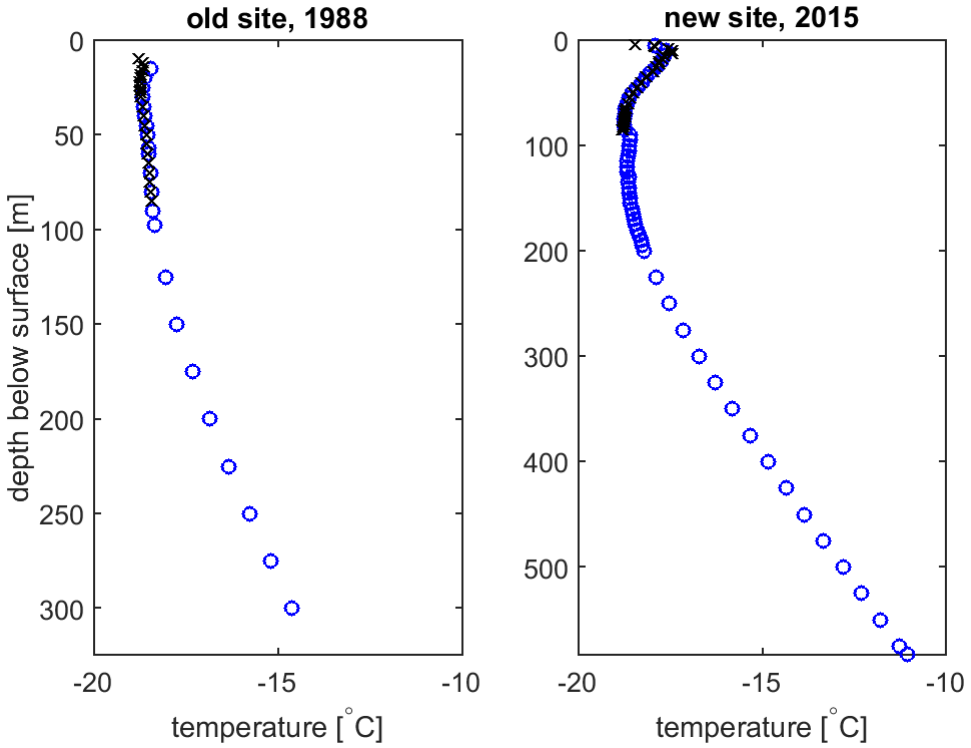

Figure 7.1: *Measured borehole temperatures from the old and new site. Both sites have profiles measured in main holes (blue circles), and a shorter, extra profile (black crosses): for the old site, this is a profile measured in a nearby hole, and for the new site, it is the measurements made without drilling liquid. The limits of the depth axes are chosen so that a comparison is possible, by making it the height of the ice sheet at the given place.*

Using the surface temperatures from ECHAM as input, we will model the temperature in the ice cap and compare with the borehole measurements. As outlined in section 2.3, several different ice parameters are needed in order to model the borehole temperature. First of these are the density

which is used directly in the equation for the change of temperature with time. Secondly, the Dansgaard-Johnsen velocity model needs different flow parameters such as accumulation, bottom sliding, and kink height. Finally the geothermal heat is needed.

The density will be found from fitting density measurements of drilled ice cores from Renland to a density profile. The flow parameters will be found by modelling the age profile of the ice as described in section 2.2 and making use of dated depth points to find the best matches for both cores. Geothermal heat will be found directly from the borehole measurements.

7.1 Density

For Renland, the density has been measured for two main cores and two firn cores (so far), one for each of the sites. The density of the firn cores is described in section 4.3.1. The density measurement of the old core goes a little more than halfway towards the bottom, but never reaches the density of ice: The core was drilled using "dry" drilling which is bad for the core quality. For RECAP, the density measurement almost reaches that of ice. The un-processed experimental data from both cores can be seen in figure 7.2. Firstly, it is obvious that the density of the two cores

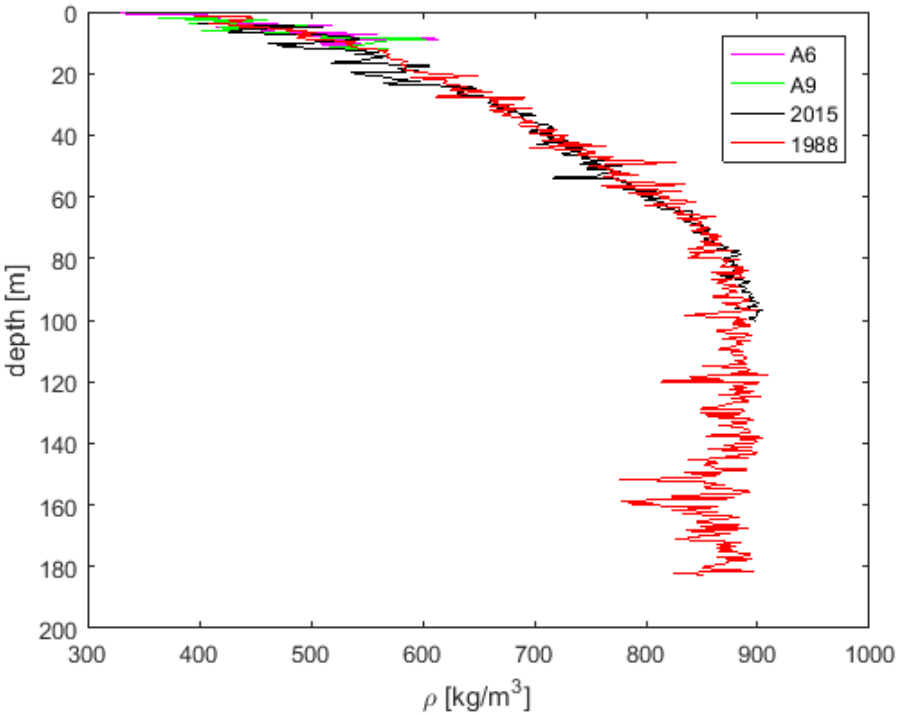

Figure 7.2: *The density profiles for the two main Renland cores, old site (red), new site (black) and the two firn cores A9 (green) and A6 (magenta).*

are similar, and thus the density profile will be treated as applicable for both places. The firn compacts into ice at a around 100 meters; at those depths, the two sites are similar and the firn flow and compaction will not be affected by the underlying different topography.

Since the old core does not eventually reach density of ice due to poor core quality, the data used for fitting is therefore cut off at the same bag depth as that of the data for the new core. The second-to-last density measurement of the new RECAP core is missing, so in order to have this somewhat important data point, that value is taken as the mean of its neighbouring bag densities.

The data was fitted to the exponential Schytt profile, equation 2.15, and to the linear logarithmic version of this, with the inverse e-folding depth, k, and density at the surface, ρ_0, as the unknown parameters. The processed density data set from all four cores and the fitting results can be seen

in figure 7.3. The values of the fitting parameters are in table 7.1. Their 95% confidence intervals

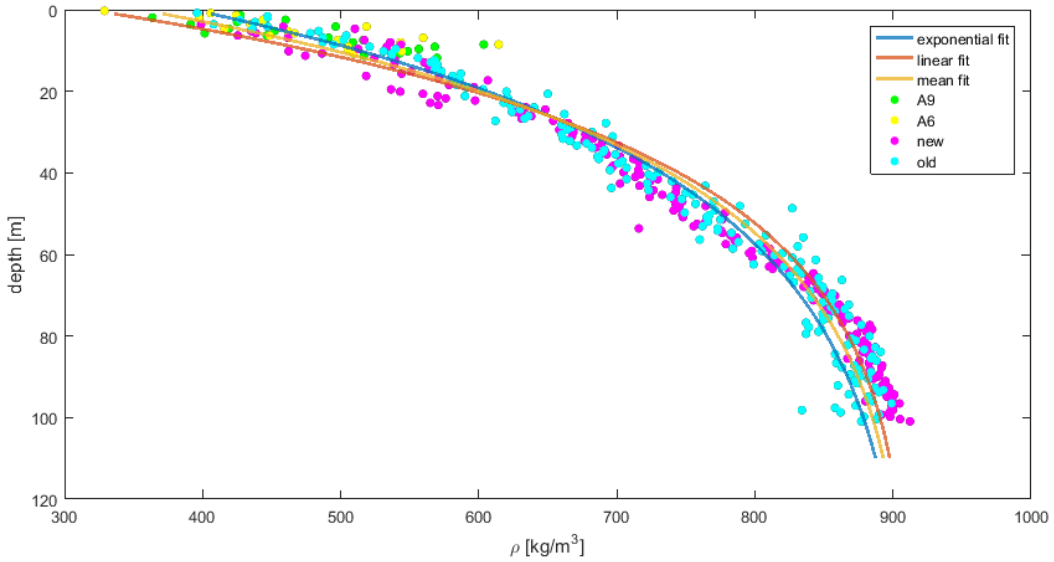

Figure 7.3: *The data processed used for fitting the Schytt profiles from the two firn cores A9 (green), A6 (yellow) and the two main cores from old site (cyan) and the new site (magenta). Also shown is the exponential (blue) and logarithmic (red) fitted profile as well as the average (mustard) of the two.*

Table 7.1: *Found Schytt density paramters*

fitting type	ρ_0 [kg/m^3]	k
exponential	392 ± 7	0.0261 ± 0.0006
logorithmic	316 ± 25	0.0312 ± 0.0007

do not overlap, and it can also be seen that the exponential fit fits better in the bottom of the density profile, whereas the logarithmic fit fits better in the top. We decide to use the mean of the two fits as the parameters for the density profile for the modelling of the temperature, giving us a density of 355 kg/m^3 for the surface snow and a e-folding factor of 0.0287 1/m, or about 35m.

Having the density profile factors also makes us able to sum up the amount of air in the ice cap, using equation 2.16, at 21.38 m. This gives us a pure ice height for the old and new site at 303.62 m and 562.73 m, respectively. This pure ice sheet height is a parameter needed by the velocity model, and therefore the age modelling.

The nature of the Schytt model is that it never reaches ice density. That means the size of the air column will be slightly overestimated. This also requires us to make a manual determination of where we think the transition from firn to ice is. Based on the original data more than the fit, we estimate that threshold to be at 100 meters depth.

7.2 Flow parameters

The velocity model by Dansgaard-Johsen, the kink-model described in section 2.1.1, needs the ice cap and kink heights, the annual accumulation (in ice equivalent) and the value of bottom sliding at the base, if any. For the purpose of the age modelling and the following temperature modelling, we assume that the velocity model is in steady state, meaning that the mentioned parameters do not change in time.

From the fitted Schytt-density profile (see previous section, section 7.1) we have the air column and the ice height. As a starting point for the other flow parameters, we can get an idea about

the annual accumulation for both sites from for instance the firn cores from shown in section 4.3.2. With a new radar topography map of Renland and using the PISM model, we get a starting point of 0.1 for the bottom sliding[i] for the new site, although it is probably lower or zero, due to the lack of bedrock topography.

These values will help in setting the range of the different parameters. We have no starting value for kink height, so here we must simply try a wide range.

7.2.1 4D gridded matrix

In addition to the three parameters, kink heigh, annual accumulation and bottom sliding, we have a fourth input to the age modelling: the depth of the match point themselves. To calculate the ages, 4-dimensional gridded matrices were created using matlab's *ngrid* (which work the same way as *meshgrid* but with column and row input reversed and for higher dimensions) of the four parameters. This allows for an element-wise evaluation of all ages for all parameters using equations 2.8 and 2.9. This gives a 4D matrix with the rows, columns, "leaves" and "stacks" representing the input values, as shown in figure 7.4. The equation used for calculating time is different whether

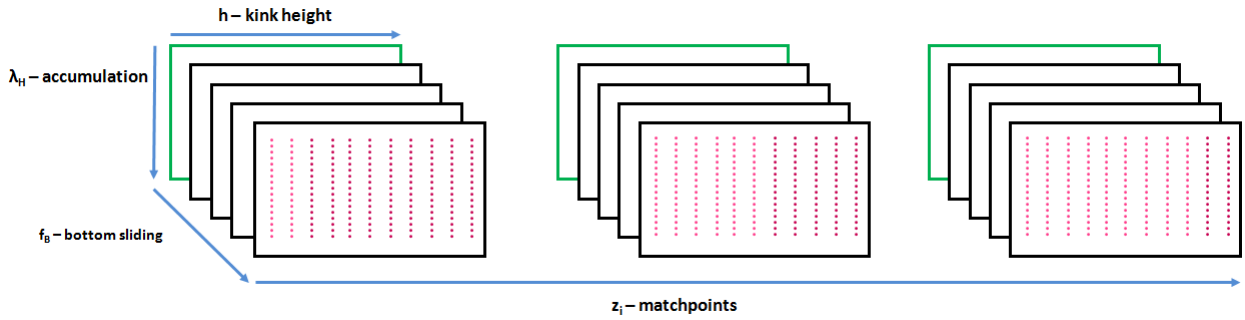

Figure 7.4: *Schematic representation of the age matrix. The rows are annual accumulation, the columns kink height, the leaves the bottom sliding and the stacks the different depth match points. The first leaf of every stack (marked with green contour) is calculated using a different equation of age since the general one does work for no bottom sliding. The columns of each stack are calculated with the equation for either above or below the kink height (marked with magenta and purple rows); the split changes as we go from a smaller hight to a greater height above the bedrock.*

the input depth is above or below the kink height – the kink height that we are varying. This means that for a certain input match depth, some of the age will be modelled with one equation, and the rest with the other, and that partitioning will be different, given by the match depth. As the equations for calculating ages when the height is below the kink height does not satisfy the situation of no bottom sliding, the integration of the simple velocity model version without bottom sliding, equation 2.10, is used. Both of these "corrections" is illustrated in figure 7.4.

The range of the parameters were initially chosen to be wide: For the new site, the kink height is from zero meters to full height of the ice cap, bottom sliding from 0 to 0.2 and yearly precipitation from 30 to 55 cm. For the old site, similar ranges where chosen.

7.2.2 Match points and misfit

Since the age modelling is based on the assumption that the ice cap is solid ice, i.e. no firn layer, we should exclude match points that are above the transition to ice density from our validation of the parameter triplets. Since we use the same density model, that transition is at the same place for both cores, and was found in section 7.1 to be 100 meters.

[i] Data extracted by Iben Koldtoft.

The depth-ages match points used for finding the best triplet of parameters are all ages matched on the GICC05 age scale. The RECAP core has not yet been dated completely, neither by counting isotopic annuals nor with a thinning model. However, there exists some preliminary ECM dating[ii] for the first 4000 years, down to about 100 meters above the bedrock. Additionally, the 8.2k event, a cold climate excursion clearly visible in water isotope data, has been found at 480.5m depth and is added to the match points as to have a lower fix point.

For the old site, the points are found through a combination of annual counting of δ^{18}O and ECM for the first thousand years and using volcanic ECM layer horizons for the next thousand. The data here goes down about 250 meters, not reaching all the way to the bottom. The dating exists in a resolution of 5 years, but for the purpose of this modelling, a down-sampling to 100 year resolution was used. For the old site, using the 8.2k event, which is at depth 283.3 meters would not improve the fit, however, because the yearly thicknesses for the old core increases with depth in the deep part [Vinther et al., 2008], contrary to regular ice flow.

The dated depth points and ages for both sites can be seen in figure 7.5.

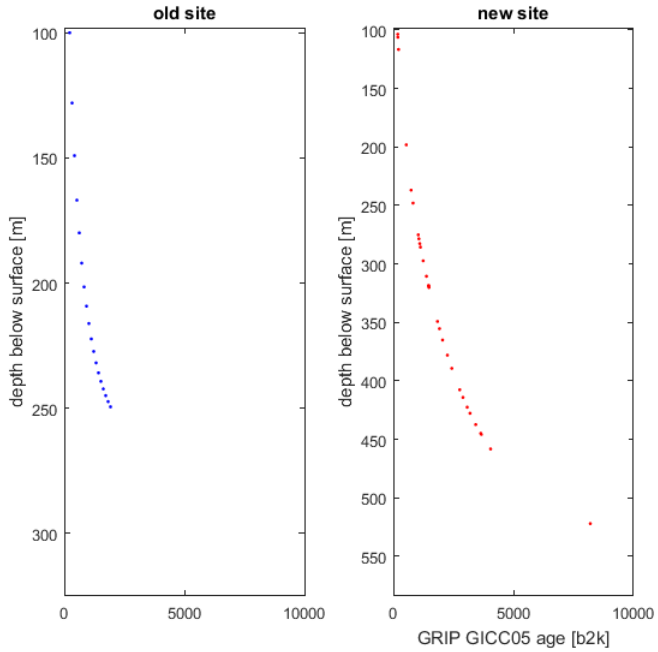

Figure 7.5: *The matched dated points of the Renland cores, old site (blue), and new site (red). The limits of the axes are chosen so that a comparison is possible.*

To asses which triplet set of parameters are best, we will compare the misfits of the ages. In the context of our 4D matrix, that means summing on the fourth dimension, the stacks, which are our depth match points, which leave us with a 3 dimensional matrix. We define the misfit as:

$$MF = \sqrt{\frac{\sum_{i=1}^{N} (t^i_{fit} - t^i_{match})^2}{N}} \tag{7.1}$$

where t_{fit} is the fitted ages, t_{match} is the matched depth-time points and N is the number of samples. The misfit is measured in units of time, for instance years. It can be understood as a sort of mean offset for all points with added weight to the far outliers; if all the offsets of the individual points where of equal magnitude, misfit would simply yield this value.

There is no obvious single minimum of misfit that we can home in on in the patterns shown in figure 7.6 for the new site and figure 7.7 for the old site. The misfits for the new site for all

[ii] Unpublished local data.

triplets with a non-zero bottom sliding all exhibit the same pattern: a downward sloping broad band of low misfit of wide width in annual accumulation going across all kink heights, and with a band of high misfit for smaller values of accumulation and a band of middle misfit for higher accumulations. For no bottom sliding, the pattern is different, with a band upward sloping and narrower in accumulation, but also going across all kink heights, and with a small band above and a wide band below of higher misfits.

For the old site, the misfit with no bottom sliding has the best fit with very low accumulation and deeper kink height and has a v-shape dip in the pattern. For the non-zero bottom sliding, there is a band similar to that of the new site of downward sloping low misfits going across almost all kink heights and accumulations but increasing in value towards the lower accumulations, with higher misfits on both sides of the band.

For new site, this best misfit triplet of 40.5 years is with kink height of 488 meters, an accumulation of 40 cm and a bottom sliding of 0.06. For the old site, the best triplet has a misfit of 57.4 years, with a kink height also high at 243 meters, a bit higher accumulation at 47 cm and a very low bottom sliding at 0.01.

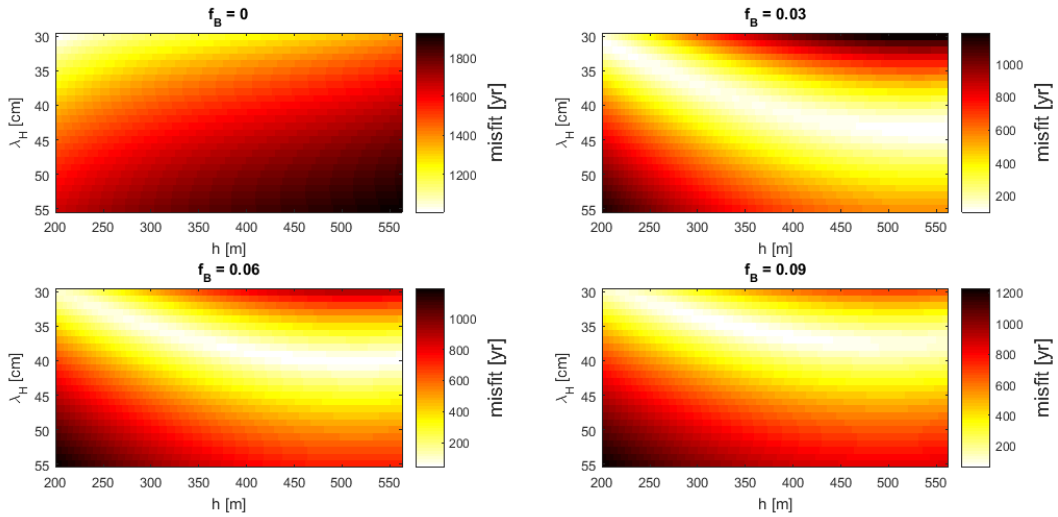

Figure 7.6: *An example of the pattern of the age misfits for the new site with bottom sliding factors of 0, 0.3, 0.6 and 0.9. The colour scale is not the same so as to show the detailed patterns.*

A way to evaluate the fit is to not look at the depth-age curve and misfit itself, but instead look at the velocity profile given by the found flow parameters. Recall, from section 2.1.1, that if the accumulation is in steady state, the kink velocity profile also represents the thickness of the annual layers at a given depth. Using as an initial check the lowest misfit triplet for both sites, the flow model can be seen in figure 7.8. It is clear that for the new site, we are fitting the lower points better than the upper. The same is the situation for the old site, although here some of the deepest points also fit less than very well.

The temperatures that we are modelling and checking against the measured borehole temperature only goes back to the late 19th century, which means that the temperature signal will not have propagated very far down. As such, we seek to have velocity model parameters that fit well in the upper part of the profile, and are less concerned with any eventual offset to the deeper match points.

We therefore truncate our fitting depth points, so that for both sites, it is based on match points down to about 800 years old, the cut-off marked in figure 7.8.

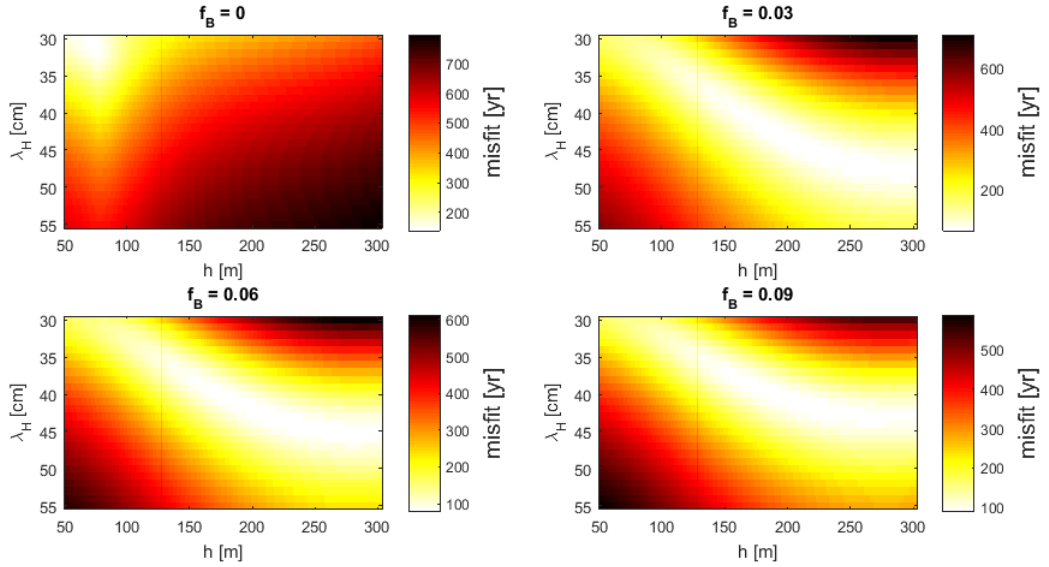

Figure 7.7: *An example of the pattern of the age misfits for the old site with bottom sliding factors of 0, 0.3, 0.6 and 0.9. The colour scale is not the same so as to show the detailed patterns.*

7.2.3 Chosen values

Using only the upper depth point matches down to about 800 years, we again evaluate the found misfit of the parameters triplets. To get a firm "lock" on the parameters, we narrow the ranges and increase the resolution of the parameters. The picked values for the parameters, the triplet with the lowest misfit are listed in table 7.2 for the old and new site. The misfit for the old site is

Table 7.2: *Chosen velocity model parameters*

	λ_H [cm]	f_B	h [m]	H_{ice} [m]	misfit [yr]
old site	47.41	0.0004	183.50	303.62	3
new site	46.17	0	559.22	562.73	11

obviously better than for the new site. They have almost the same annual accumulation, which is not surprising given their proximity, and they also have very similar bottom sliding, almost none. For the kink height, however, it is a little more than half way to the top for the old site, whereas for the new site, it is *at* the top. This and the larger misfit would indicate that the new site does not flow according to a kink model, and could be a cause of discrepancies/errors when using this velocity model. The yearly thicknesses for the tuned modelling can be seen in figure 7.8 for the new and old site. It can be seen that the model now fit the upper part better than when using all the depth match points, especially for the old site, while the model still has trouble matching its points for the new site.

7.3 Modelling borehole temperature

From the previous sections we have a density model and flow parameters. The last value we need is the geothermal heat, the incoming heat from the bedrock at the bottom of the ice cap. That is found from simple application of Fourier's law, $Q_{geo} = -k\ dT/dz$. Using the slope from the five deepest points and their mean temperature for the thermal conductivity, we get a geothermal heat of 46.2 mW for the new site. We will use the same value for the old site, instead of calculating it from its borehole profile, as the measurements do not reach all the way to the bottom.

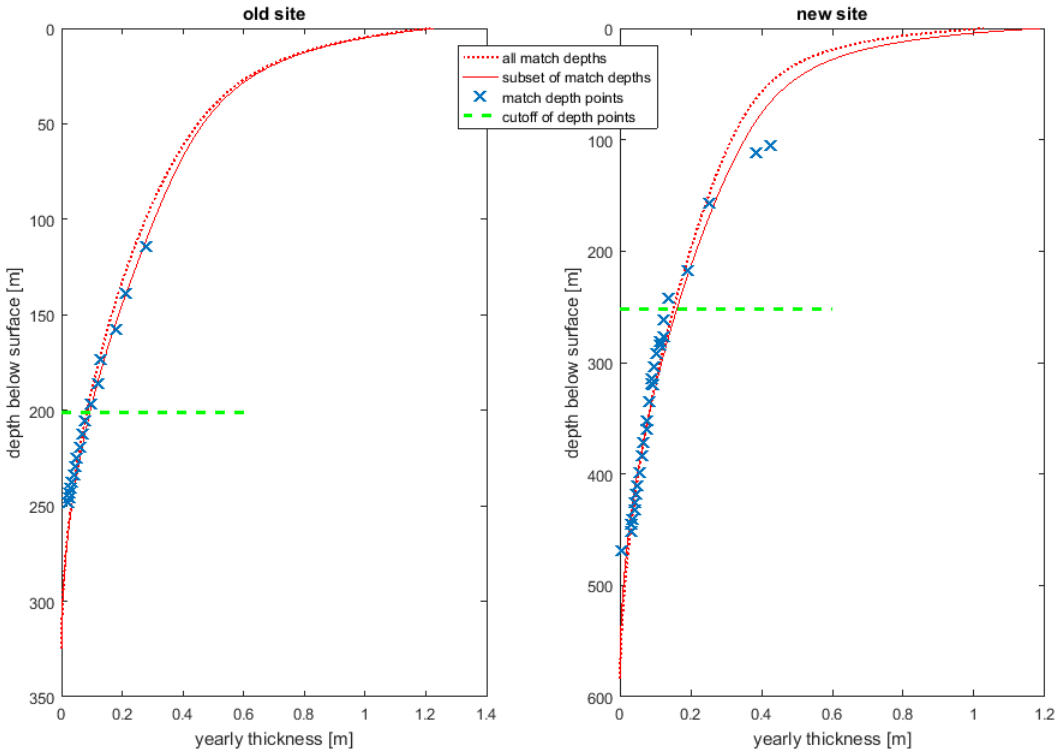

Figure 7.8: *Velocity profile, and thereby mean yearly thicknesses, for both sites. Shown are depth match points (blue crosses), cut-off for match points (green line), and model fit with all (red dotted line) and with part of the depth points (red full line).*

7.3.1 Crank-Nichelson scheme

To solve the non-steady state situation numerically, we use a Crank-Nichelson scheme [1996]. In order to not make the derivation overly cluttered, I will present it for the simple case; in the end, by comparison with the full equation, we will see that solution is analogous.

In the simple case, we have no firn layer and only vertical advection and the equation therefore has three terms, being the same as equation 2.11 but without any term in the horizontal direction:

$$\frac{\partial T}{\partial t} = \kappa \frac{\partial^2 T}{\partial z^2} - w(z) \frac{\partial T}{\partial z} \tag{7.2}$$

We let the j-index denote the spacing coordinate, and i-index the time coordinate, we write up the terms on discrete form:

$$\frac{\partial T}{\partial t} = \frac{T_{i+1,j} - T_{i,j}}{\Delta t} \tag{7.3}$$

where Δt is the temporal spacing.

$$\frac{\partial T}{\partial z} = \frac{1}{2} \left(\frac{T_{i+1,j+1} - T_{i+1,j-1}}{2\Delta z} + \frac{T_{i,j+1} - T_{i,j-1}}{2\Delta z} \right) \tag{7.4}$$

where Δz is the spatial spacing.

$$\frac{\partial^2 T}{\partial z^2} = \frac{1}{2} \left(\frac{\frac{T_{i+1,j+1} - T_{i+1,j}}{\Delta z} - \frac{T_{i+1,j} - T_{i+1,j-1}}{\Delta z}}{\Delta z} + \frac{\frac{T_{i,j\pm+1} - T_{i,j}}{\Delta z} - \frac{T_{i,j} - T_{i,j-1}}{\Delta z}}{\Delta z} \right) \tag{7.5}$$

which can be simplified slightly by recognising that we have two of each of the current spatial

terms:

$$\frac{\partial^2 T}{\partial z^2} = \frac{1}{2}\left(\frac{T_{i+1,j+1} - 2T_{i+1,j} + T_{i+1,j-1}}{\Delta z^2} + \frac{T_{i+1,j} - 2T_{i,j} + T_{i,j-1}}{\Delta z^2}\right) \tag{7.6}$$

With this discrete form, equation 7.2 is now re-written:

$$\begin{aligned}\frac{T_{i+1,j} - T_{i,j}}{\Delta t} = \frac{\kappa}{2}&\left(\frac{T_{i+1,j+1} - 2T_{i+1,j} + T_{i+1,j-1}}{\Delta z^2} + \frac{T_{i+1,j} - 2T_{i,j} + T_{i,j-1}}{\Delta z^2}\right) \\ &- \frac{w(z)}{2}\left(\frac{T_{i+1,j+1} - T_{i+1,j-1}}{2\Delta z} + \frac{T_{i,j+1} - T_{i,j-1}}{2\Delta z}\right)\end{aligned} \tag{7.7}$$

What we are interested in is the temperature profile, so we therefore re-arrange to have the temperature terms on their own and everything else outside in parenthesis:

$$\begin{aligned}T_{i+1,j} - T_{i,j} = &\frac{\kappa\Delta t}{2\Delta z^2}\left(T_{i+1,j+1} - 2T_{i+1,j} + T_{i+1,j-1} + T_{i+1,j} - 2T_{i,j} + T_{i,j-1}\right) \\ &- \frac{w(z)\Delta t}{4\Delta z}\left(T_{i+1,j+1} - T_{i+1,j-1} + T_{i,j+1} - T_{i,j-1}\right)\end{aligned} \tag{7.8}$$

What we wish to find in the end is the temperature for the next time step, $i+1$, for the entire column, j_n; and the input data, that we have, is the temperature now, i, for all of the column, j_n. We therefore sort the terms of the two different time steps so that one is to the left and one to the right of the equal sign:

$$\begin{aligned}&\left(-\frac{\kappa\Delta t}{2\Delta z^2} + \frac{w(z)\Delta t}{4\Delta z}\right)T_{i+1,j+1} + \left(2\frac{\kappa\Delta t}{2\Delta z^2} + 1\right)T_{i+1,j} + \left(-\frac{\kappa\Delta t}{2\Delta z^2} - \frac{w(z)\Delta t}{4\Delta z}\right)T_{i+1,j-1} = \\ &\left(\frac{\kappa\Delta t}{2\Delta z^2} - \frac{w(z)\Delta t}{4\Delta z}\right)T_{i,j+1} + \left(-2\frac{\kappa\Delta t}{2\Delta z^2} + 1\right)T_{i,j} + \left(\frac{\kappa\Delta t}{2\Delta z^2} + \frac{w(z)\Delta t}{4\Delta z}\right)T_{i,j-1}\end{aligned} \tag{7.9}$$

Here the signs are chosen so that the temperature terms themselves or individual factors in front of them are always positive, but the full factor in front of a temperature-term for a certain space and time carries the sign. This way, we can we-write the equation to a simpler form by denoting the non-temperature terms:

$$s_j = \frac{\kappa\Delta t}{2\Delta z^2} \qquad \text{and} \qquad r_j = \frac{w(z)\Delta t}{4\Delta z} \tag{7.10}$$

The equation now reads:

$$\begin{aligned}&(-s_j + r_j)T_{i+1,j+1} + (1 + 2s_j)T_{i+1,j} + (-s_j - r_j)T_{i+1,j-1} = \\ &(s_j - r_j)T_{i,j+1} + (1 - 2s_j)T_{i,j} + (s_j + r_j)T_{i,j-1}\end{aligned} \tag{7.11}$$

The left hand side can now be written as tridiagonal matrices multiplied by the temperature profile for the next time step, $i+1$, and the right hand side as a vector whose elements correspond to the current time, i:

$$\begin{bmatrix} b_1 & c_1 & 0 & \cdots & 0 \\ a_2 & b_2 & c_2 & \cdots & \vdots \\ 0 & a_3 & b_3 & \ddots & \vdots \\ \vdots & \vdots & \ddots & \ddots & c_{n-1} \\ 0 & \cdots & \cdots & a_n & b_n \end{bmatrix} \begin{bmatrix} T_{i+1,1} \\ T_{i+1,2} \\ T_{i+1,3} \\ \vdots \\ T_{i+1,n} \end{bmatrix} = \begin{bmatrix} f_1 \\ f_2 \\ f_3 \\ \vdots \\ f_n \end{bmatrix} \tag{7.12}$$

The matrix can be explained by looking at its second row: the red element, a, corresponds to the previous spatial point $j-1$, the blue, b, to the current point, j, and green, c, to the next point,

$j+1$. From this, we also get that

$$a_j = -r_j - s_j, \qquad b_j = 1 + 2s_j \qquad \text{and} \qquad c_j = r_j - s_j \tag{7.13}$$

for when $1 < j < n$. The elements in vector f is the weighted sum of the temperatures at the current point, the point lying before, and the point lying after, just as for the left hand side, but with different weightings:

$$f_j = (s_j - r_j)T_{i,j+1} + (1 - 2s_j)T_{i,j} + (s_j + r_j)T_{i,j-1} \tag{7.14}$$

also within the interval $1 < j < n$.

In order to be able to do the calculation, we need the boundary conditions for both the elements a, b, and c, and the vector f. We find these by considering the physical situation, we are modelling, and what the factors need to be for the left and right hand side of equation 7.12 to satisfy this.

As input in our model, we have the surface temperature, i.e. the temperature at spatial point n. Setting this to be the temperature for the next time step gives us the upper boundary: Letting f_n be the surface temperature, we can find a_n and b_n by extracting the multiplication of the last row of the matrix $\mathbf{M}$ with the vector T:

$$0(T_{i+1,(1:n-2)}) + a_n(T_{i+1,n-1}) + b_n(T_{i+1,n}) = f_n = T(z = H) \tag{7.15}$$

where H is of course the height of the ice cap. From this, we can see that $a_n = 0$ and $b_n = 1$.

For the lower boundary, we must make a different boundary condition, as we do not know the temperature. But, as described in section 2.3, the slope of the temperature profile at the very bottom is determined by the geothermal heat, coming from the bedrock. Based on this, we let f_1 be geothermal heat, Q_{geo} divided by the thermal conductivity, $K(T)$ times the spatial step, $(dT/dz)\Delta z$, and find the elements b_1 and c_1 from the first row of the matrix:

$$b_1(T_{i+1,1}) + c_n(T_{i+1,2}) + 0(T_{i+1,(3:n)}) = f_1 = \frac{Q_{geo}}{K(T)}\Delta z \tag{7.16}$$

From this, we get that $b_1 = -1$ and $c_1 = 1$, since the positive direction of z is upwards. The temperature used for the value of conductivity will be the bottom temperatures.

Since the naming of the diagonal elements is based on their row index, there is no c_n or a_1 element. The full end matrix now reads:

$$\begin{bmatrix} -1 & 1 & 0 & \cdots & 0 \\ a_2 & b_2 & c_2 & \cdots & \vdots \\ 0 & a_3 & b_3 & \ddots & \vdots \\ \vdots & \vdots & \ddots & \ddots & c_{n-1} \\ 0 & \cdots & \cdots & 0 & 1 \end{bmatrix} \begin{bmatrix} T_{i+1,1} \\ T_{i+1,2} \\ T_{i+1,3} \\ \vdots \\ T_{i+1,n} \end{bmatrix} = \begin{bmatrix} f_1 \\ f_2 \\ f_3 \\ \vdots \\ f_n \end{bmatrix} \tag{7.17}$$

The right hand side could also be expressed by a tridiagonal matrix and a vector, analogous to the left hand side with slightly changed elements. And in the same way, the left hand side could be expressed as a single vector. What we are after, however, is the temperature profile for the next time step, so we very much wish for the vector $T_{i+1,n}$ to be "extracted". We find this vector by inversion:

$$\mathbf{M}T = f \qquad \Rightarrow \qquad T = \mathbf{M}^{\top} f \tag{7.18}$$

In practise, we use the *mldivide* in Matlab, also known as the \ operator. The new-found temperature profile, T, is then used as the temperatures for the elements for input into vector f in the next calculation of the temperature profile for the next time step, and so forth.

With firn layer: density and thermal dependency, and compaction

The factors s_j and r_j come from the diffusive term and the convective term, and the components of s_j and r_j are comprised of κ and $w(z)$ and the result of the discretisation. We can use this to easily ascertain what the components of s_j and r_j are for the full temperature equation with a firn layer, equation 2.14.

First, again we ignore any convection in the horizontal direction, since any temperature changes will be small:

$$\begin{aligned}\frac{\partial T}{\partial t} = \kappa\frac{\partial^2 T}{\partial z^2} + \left[\left(\frac{\kappa}{\rho} + \frac{\partial \kappa}{\partial \rho}\right)\frac{\partial \rho}{\partial z} - w(z)\right]\frac{\partial T}{\partial z} \\ + \left[\frac{\partial \kappa}{\partial T} + \frac{\kappa}{c}\frac{\mathrm{d}c}{\mathrm{d}T}\right]\left(\frac{\partial T}{\partial z}\right)^2 + L\frac{\Lambda}{\rho^3}\frac{d\rho}{dz}\frac{g}{c}\end{aligned} \tag{7.19}$$

It is straight away obvious that the s_j factor remains the same, as the diffusive term has not changed. The compaction term has no relation to the change in temperature, so it will simply be added on to the right hand side, the vector f, of our Crank Nicholsen-scheme. The squared advection term is not possible to treat with conventional numerical methods, so in order to get around that, we *linearise* the term: this means we "extract" one (dT/dz) from it, and we-write that into discrete form:

$$\left[\frac{\partial \kappa}{\partial T} + \frac{\kappa}{c}\frac{\mathrm{d}c}{\mathrm{d}T}\right]\left(\frac{\partial T}{\partial z}\right)^2 = \left[\frac{\partial \kappa}{\partial T} + \frac{\kappa}{c}\frac{\mathrm{d}c}{\mathrm{d}T}\right]\left(\frac{\partial T}{\partial z}\right)\left[\frac{T_{i,j+1} - T_{i,j-1}}{2\Delta z}\right] \tag{7.20}$$

where the central difference in temperature is used, the difference over the distance of two points. We now have the same term as of the simple temperature equation, albeit with a lot more factors in front of the vertical advection. Denoting the central difference D:

$$\left[\left(\frac{\kappa}{\rho} + \frac{\partial \kappa}{\partial \rho}\right)\frac{\partial \rho}{\partial z} - w(z) + \left(\frac{\partial \kappa}{\partial T} + \frac{\kappa}{c}\frac{\mathrm{d}c}{\mathrm{d}T}\right)D\right]\left(\frac{\partial T}{\partial z}\right) \tag{7.21}$$

The factor r_j will then contain, as opposed to only $w(z)$, *all* of what is in front of the advection term. We find the equations for diffusion and the derivatives with respect to density from equation 2.13, and for the density from equation 2.15:

$$\frac{\partial \kappa}{\partial \rho} = \kappa\left(\frac{1}{\rho(z)} - \frac{1}{2\rho_{ice}}\right)\left(1 + \log\left(\frac{\rho(z)}{\rho_{ice}}\right)\right) \tag{7.22}$$

$$\frac{\partial \rho}{\partial z} = k(\rho(z) - \rho_{ice}) \tag{7.23}$$

where $\rho(z)$ is of course the density profile. The derivatives with respect to temperature are straightforward with regards to the thermal capacity, but for the diffusivity, equation 2.13, we must use the chain rule as the diffusivity is calculated from the capacity and conductivity, equation 2.12, both of which depend on the temperature:

$$\frac{\mathrm{d}c}{\mathrm{d}T} = 7.122 \tag{7.24}$$

$$\begin{aligned}\frac{\partial \kappa}{\partial T} = \frac{\partial}{\partial T}\left(K(T)\frac{1}{c(T)}\right)P = \left(\frac{\partial K}{\partial T}\frac{1}{c(T)} + \frac{\partial c(T)^{-1}}{\partial T}K\right)P = \\ \left(-0.0057K_{ice}\frac{1}{c} - 7.122\frac{1}{c^2}K_{ice}\right)P = -0.0057\kappa - 7.122\frac{\kappa}{c}\end{aligned} \tag{7.25}$$

where P is all the terms relating to density from the equation of thermal diffusivity, 2.13. The

terms originally stemming from the squared vertical advection can be simplified further:

$$\left(\frac{\partial \kappa}{\partial T} + \frac{\kappa}{c}\frac{\mathrm{d}c}{\mathrm{d}T}\right) D = \left(-0.0057\kappa - 7.122\frac{\kappa}{c} + \frac{\kappa}{c}7.122\right) D = -0.0057\kappa D \tag{7.26}$$

We can now write up the full equation for the temperature with a firn layer and thereby find the factor r_j, stemming from the components in front of the vertical advection. The s_j factor is the same as before. Remember, the factors consist of all the components in front of the diffusivity and advection in addition to components from the discritisation:

$$\frac{\partial T}{\partial t} = \kappa\frac{\partial^2 T}{\partial z^2} - \left[-\left(\frac{\kappa}{\rho} + \frac{\partial \kappa}{\partial \rho}\right)\frac{\partial \rho}{\partial z} + w(z) + 0.0057\kappa D\right]\left(\frac{\partial T}{\partial z}\right) + L\frac{\Lambda}{\rho^3}\frac{d\rho}{dz}\frac{g}{c} \tag{7.27}$$

$$s_j = \frac{\kappa \Delta t}{2\Delta z^2} \qquad \textit{and} \qquad r_j = \left[-\left(\frac{\kappa}{\rho} + \frac{\partial \kappa}{\partial \rho}\right)\frac{\partial \rho}{\partial z} + w(z) + 0.0057\kappa D\right]\frac{\Delta t}{4\Delta z} \tag{7.28}$$

where the sign change in the full equation is so that everything in front of the advection term is exactly as in the simple equation. Finally, the elements f_j become:

$$f_j = (s_j - r_j)T_{i,j+1} + (1 - 2s_j)T_{i,j} + (s_j + r_j)T_{i,j-1} + L\frac{\Lambda}{\rho^3}\frac{d\rho}{dz}\frac{g}{c} \tag{7.29}$$

And of course, all the boundary conditions are the same for the model with a firn layer and without.

7.4 Comparing modelled and measured borehole temperatures

We start the temperature modelling with inputting a sufficiently large amount of time, 100 thousands years, of the same temperature. We tune this temperature so that the steady state solution fits with the measured deeper part of the temperature profile.

Hereafter, the temperature history from Southern East Greenland is added as the input surface temperature from DMI station 4360 Tasiilaq (see section 5.1) for the years 1895 to 1959. And lastly, the temperatures from ECHAM is added up until the the time of the drilling for the two sites. For both DMI and ECHAM, we run with monthly input. For the 12 continuous missing

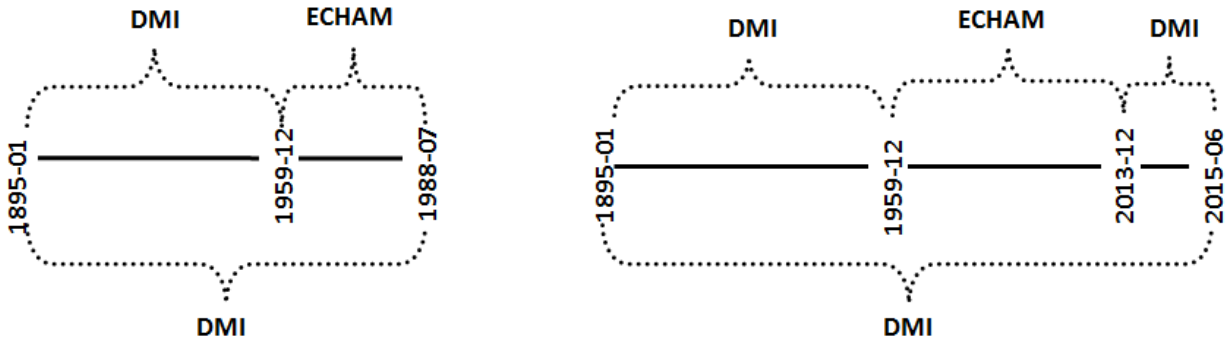

Figure 7.9: *The input data sources for the temperature modelling: DMI station 4360 and ECHAM (top part) or only DMI station 4360 (bottom part) in the relevant intervals for the old site (left) and new site (right).*

months of DMI station 4360, we repeat the previous relevant months. For the two single monthly values missing, we take the mean of the neighbouring months. For the old site, the temperature input from ECHAM will run up to including July 1988. ECHAM data stops 18 months before drilling of RECAP, the new site, so for this the last part of the surface temperature input comes from the DMI station.

We also run a model with only DMI station 4360 as surface temperature input, to investigate whether using ECHAM data is better than using a shifted temperature measurement, for both

sites and corresponding time intervals. A schematic of the input sources can be seen in figure 7.9.

We apply a shift to the surface temperature inputs, so that their temperature values have the right magnitude. We use the top of the borehole profile that is not controlled by the geothermal heat, which has a mean value of -18.47 °C for both sites, and compare with the the temperature of the overlapping interval of the two cores, 1960-July 1988. This gives a positive shift of only 0.52 °C for ECHAM, and a negative of 16.87 °C for DMI station 4360.

The borehole measurements and the modelled temperature profile can be seen in figure 7.10. Overall, both the combined surface temperature input from DMI and ECHAM and only from DMI model the measurements quite well. It is clear that the geothermal heat has a high influence on the temperature profile, as could also be seen from just the measurements, as expected due to the relative smallish height of the Renland ice cap compared to for instance the main Greenland ice sheet. The small misfit in the middle parts could be due to the shifts not being correct, or rather, that the input assuming a temperature steady state condition up until the start of the model input, 1885, is incorrect.

Detail of the upper part is shown in figure 7.11. Naturally, the previous winter cold and summer warmth can be seen. A warming is present in both the old site and the new site, starting at around 30 and 80 meters depth, respectively, indicating a warming that started before 1980's and continued until present day. For the old site, the warming starts later for the DMI input than the ECHAM input, which is also true for the new site, but of course less apparent since the signal has travelled further down and been advected and diffused.

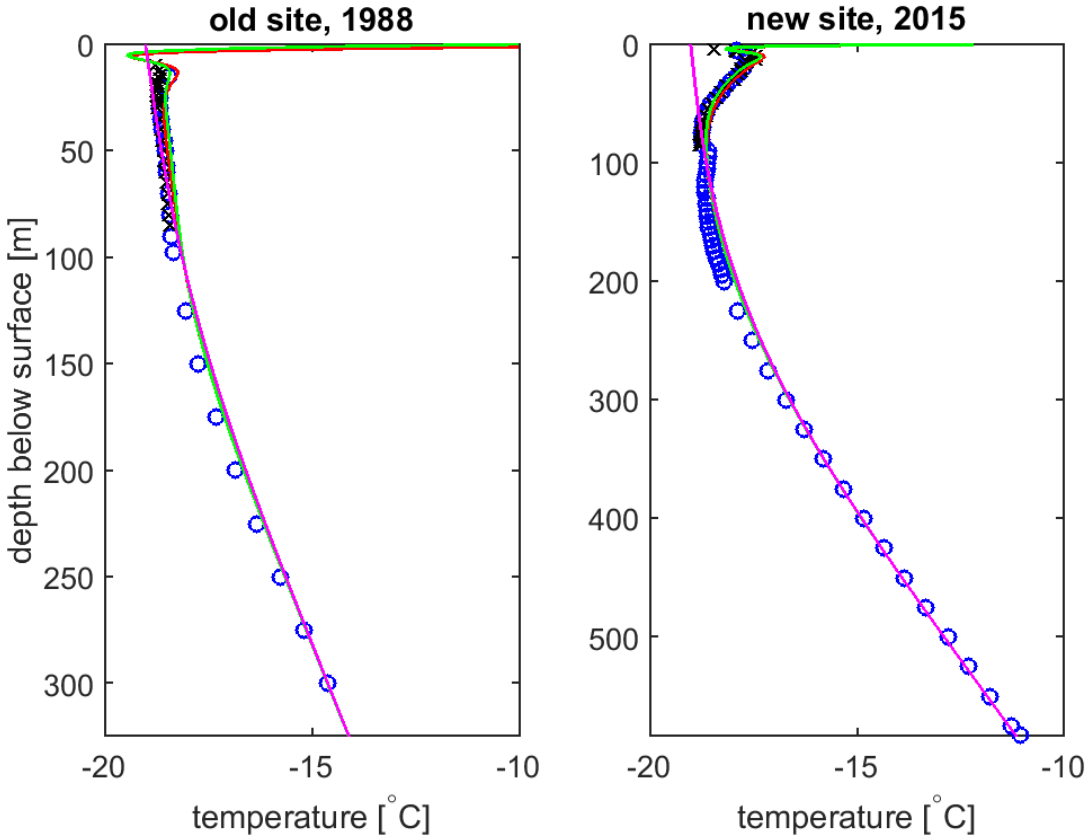

Figure 7.10: *Modelled borehole temperature profile (red for combined DMI and ECHAM and green for DMI) and comparison with steady state profile (magenta) and measurements (blue circles and black crosses) for both sites.*

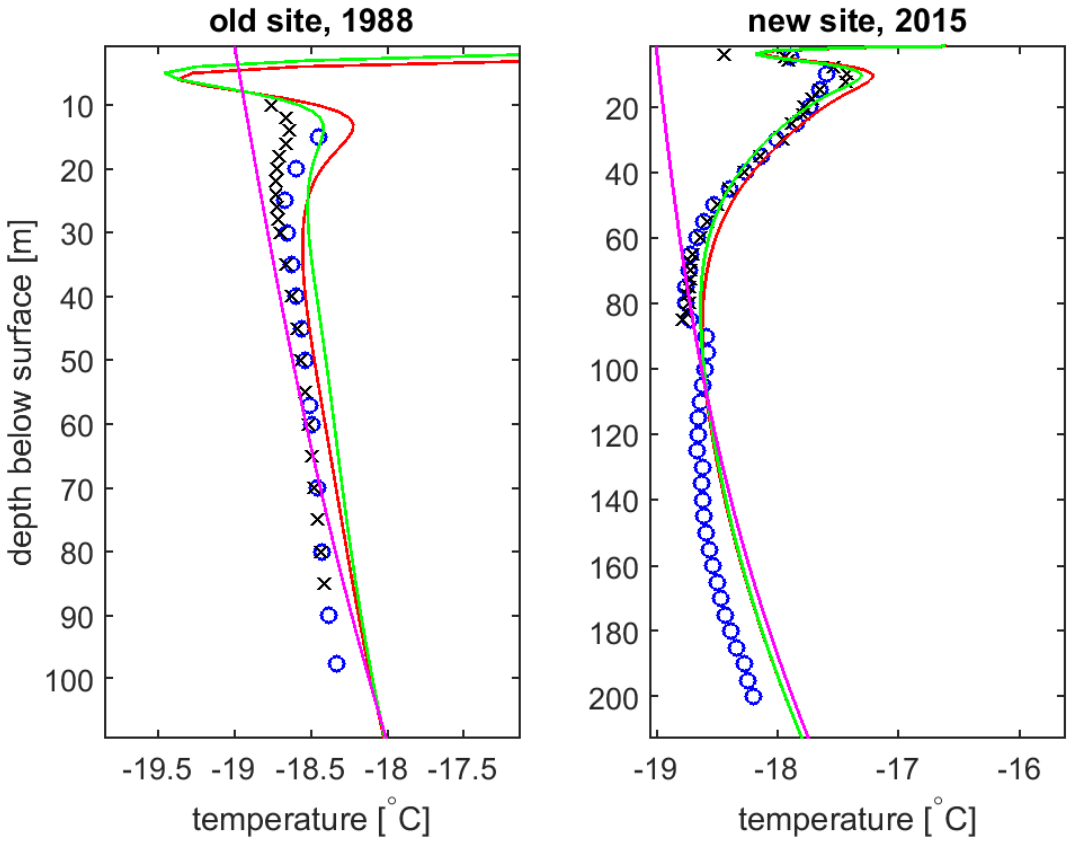

Figure 7.11: *Zoom in on modelled borehole temperature profile (red for combined DMI and ECHAM and green for DMI) and comparison with steady state profile (magenta) and measurements (blue circles and black crosses) for both sites.*

CHAPTER 8

Discussion

This chapter makes the inter-parameter comparison of our available data sets, where in the previous chapters, only data of the same type had been compared. First, however, it will address some of the more technical details of the needed background models that was found in chapter 7, namely the density model and the flow model.

It ends by presenting an overview of what findings and results we can draw about the climate of Renland from this study based on modern data to possible be used in a paleo climatic sense, based on the three climate parameters *temperature, precipitation* and *isotopic composition.*

8.1 Flow and density model

The density model in section 7.1 does quite well. However, as the borehole and modelled temperature profiles show, it is in the upper part that we see the warming develop. As such, it is important to take care that the model employed is correct as this will affect the upper ~100 metres, a depth which for the old but also new site includes the warming (see figure 7.11). A possible improvement could be to use the Herong-Langway model: taking the logarithmic behaviour of the density data, it can be seen that there is two different linear regimes, as seen in figure 8.1.

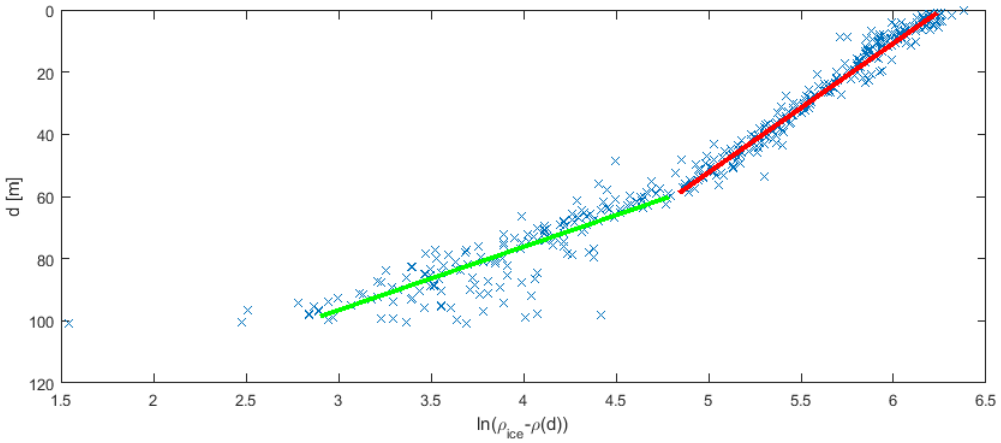

Figure 8.1: *The logarithm of the density data versus shown versus depth, with two approximate slopes manually superimposed.*

The parameters for the flow modelling was found via a simple forward misfit model. As shown in section 7.2, the fit was a lot better for the old site than the new. While the kink height for the old site is quite high compared to those normally found for the main Greenland ice sheet, it is not lying *at* the level of the ice cap height as was found for the new site.

During the "tuning" of the ranges and resolution of the fitting parameters (accumulation, kink heigh and bottom sliding) it was seen that while the old site seem to have a simple misfit

distribution which allowed for straightforward decrease of ranges and increase of resolution, the new site's misfit distribution was less regular. As an example, when one parameter got increased resolution, it found a triplet of lowest misfit, and then when that parameter was changed back to lower resolution so that another could be higher, it would not necessarily choose a similar misfit lying close to: especially for the kink height, the variation was great, although the lowest triplet still had misfit of around more than ~10 years. A visual way to orient oneself of the misfit distribution is to plot a suitable number of triplets as a scatter plot in 3D space where colour would indicate the magnitude of misfit, possibly highlighting the presence of more than a single minima. However, the triplets plotted of course also depend on the tuning of the model parameters.

The direct solution is to increase the computational memory available for the calculation so that all parameters can have resolutions high enough. This, however, also raises the question of how accurate such a model parameter could, or rather should, physically be. When taking into account the uncertainty of the dated match points, does it then make sense to estimate e.g. the accumulation to within a millimetre? As seen, the bottom sliding as found by tuning the parameters is in the fourth decimal; one could argue then that instead, the bottom sliding should just be held at zero, which certainly would decrease the misfit complexity as we only have to find two best fitting parameters, but as explained, the old site was not the one with difficulties.

There is also the possibility of using a different approach of using an inverse model rather than a forward one to find the best parameters for the flow model. However, it is possible that even an inverse fitting would not create a better fit: The flow model used for the borehole temperature modelling does not do very well for the new site. The velocity model, even when only fitted to the upper most parts, still has a misfit of more than 10 years, and as evident by the yearly thicknesses (see figure 7.8), does not have the correct thinning. It seems that the new site has faster, or different, thinning than the kink-model can match, and the misfit was even greater when using all of the depth points. While it must not be ignored that the possibility of additional depth points could change this picture, the results suggest that a different flow model is needed to accurately represent the new site on Renland.

Despite these problems with the underlying flow model, we still believe that the results of the temperature modelling are a good match, as we truncated the depth points and as the same behaviour is seen for the old site, whose flow models works, and the new site.

8.2 Definition of seasons

As mentioned in chapter 7, the temperatures for ECHAM only required a very small shift to match the borehole temperatures, while the isotopes, as seen in chapter 6, are heavyer than the measured values from both the old core and in the firn cores. The last is what would be expected from using the simple relation that the higher the altitude, the heavyer (more positive) the isotopes are, and in the ECHAM model, the Renland grid point is more than one kilometre lower than the real elevation of the ice cap. At such, it is surprising that the temperature agree well with measurements, especially when, in the comparison with DMI data for station 4339 Itt., there was a greater temperature difference even though the difference in heights are only 100 meters.

Looking at the distribution of the δ^{18}O-values throughout the year for ECHAM and the firn-cores, as also seen for the older interval, the reason for the higher isotopic mean value is a longer lasting "summer" season, as seen by a wider peak in figure 6.3. This is not seen in the comparison of temperature for Itt., where the timing of the season fits, and the summer is colder. Whether this warmer and wider summer signal is seen in the temperature for the grid point of Renland can be checked for ECHAM itself by comparing the temperature and isotopic values throughout the year, as seen in figure 8.2. It is seen that light values of the isotopes are shorter periods, and the heavier values are wider. The temperature is more evenly spread throughout the year than the

isotopes. It is also seen that the troughs and peaks of temperature and isotopes are not coinciding exactly.

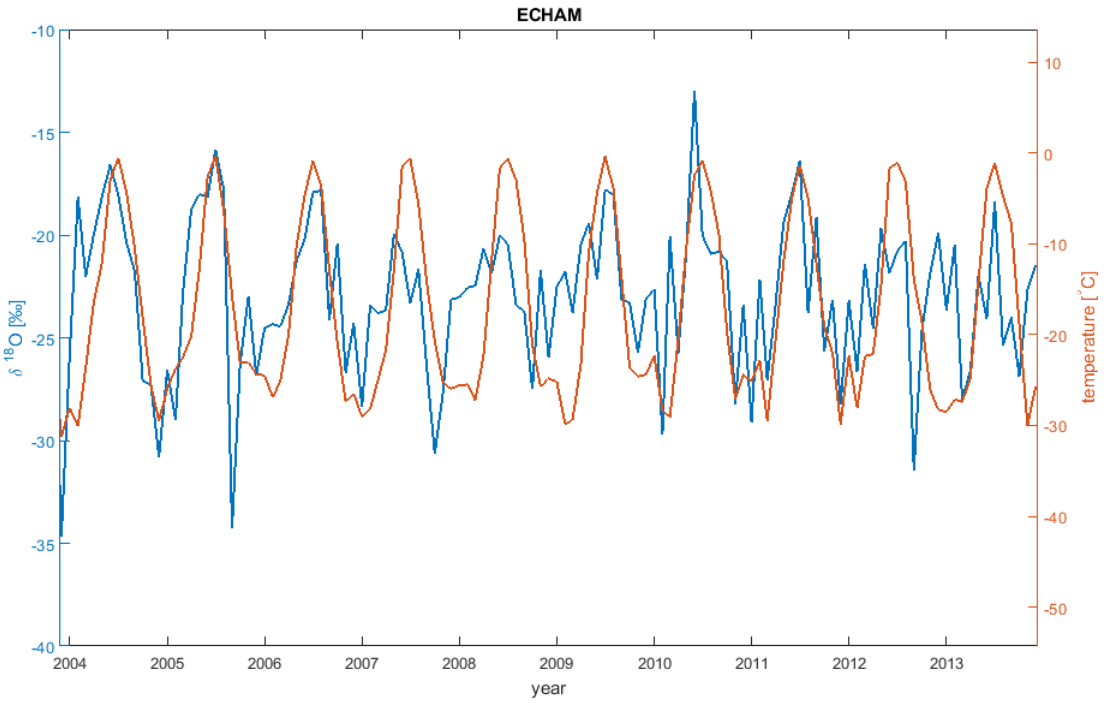

Figure 8.2: *δ^{18}O-values (blue, left axis) and temperature (red, right axis) for EHCAM for the recent interval of 2004-2013.*

By making the same comparison in figure 8.3 for ISOCAM, it can be seen that the temperature display a clear seasonal signal, which is not seen in the isotopic data. Some years do look more regular although with a very wide warm season, for instance 2008 and 2010, and 2007 even have a more defined summer peak, while others, for instance 2005 or 2011, appear less cyclic. Comparing with ECHAM, as seen in figure 6.5, the timing of the coldest values does not coincide between the two models, but neither does the coldest value of one model throughout the different years, as it sometimes falls at the end of a year and sometimes at the beginning. Comparing the timing of warmest values is less readily done due to the wide summer seasons. The transition to year 2011, 2012 and 2013 of ECHAM appear especially imprecise, with the first month of 2013 even having a high value. For ISOCAM, the same impreciseness in timing can be seen: although the transition to year 2008 and possibly 2009, 2010 and 2011 display more clear winters values, year 2012 seem to have an "extra" season with low values around the winter months and high values at the transition.

As summarized in table 6.1, the spread, measured as seasonal amplitude, of ISOCAM is a closer match to that of the firncores than ECHAM. This used definition/way of calculating "seasonal amplitude" is however possibly not a good measurement for how well the models work: for ECHAM, it appears that the higher spread for some years are due to single months of very high and low values, for instance for year 2005, 2010, and the low value of 2012. For 2010, the seasonal amplitude is calculated with values only two months apart (July and September). For other years, as just described, some winter trough is not an obvious single dip in the profile. For ISOCAM, the same picking of the "wrong" lows and highs happen for instance in year 2012 where the lowest value are in September and the highest in December. In addition, the summer peak is not always apparent and in some cases the warmest value appear almost identically twice, for instance in the year 2007 or 2008.

A new way of defining and calculating the seasonal amplitude could alleviate these problems. One way is to use the same months as when there are highs and lows in the temperature data,

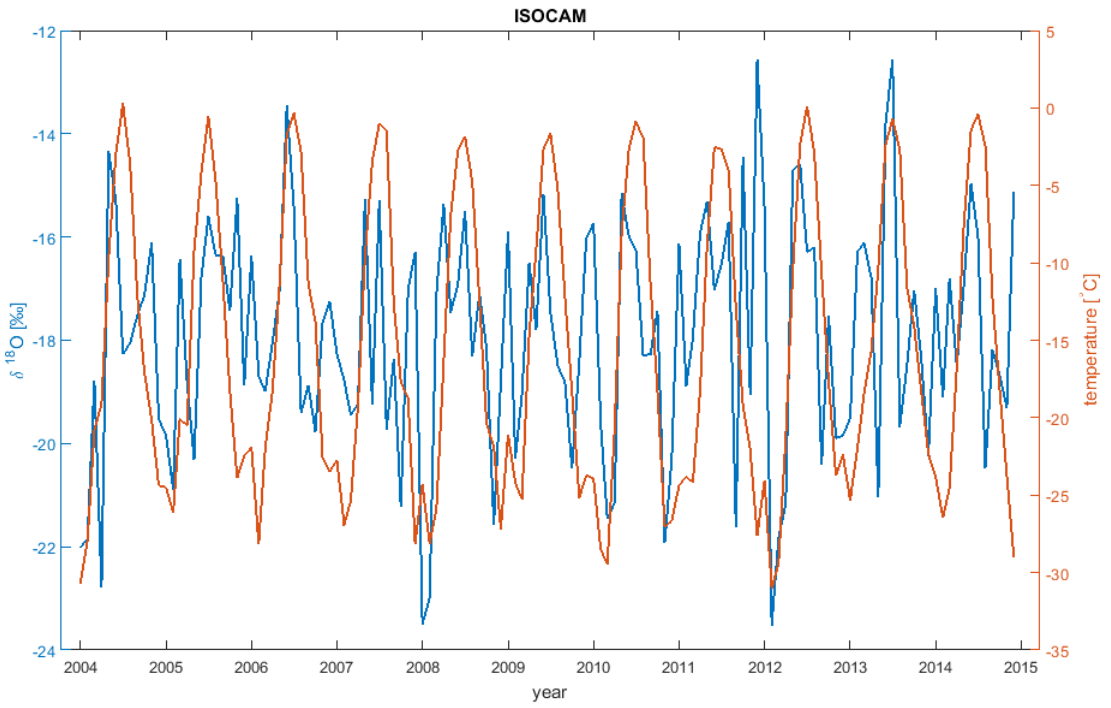

Figure 8.3: *δ^{18}O-values (blue, left axis) and temperature (red, right axis) for ISOCAM for the recent interval of 2004-2014.*

which would necessitate that isotopes and temperature exhibit a seasonal cycle of the same timing. One could also pick the same months for all years for one or both models, or look for the highest and lowest value in a for instance three month interval around what should theoretically be the warmest and coldest months, or as indicated pointed out by the temperature data, thus not having to worry about the interim months. This would allow for the coldest and warmest months to not have to be at the same time of the year for all years, but, however, that implies that we believe the model has the right behaviour in those certain periods and that only the other months are have error. Lastly, the highs and lows to base the amplitude on could be chosen manually, but that would not get rid of the underlying problem of especially ISOCAM not displaying a clear seasonal cycle, making it hard to pick a sound high and a low.

8.3 Climate signal for Renland

It was found that the two firn cores, from the sites of the old and new main core, are not isotopically significantly different (see chapter 4). However, it cannot be discounted that this is due to the relatively high resolution of the profile and with it intrinsic noise: for instance, a difference of as much as 4 ‰ can be seen in samples of the same date. The overall difference of about 0.4 lower in value of δ^{18}O for the A9 firncore matches what is seen from isotopic CFA RECAP profile[i] which consistently lies higher than the old core with about the same amount. Comparison with the old main core showed a warming in the isotope values in the recent years.

The lack of agreement between modelled and dated depths for the new site suggest that the flow scheme for the old and new site are not the same, and specifically that a Dansgaard-Johnson model is not the right way to conceptualize the flow. The firn cores do suggest, however, that the accumulation of the two sites are very similar, so the reason for the different flow regimes are to be found below the surface. It is very possible that the fact that the old site is on a slope and that

[i]Preliminary unpublished local data.

the new site is in the bottom of a valley affects how the ice can flow.

By looking at the averaged yearly data, while loosing the monthly details, it also removes possible noise and model inner-annual timing problems, and gives a clearer view into a possibly changing climate when using the longer interval that the ECHAM data spans. The validation for ECHAM was only done in the two separate time intervals; making it over the full interval that we have DMI and ECHAM data for would naturally give a comparison of higher certainty.

As seen in chapter 6, while offset to heavier values, the development of the δ^{18}O-values over the years from ECHAM match the measurements from the firn cores (figure 6.1) very well and the old main core (figure 6.9) well. As seen in figure 8.4, the development toward warmer values is displayed in the temperature data for ECHAM, but not the isotopes, as it was for the old and A9 core. The temperature and isotope data for ECHAM has an overall cross-correlation factor of 0.44. The offset in isotope values of ECHAM to firncores can be explained by the difference in height of the real and modelled site, however, this offset is not seen in the temperatures when using the boreholes as a measurement source. It is not surprising that ECHAM does better than ISOCAM, being nudged, but both models actually capture the overall precipitation.

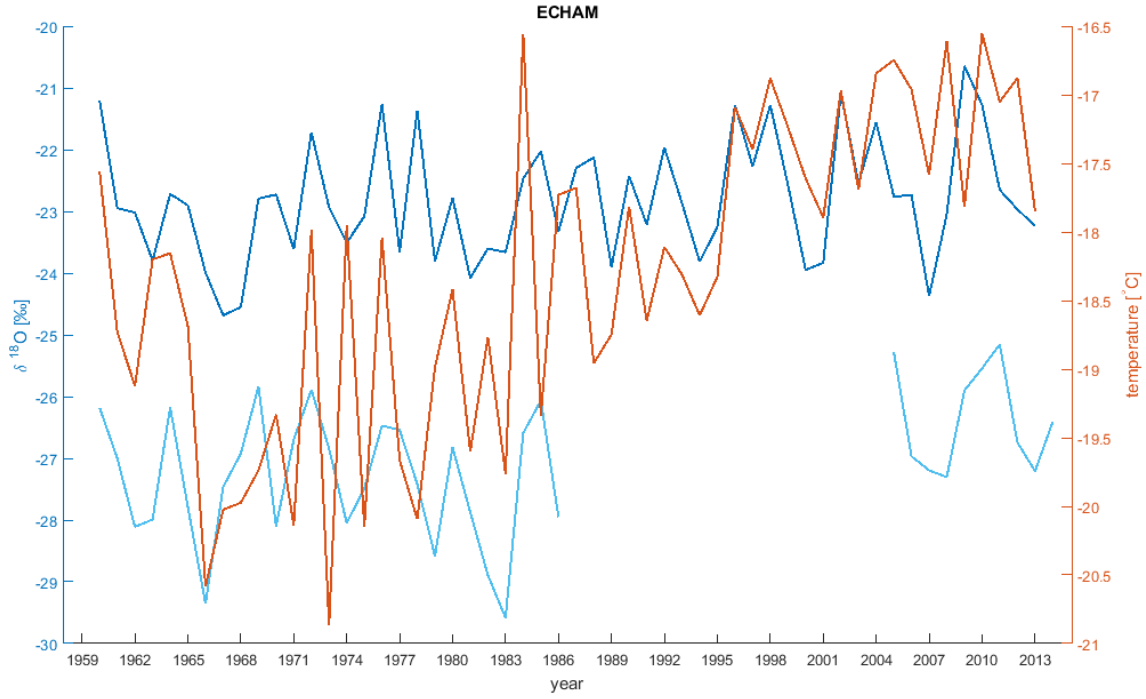

Figure 8.4: *Comparison of the yearly meaned δ^{18}O-values (left axis) for ECHAM (dark blue) and old main core and firncore A9 (light blue), overlayed with the temperature (right axis) from EHCAM (rust).*

As we saw in chapter 7, both the temperature data from ECHAM and the shifted measurements from DMI station 4360 model the borehole temperature very well, with the latter needing a natural shift in temperature to get the right amplitude, but still representing this trend of a significant warming, as modelled in ECHAM and measured in the boreholes. This would indicate that the temperature trend of ECHAM is not (only) a result of the better representation of the climate, but also a warming in the area in the relevant period: it is seen that the warming in the borehole for the new core is a lot more significant than for the old core.

CHAPTER 9

Conclusion

The two firn cores from near the sites of the old and new main cores where processed and found to be climatologically no different. During the background for the temperature modelling, it was found that the flow at the two sites, however, does not follow the same pattern.

From comparison, ECHAM shows very good agreement with the yearly development of the isotopes in the recent interval especially, and with the measured borehole temperatures. Both models agree with each other and the firn cores in regards to total amount of precipitation, but not the timing hereof, and likewise, the seasonal variability of ECHAM and ISOCAM did not show good matching of isotopes.

Additionally, it was shown that the temperature trend exhibited by the borehole is also displayed by the measurements of a station even further away, at the coast of Greenland.

Going from very local (firn core to firn core), to broader (ECHAM and ISOCAM grid scale) and finally to regional scale (DMI station Tasiilaaq) and still have a climatological match suggest that the climate signal experience by Renland and present in the ice core (and the borehole) is of a broader scale and possibly experienced by the entire area of South Eastern Greenland.

This means that for understanding the climate of Renland, we can use more than just what is available from the ice cores, but also both measured climatic data like temperature, but possibly also the whole suit of parameters available from ECHAM: when both the temperature, isotopes and precipitation appear to be correct, as seen on a yearly scale, it lends support to that the underlying physics and relations of the model are correct, and thus the other parameters calculated by it will be usable.

Whether this is also the case for other sites than Renland cannot be concluded on the basis of this study, and would require a larger comparison of measurement and data, preferably at a place outside the regional scale of the southeast of Greenland. Additionally, a temporally longer comparison would yield higher a certainty, also taking into account that ECHAM agrees somewhat better in the recent interval than earlier.

9.1 Outlook

When comparing the timing of the firn cores and models, as in figure 6.3, it is important to remember that the timing of the isotopic samples of the firn cores are chosen by marking the lowest value as the first of a new year, as described in section 4.3.2. This means that the winter season should coincide somewhat, but the timing of the summer does not necessarily fit, nor does the interim months. This could be improved by a different dating of the individual samples, for instance at least a summer horizon too. However, this would still not allow for a spread around the seasons for when exactly a low and high occur, and it still does not address the crude approximation/assumption it is that the all samples within a year correspond to the same duration. The comparison between models and measurements becomes muddied by how much one believes in the detail of the dating of the firn cores and in the values themselves and the timing of the model data.

Ideally, one could get around the dating issues by comparing the isotopes on a physical depth scale instead of on a dated time scale, just as we compared the firn cores themselves on their respective depth scales. For the models, we simply use the precipitation data to create artificial "water cores", and for the firn cores, we use the density data to also get the depth in water equivalent. Of course only the dated interval matching the intervals of the model data, 2006-2013 including, are used, as otherwise, the "surface" of these "cores" would not correspond to the same time of "drilling". This means that we are still depending on the dating of the firn cores, as well as the models, at the end and start of the interval. The water cores are shown in figure 9.1.

While the yearly cycle was seen in the firn cores on a depth scale and was even good enough to use for dating, it is not apparent in neither ISOCAM nor ECHAM. The values and depths of individual samples of the firn cores are of course determined by the fact that they were cut into 5 cm samples: a for instance 10 cm sampling scheme would smooth the curves. The longer intervals of precipitation for the models is of course due to it being monthly data, and also, compared with the artificially linearly spread firn core samples, we do not expect actual or modelled precipitation to be equally distributed over a year, nor over one month even.

Making the artificial "water cores" for the models with higher temporally resolved data might aide in the comparison: one could even use the dating of the firn cores and the sliding time duration of the samples to make weighted means of the isotopic model data of the same "lengths", after which summed up to a depth. But even so, that would not make the water depth isotope profiles of the models fit the firn cores, as is apparent in the figure. But, on the other hand, the firn cores themselves do not have matching precipitation. If there is a spread in the timing and/or amount of the precipitation on the ice cap itself over two kilometres (distance between the old and new site), it would be unreasonable to expect the models that does not even resolve the ice cap and cover a larger grid area than it, to have the matching precipitation at this temporal resolution.

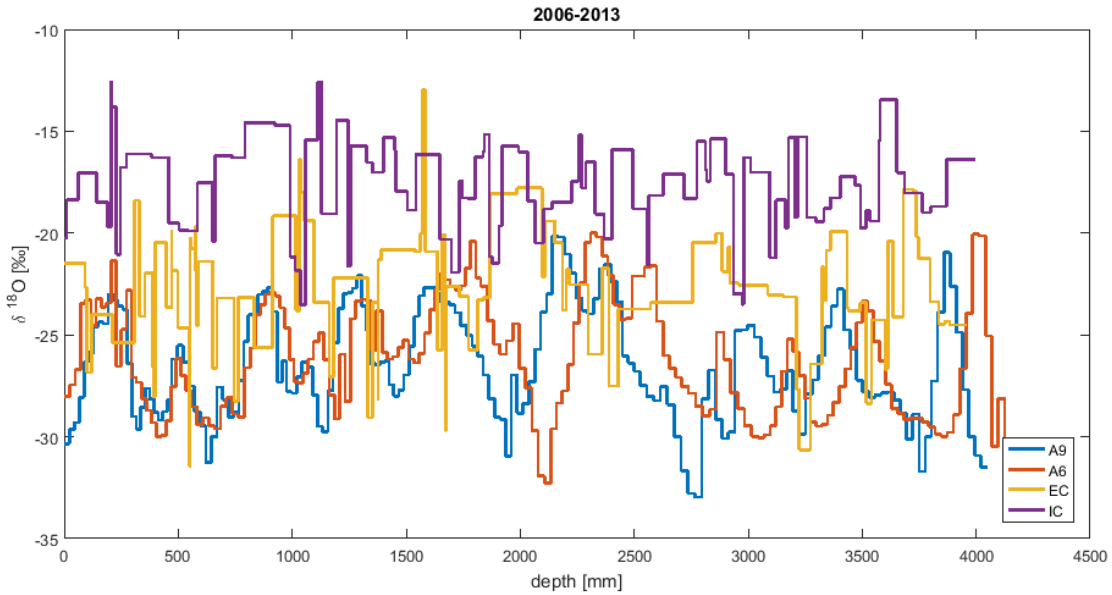

Figure 9.1: *δ^{18}O-values for firn cores A9 (blue) and A6 (red) and models ECHAM (yellow) and ISOCAM (purple) on water equivalent depth scale.*

What can still be seen though, is that the precipitation events happens often as big and warm and short and cold periods, matching the wide summer seasons seen in the dated isotopic profiles for the models. Overall, as also seen in chapter 6 and in the summery table 6.1, the amount of precipitation agrees remarkably well with the firn cores, giving if not all then at least the end point horizons of the dating of the firn cores credibility, as well as believability to the models.

So while ISOCAM exhibits the right precipitation and ECHAM has the right temperature, precipitation and isotopic composition when seen separately and at a yearly resolution, the detailed behaviour and combination of those parameters still leave room for improvement of the GCM's. If working, there would be no need for dating an ice core as the measurement profiles could be directly compared to the GCM data, from where the timing could be gotten. If so, the only source of errors would be due to eventual errors in the logging depth[i].

[i]Though careful attention is paid in the field to accuracy and precision, logging the depth of an ice core is no trivial matter.

Bibliography

Center of Ice and Climate. The GICC05 time scale, 2016. URL http://www.iceandclimate.nbi.ku.dk/research/strat_dating/annual_layer_count/gicc05_time_scale/.

H Craig. Isotopic Variations in Meteoric Waters. *Science (New York, N.Y.)*, 133(3465):1702–1703, 1961. ISSN 0036-8075. doi: 10.1126/science.133.3465.1702.

J. Crank and P. Nicolson. A practical method for numerical evaluation of solutions of partial differential equations of the heat-conduction type. *Advances in Computational Mathematics*, 6(1):207–226, dec 1996. ISSN 1019-7168. doi: 10.1007/BF02127704. URL http://link.springer.com/10.1007/BF02127704.

K. M. Cuffey and W. S. B Paterson. *The physics of glaciers*. Elsevier Ltd, 4th edition, 2010. ISBN 9780123694614.

D. Dahl-Jensen. Past Temperatures Directly from the Greenland Ice Sheet. *Science*, 282(5387):268–271, 1998. ISSN 1095-9203. doi: 10.1126/science.282.5387.268.

W. Dansgaard. Stable isotopes in precipitation. *Tellus*, 16(4):436–468, 1964. ISSN 0280-6495. doi: 10.3402/tellusa.v16i4.8993.

W. Dansgaard and S.J. Johnsen. A Flow Model and a Time Scale for the Ice Core from Camp Century, Greenland. *Journal of Glaciology*, 8(53):215–223, 1969. ISSN 00221430.

Pier A. de Groot. *Handbook of Stable Isotope Analytical Techniques Volume I*. Elsevier Ltd, 1st edition, 2004. ISBN 978-0444511140.

DMI. Tekniske Rapporter, 2016. URL http://www.dmi.dk/laer-om/generelt/dmi-publikationer/2013/.

M. M. Herron and C. C. Langway. Firn densification: an empirical model. *Journal of Glaciology*, 25(93):373–385, 1980. ISSN 00221430. doi: 10.3198/1980JoG25-93-373-385.

S. J. Johnsen, W. Dansgaard, and J. W. C. White. The origin of Arctic precipitation under present and glacial conditions. *Tellus B*, 41B(4):452–468, 1989. ISSN 02806509. doi: 10.1111/j.1600-0889.1989.tb00321.x.

Sigfus J Johnsen. Stable isotope profiles compared with temperature profiles in firn with historical temperature records. *Isotopes and Impurities in Snow and Ice - Symposium 118*, pages 388–392, 1977.

Sigfus J Johnsen, H. B. Clausen, Willi Dansgaard, Niels S. Gundestrup, Margareta Hansson, Peter Jonsson, J. P. Steffensen, and Arny E. Sveinbjørnsdottir. A "deep" ice core from East Greenland. *Meddelselser om Grønland, Geoscience*, 29:3–22, 1992.

Jean Jouzel and Liliane Merlivat. Deuterium and oxygen 18 in precipitation: Modeling of the isotopic effects during snow formation. *Journal of Geophysical Research*, 89(D7):11749, 1984. ISSN 0148-0227. doi: 10.1029/JD089iD07p11749.

M Majoube. Fractionnement en oxygene-18 et en deuterium entre l'eau et sa vapeur. *Journal de Chimie et Physique*, 58:1423–1436, 1971.

Liliane Merlivat and Jean Jouzel. Global climatic interpretation of the deuterium-oxygen 18 relationship for precipitation. *Journal of Geophysical Research*, 84(C8):5029, 1979. ISSN 0148-0227. doi: 10.1029/JC084iC08p05029.

Willem G. Mook. *Environmental Isotopes in the Hydrological Cycle Principles and Applications*, volume 1+2. IAEA, 2001.

V Schytt. The inner structure of the ice shelf at Maudheim as shown by core drilling. *Norwegian-British-Swedish Antarctic Expedition, 1949–52*, (Scientific 4, Glaciology 2):115–151, 1958.

The Ohio State University. Greenland Mapping Project, 2016. URL https://bpcrc.osu.edu/gdg/data/gimpdem.

B. M. Vinther. The REnland ice CAP project (Sapere Aude). URL http://recap.nbi.ku.dk/forsidebokse/recap_proposal/RECAP_proposal.pdf.

B. M. Vinther, H. B. Clausen, D. A. Fisher, R. M. Koerner, S. J. Johnsen, K. K. Andersen, D. Dahl-Jensen, S. O. Rasmussen, J. P. Steffensen, and A. M. Svensson. Synchronizing ice cores from the Renland and Agassiz ice caps to the Greenland Ice Core Chronology. *Journal of Geophysical Research Atmospheres*, 113(8):1–10, 2008. ISSN 01480227. doi: 10.1029/2007JD009143.

B M Vinther, S L Buchardt, H B Clausen, D Dahl-Jensen, S J Johnsen, D a Fisher, R M Koerner, D Raynaud, V Lipenkov, K K Andersen, T Blunier, S O Rasmussen, J P Steffensen, and a M Svensson. Holocene thinning of the Greenland ice sheet. *Nature*, 461(7262):385–388, 2009. ISSN 0028-0836. doi: 10.1038/nature08355. URL http://dx.doi.org/10.1038/nature08355.

G. E. Weller and P. Schwerdtfeger. Thermal properties and heat transfer processes of the snow of the central Antarctic plateau. In *Symposium on Antarctic Glaciological Expolation (ISAGE)*, pages 284–298. IAHS Publ. no. 86, 1970.